Characterization of the molecular features of Oncostatin M determining receptor activation

INAUGURALDISSERTATION

zur Erlangung des Doktorgrades der Naturwissenschaften

- *Doctor rerum naturalium* -
(Dr. rer. nat.)

Eingereicht am Fachbereich Biologie und Chemie
der Justus-Liebig-Universität Giessen

vorgelegt von

Juan Manuel Adrián Segarra

Bad Nauheim, 2017

Die vorliegende Arbeit wurde am Max-Planck-Institut für Herz- und Lungenforschung in Bad Nauheim angefertigt.

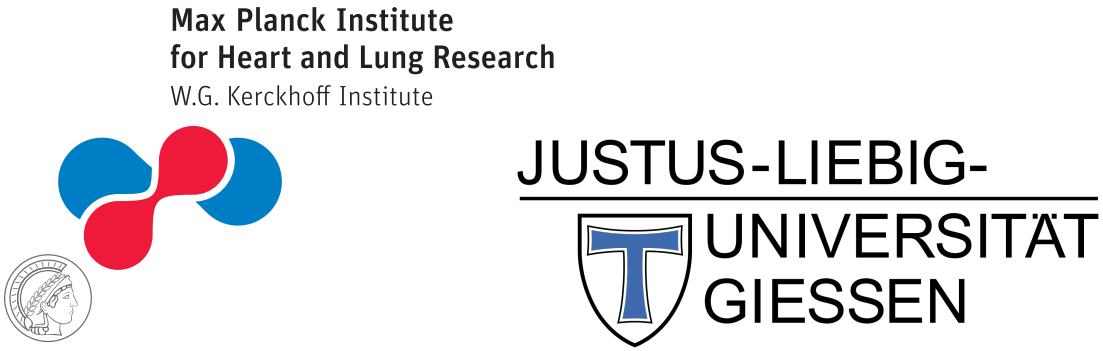

Erstgutachter:
Prof. Dr. Dr. Thomas Braun
Abteilung Entwicklung und Umbau des Herzens
Max-Planck-Institut für Herz- und Lungenforschung
Ludwigstrasse 43
61231 Bad Nauheim

Zweitgutachter:
Prof. Dr. Katja Sträßer
Institut für Biochemie
Justus-Liebig-Universität Gießen
Heinrich-Buff-Ring 17
35392 Giessen

Table of contents

1. Introduction

1.1. Analysis of protein structure and function

The function of a protein is largely a consequence of its structure, with different functions being associated with particular three-dimensional folds in the proteins performing them. (Hegyi & Gerstein 1999) Describing the three-dimensional structure of a protein from its amino acid sequence is not trivial, leading to a number of techniques being developed over the years to obtain high-quality structural information. The first of these was x-ray crystallography, which involves the production of protein crystals from purified protein samples: these crystals are then exposed to an x-ray beam, and the diffraction patterns caused by the crystal used to obtain information about its structure. (Lieberman et al. 2013)

While significant improvements in resolution have been achieved since the first protein structures were described, x-ray crystallography is not without disadvantages: creating protein crystals for water-insoluble proteins (e.g. membrane proteins) remains a considerable challenge, and the crystallization process might result in a loss of information regarding the native structure of the protein. (Yonath 2011) Obtaining information regarding protein-protein interactions through this method requires the co-crystallization of both proteins: while difficult, this feat has shed light into the arrangement of a number of protein complexes since it was first described. (Wiesmann et al. 1999)

A second technique, nuclear magnetic resonance (NMR), has been particularly useful to determine protein dynamics since it does not require crystallization: it is based on the effect of a magnetic field on atom behavior, which is influenced by the presence of other neighboring atoms. (Marion 2013) Although normally restricted to proteins in solution smaller than 30-40 kDa and requiring large amounts of soluble protein, NMR has been applied with great success to monitor intermolecular interactions, including drug-target and transient protein-protein interactions. (Pellecchia et al. 2008) (Liu et al. 2016)

In addition, recent advances have resulted in cryo-electron microscopy becoming the method of choice to study membrane protein structures, as it is able to derive high-resolution structural information from two-dimensional crystals of proteins inserted in a phospholipid bilayer. (Goldie et al. 2014) Mass spectrometry (MS) has also emerged as a powerful tool to characterize secondary protein structures: techniques such as ion mobility MS or hydrogen/deuterium exchange MS are nowadays able to detect structural differences or probe protein-ligand interactions. (Chalmers et al. 2006) (Leurs et al. 2015) The increasing number of three-dimensional structures

described through these means has also resulted in more accurate protein structure prediction, using homology modeling to initiate structure-based studies in molecules for which no experimental data is yet available. (Schmidt et al. 2014)

The study of protein function, on the other hand, relies on molecular biology tools: site-directed mutagenesis has been extensively used to study the role of specific protein residues in protein function, as the importance of the mutated residues can be determined by comparing the biological function of the native and mutant variants. (Morrison & Weiss 2001) Domain shuffling among related proteins with differing functions can also be very informative, as the biological activities of the chimeric proteins thus created offer critical insight into the structural determinants influencing protein function. (Lafuse 1991) In this way, studies on protein structure and function are closely interrelated: the availability of structural information permits restricting the design of mutant protein variants to putative active sites or interacting regions, while the mutants thus created can confirm and add to the information offered by structural models. (Wildhagen et al. 2011) The application of these different methods has resulted in a deeper understanding of protein-protein interactions, such as those taking place between ligands (e.g. cytokines) and their specific receptors. (Newell et al. 2000)

1.2. The interleukin-6 family of cytokines

Cytokines are a broad category of small intercellular signaling peptides, usually with a molecular weight between 8-30 kDa. (Cannon 2000) Cytokines exert their actions by binding to and activating specific receptors located in the surface of their target cells, in a similar way to classic protein hormones. (Kishimoto et al. 1994) However, in contrast to hormones cytokines are mostly absent in the circulation and their concentrations only increase drastically in response to trauma or infection; in addition, cytokines can be produced by virtually all nucleated cells, while classic hormones are secreted from discrete glands such as the adrenal gland or the pancreas. (Cannon 2000)

Cytokines can be subdivided into different groups based on the presence of shared structural elements in their receptors. (Schwartz et al. 2016) One of the main cytokine classes is the interleukin-6 (IL-6) family, named after its first identified member, IL-6: a pleiotropic cytokine acting via the glycoprotein 130 (gp130) receptor. (Hirano et al. 1985) (Hirano et al. 1986) (Taga et al. 1989) (Hibi et al. 1990) In the following years other cytokines have been added to the IL-6 class, which nowadays comprises ten different members: these are IL-6, interleukin-11 (IL-11), interleukin-27 (IL-27), interleukin-31 (IL-31), leukemia inhibitory factor (LIF), oncostatin M (OSM), ciliary neurotrophic factor (CNTF), cardiotrophin-1 (CT-1),

cardiotrophin-like cytokine (CLC) and neuropoietin (NP). (Ip et al. 1992) (Gearing et al. 1992) (Yin et al. 1993) (Pennica et al. 1995) (Elson et al. 2000) (Pflanz et al. 2004) (Derouet et al. 2004) (Dillon et al. 2004)

The different members of the IL-6 family present very little sequence homology, although they all adopt a common secondary structure: all of them form a four-helical bundle with an up-up-down-down topology, linked by loops. (Bazan 1990) (Robinson et al. 1994) (McDonald et al. 1995) (Somers et al. 1997) (Deller et al. 2000) Besides these similarities in their secondary structure, all of these cytokines recruit gp130 in their signaling receptor complexes: the only exception is IL-31, which replaces gp130 with the IL-31 receptor alpha (IL-31RA), a markedly similar receptor originally described as a gp130-like cytokine receptor. (Dreuw et al. 2004)

In addition to gp130 there are other signaling receptors interacting with the IL-6 class ligands: these include the LIF receptor (LIFR), OSM receptor (OSMR), IL-27 receptor subunit alpha (IL-27RA) and IL-31RA. (Gearing et al. 1991) (Mosley et al. 1996) (Pflanz et al. 2002) (Diveu et al. 2003) IL-6 family cytokines exert their actions through signaling receptor dimers, with IL-6 and IL-11 activating a gp130 homodimer and most other members (LIF, CNTF, CLC, CT-1, NP and OSM) being able to signal via a LIFR/gp130 heterodimer. (Murakami et al. 1993) (Yin et al. 1993) (Gearing et al. 1992) (Davis, Aldrich, Stahl, et al. 1993) (Pennica et al. 1995) (Elson et al. 2000) (Derouet et al. 2004) Additionally, OSM has the exceptional ability within the family of being able to recruit a second receptor complex, comprised of an OSMR/gp130 heterodimer. (Mosley et al. 1996) IL-27 activates an IL27-RA/gp130 dimer, while IL-31 utilizes an OSMR/IL31-RA complex. (Pflanz et al. 2004) (Dillon et al. 2004)

In some cases the activation of these signaling receptor complexes requires the participation of non-signaling receptors, which include the IL-6 receptor (IL-6R) for IL-6, the IL-11 receptor alpha (IL-11RA) for IL-11, the Epstein-Barr virus induced 3 (EBI3) for IL-27 and the CNTF receptor (CNTFR) for CNTF, CLC and NP. (Taga et al. 1989) (Baumann et al. 1996) (Devergne et al. 1997) (Davis, Aldrich, Ip, et al. 1993) (Elson et al. 2000) (Derouet et al. 2004) Although not directly involved in intracellular signaling, the aforementioned cytokines are unable to efficiently recruit their signaling receptors unless they are first bound to their non-signaling receptor. (Davis, Aldrich, Ip, et al. 1993) (Stahl et al. 1993) (Nandurkar et al. 1996) The different existing IL-6 type ligand-receptor interactions have been summarized in Figure 1.

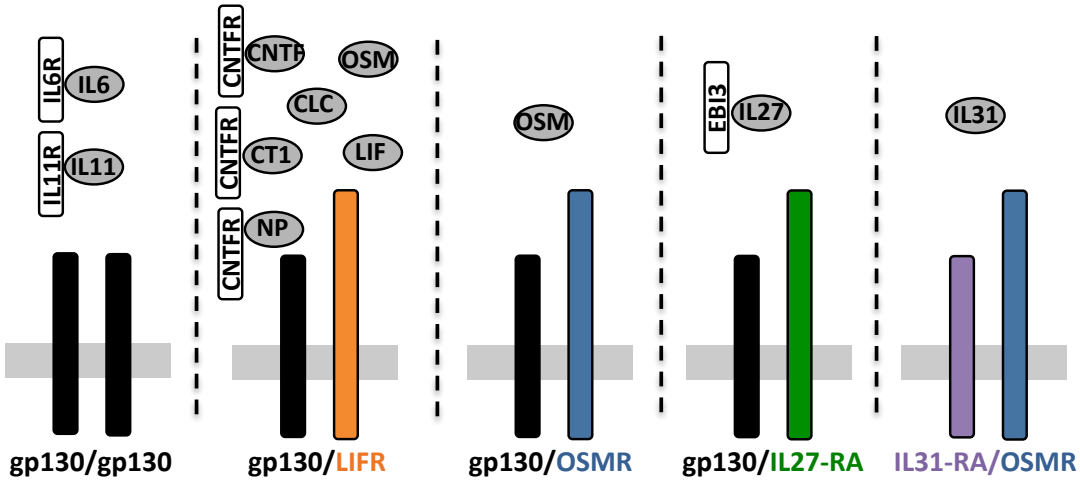

Figure 1: Cytokine-receptor interactions within the IL-6 cytokine family. IL-6 cytokines signal through several different signaling receptor complexes: IL-6 and IL-11 employ a gp130/gp130 homodimer, with LIF, CNTF, CLC, CT-1, NP and OSM binding to a LIFR/gp130 heterodimer. OSM can also use the OSMR/gp130 complex, while IL-27 utilizes the IL27-RA/gp130 complex and IL-31 binds to OSMR/IL-31RA. In some cases non-signaling receptors are required for the cytokine to be able to recruit the signaling complex: these are IL-6R (for IL-6), IL-11RA (for IL-11), EBI3 (for IL-27) and CNTFR (for CNTF, CLC and NP).

1.3. Biological relevance of oncostatin M

OSM is the only IL-6 type cytokine able to activate two different signaling complexes with high affinity (LIFR/gp130 and OSMR/gp130), so it should come as no surprise that this cytokine influences a wide array of biological processes. (Thoma et al. 1994) (Hermanns 2015) It appears to be of particular importance in the liver, where the role of OSM has been very well characterized: one of its functions is the regulation of cholesterol metabolism through the modulation of the levels of low-density lipoprotein (LDL) receptors in liver cells. (Grove et al. 1991) This cytokine can also promote hepatocyte proliferation through activation of the OSMR, a process that is particularly important in liver regeneration after injury and in the expansion and maintenance of primary hepatocyte cultures in vitro. (Nakamura et al. 2004) (Levy et al. 2015) Additionally, it is also able to regulate the acute phase protein response of hepatocytes during inflammatory processes. (Richards et al. 1992) (Wang et al. 2000)

OSM has also been shown to be an important modulator of hematopoiesis, stimulating both the hematopoietic progenitor cells directly as well as the stromal cells influencing the hematopoietic microenvironment. (Tanaka et al. 2003) Several other studies have documented the influence of OSM in other physiological processes such as cartilage catabolism, adipogenesis inhibition, bone remodeling or

central nervous system development. (de Hooge et al. 2003) (Miyaoka et al. 2006) (Guihard et al. 2012) (Morikawa et al. 2004)

However, given that the main sources of OSM in the organism are thought to be immune cells such as monocytes, macrophages, dendritic cells and neutrophils, the importance of this cytokine appears to be magnified in the context of different pathological conditions (Zarling et al. 1986) (Malik et al. 1989) (Grenier et al. 1999) (Suda et al. 2002) This cytokine was originally described as an inhibitor of proliferation of several cancer cell lines, but this antitumorigenic effect is not universal: the opposite effect has been reported for other cancer cells lines, and most recently *in vivo* in a murine model of glioblastoma. (Zarling et al. 1986) (Horn et al. 1990) (Jahani-Asl et al. 2016)

Its influence in inflammatory joint diseases such as rheumatoid arthritis has been studied in depth: the evidence collected so far suggests that OSM is able to induce maximal responses to other inflammatory cytokines in arthritis, promoting joint destruction. (Hui et al. 2005) (Richards 2013) This proinflammatory effect is also apparent in other chronic inflammatory diseases, such as allergen-induced airway inflammation in the lung, inflammatory skin lesions, inflammatory bowel disease, atherosclerosis or dilated cardiomyopathy. (O'Hara et al. 2003) (Boniface et al. 2007) (Guilloteau et al. 2010) (Hui et al. 2005) (West et al. 2017) (Albasanz-Puig et al. 2011) (Pöling et al. 2014)

Conversely, activation of OSM signaling has been linked to beneficial effects in other preclinical disease models: in the heart OSM stimulation leads to cardiomyocyte dedifferentiation and functional recovery after myocardial infarction, while OSMR/gp130 activation is crucial for the necessary recruitment of macrophages at the site of infarction that leads to cardiac healing. (Kubin et al. 2011) (Lörchner et al. 2015) Activation of the OSMR/gp130 complex has also been linked with protective effects in *in vivo* models of ischemic stroke, spinal cord injury, obesity-induced hepatic insulin resistance and steatosis (Guo et al. 2015) (Slaets et al. 2014) (Luo et al. 2016) The main biological actions of OSM are illustrated in Figure 2.

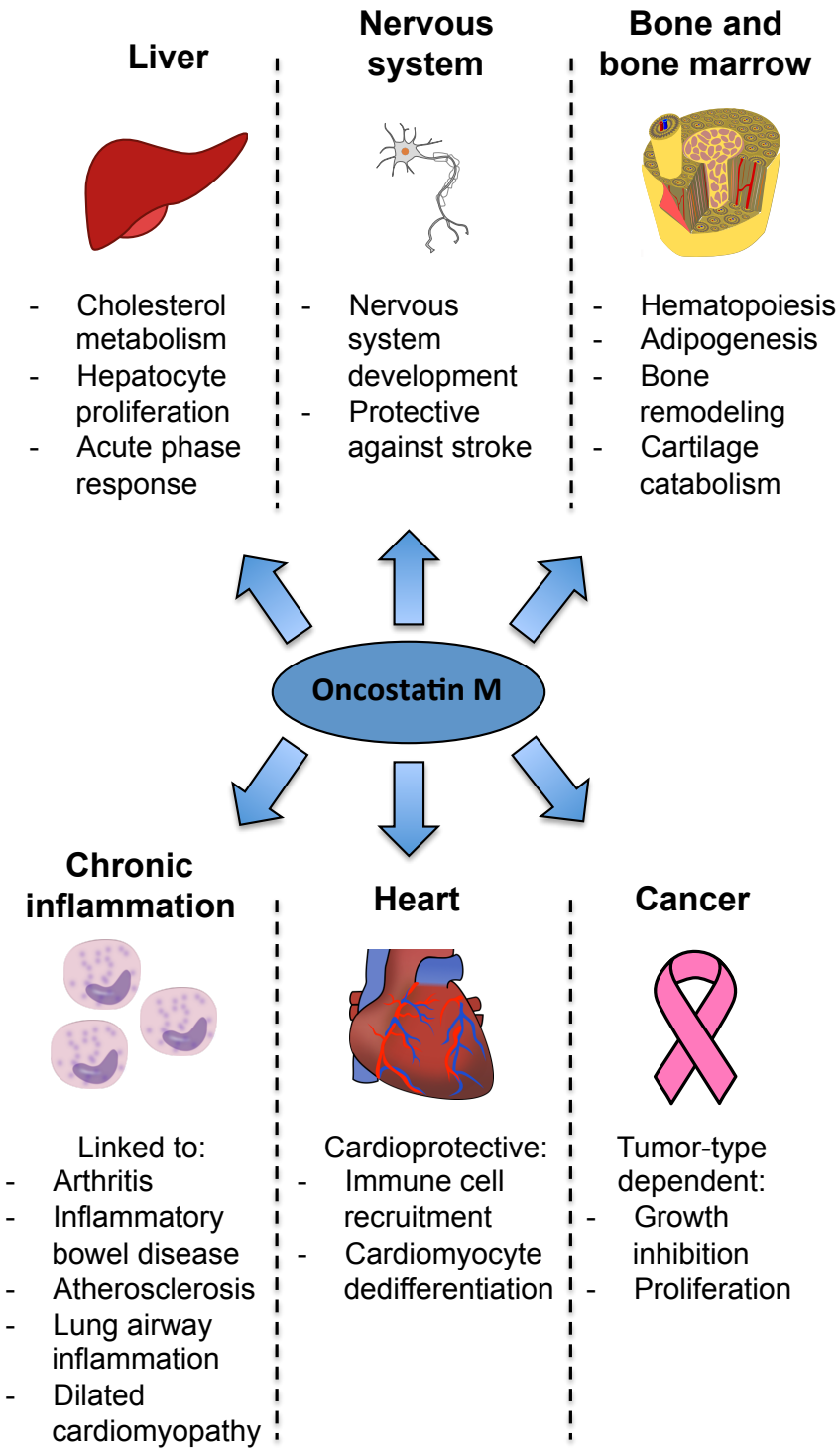

Figure 2: Main biological activities of OSM. OSM influences a wide array of biological processes in physiological conditions, particularly in the liver, the central nervous system and the bone marrow. In addition, it can also influence several pathological situations, such as different chronic inflammatory diseases, acute myocardial injury and cancer. Detailed explanations of these processes and references can be found in the main text. All images were obtained under an unlimited use license from Openclipart (www.openclipart.org).

1.4. Oncostatin M cytokine-receptor interactions and intracellular signaling

OSM cytokine-receptor interaction roughly follows the general paradigm for helical cytokines and the extracellular domain of its receptor complexes, first described for growth hormone 25 years ago. (de Vos et al. 1992) OSM has two distinct receptor binding sites: site II is formed by the residues in the middle of helices A and C, while site III encompasses the N-terminal parts of the AB loop and the D-helix as well as the BC loop. (Deller et al. 2000) Other members of the IL-6 class share this binding site arrangement, such as LIF, which is the closest to OSM in structural terms. (Rose & Bruce 1991) (Hudson et al. 1996)

In order to initiate signaling OSM binds first to gp130 through site II, after which a second signaling receptor (LIFR or OSMR) is recruited via site III. (Mosley et al. 1996) Ligand-receptor interaction through site III in both LIF and OSM is dependent on a conserved FXXK binding motif located in the N-terminal region of the D-helix of the cytokines. (Hudson et al. 1996) (Deller et al. 2000) However, the key features enabling OSM alone to interact with the OSMR/gp130 complex remain unknown so far: the most distinctive structural feature of OSM is an extended loop between helices B and C, but a previous study found that deletions in this region did not impair OSMR recruitment. (Chollangi et al. 2012) The three-dimensional structures of both OSM and LIF are represented in Figure 3.

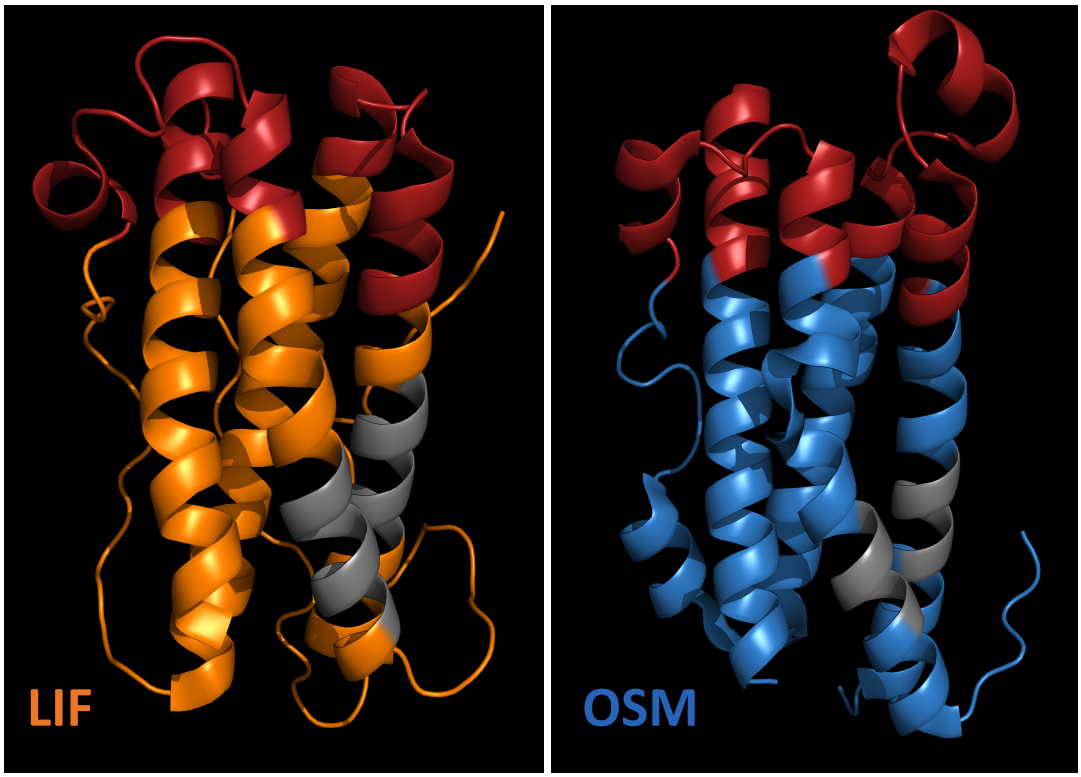

Figure 3: Secondary structure and receptor binding site locations of OSM and LIF. The three-dimensional structures of LIF (in orange**)** and OSM (in blue) are depicted, with its receptor binding sites highlighted. The common region binding to gp130 in LIF and OSM (site II), formed by amino acids in helices A and C, is shown in grey. The binding site for LIFR in LIF and for OSMR/LIFR in OSM, comprising residues in the N-terminal AB loop, the BC loop and the N-terminal D-helix regions, is marked in red.

After binding to the ligand the receptors within the signaling complex undergo conformational changes, causing their cytoplasmic regions to become closer: this allows tyrosine kinases of the Janus kinase family (JAK) such as JAK1, JAK2 and TYK2, which are found in association with the membrane-proximal region of these receptors, to phosphorylate each other and initiate signal transduction. (Lütticken et al. 1994) (Stahl et al. 1994) (Hermanns et al. 1999) (Radtke et al. 2002) The involvement of other types of kinases, such as Src and Tec family kinases, has also been reported in the past. (Heinrich et al. 1998) (Heinrich et al. 2003)

Signal transducer and activator of transcription (STAT) family proteins also play a central role in IL-6 type cytokine signaling: STATs are recruited to either phosphorylated receptor tyrosine motifs or to the JAKs and become phosphorylated themselves, leading to dimer formation and accumulation in the cell nucleus, where they act as transcription factors to modulate gene expression. (Shuai et al. 1993) (Shuai et al. 1994) Phosphorylation of STAT3 and STAT1 has been reported after receptor complex binding for all family members, while STAT5 and STAT6 are phosphorylated specifically by activation of the OSMR. (Lütticken et al. 1994) (Sadowski et al. 1993) (Wang et al. 2000) (Fritz et al. 2006)

Besides the JAK/STAT signaling pathway just described, IL-6 type cytokines also initiate other signaling cascades, such as the one comprised by the Ras-Raf-mitogen-activated protein kinases (MAPKs). (Schiemann et al. 1997) (Hermanns et al. 2000) Among the MAPKs activated by the IL-6 cytokines are ERK1/2, known to be involved in maintenance of cell survival, but also stress-activated members of the MAPK family such as p38 or c-Jun N-terminal kinase (JNK). (Wang et al. 2000) (Zauberman et al. 1999) The third main signaling pathway activated by these receptor complexes is the one mediated by the proteins phosphoinositide 3-kinase/protein kinase B (PI3K/Akt), also associated with cell survival. (Negoro et al. 2001) Moreover, the OSMR exhibits the ability to signal through additional pathways, such as the one mediated by PI3K and the protein kinase C delta, that drive some of its unique actions. (Smyth et al. 2006) (Underhill-Day & Heath 2006) The main signaling components driving OSM responses are represented in figure 4.

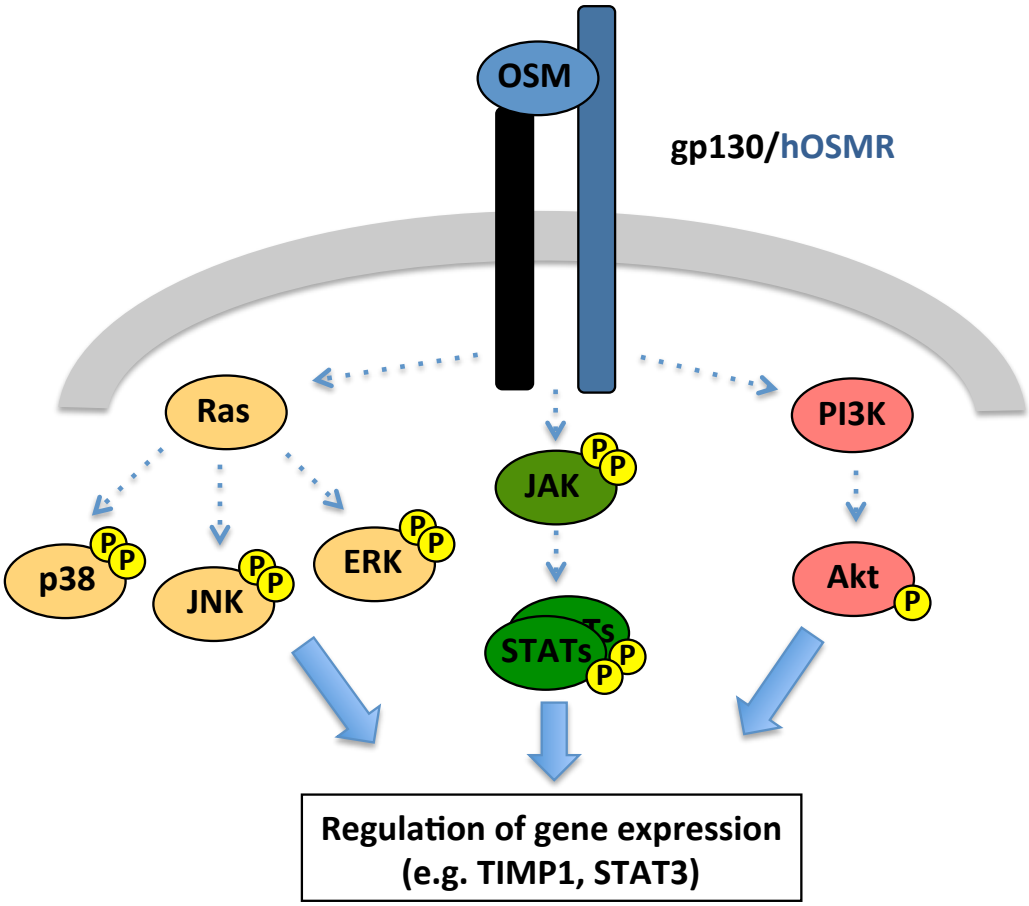

Figure 4: Main signaling pathways activated by OSM. Following binding of OSM, the OSMR is able to initiate an array of signaling events involving phosphorylation (P) of different signaling mediators. The three main cascades modulating gene expression in response to OSM are the JAK/STAT, Ras/Raf/MAPK (including ERK1/2, JNK and p38) and PI3K/Akt pathways.

Although all these signaling cascades contribute to mediate OSMR activity, in most of the biological functions reported so far STAT3 phosphorylation appears to play a crucial role. As an example, STAT3 is necessary for hematopoiesis, with a dominant negative form of STAT3 suppressing this process during mouse development. (Takizawa et al. 2003) In the heart STAT3 is required for cardioprotection against ischemic injury, being responsible for the OSM-regulated secretion of chemokines that leads to cardiac healing after myocardial infarction. (Hilfiker-Kleiner et al. 2004) (Lörchner et al. 2015) Liver regeneration after injury is also dependent on STAT3 activation, and as a result is impaired in mice lacking the OSMR. (Li et al. 2002) (Nakamura et al. 2004) Moreover, STAT3 is also involved in the progression of chronic inflammatory diseases mediated by OSM such as atherosclerosis, which is alleviated by reduced STAT3 levels. (Zhang et al. 2017) The importance of STAT3 for OSM-derived signaling is further reflected in the fact that, while all IL-6 class cytokines lead to downstream STAT3 activation, OSM shows the strongest effect on

STAT3 in stimulation experiments with a variety of cell types. (Chattopadhyay et al. 2007)

1.5. Oncostatin M species-specific receptor activation profile

A crucial particularity of OSM is the species-dependent receptor activation ability it displays: as stated before, human OSM (hOSM) is able to activate both human LIFR/gp130 (hLIFR) and human OSMR/gp130 (hOSMR). (Mosley et al. 1996) On the other hand its murine ortholog appears to signal through the murine OSMR/gp130 (mOSMR) complex almost exclusively, although minor mouse LIFR/gp130 (mLIFR) activation has recently been reported in the context of bone remodeling. (Ichihara et al. 1997) (Lindberg et al. 1998) (Walker et al. 2016)

To make matters more complex the human cytokine is unable to bind to the murine OSMR/gp130 (mOSMR), and in turn mouse OSM (mOSM) cannot activate either of the human receptor complexes. (Lindberg et al. 1998) (Drechsler et al. 2012) The species-specific receptor activation abilities of each ortholog are schematically represented in Figure 5.

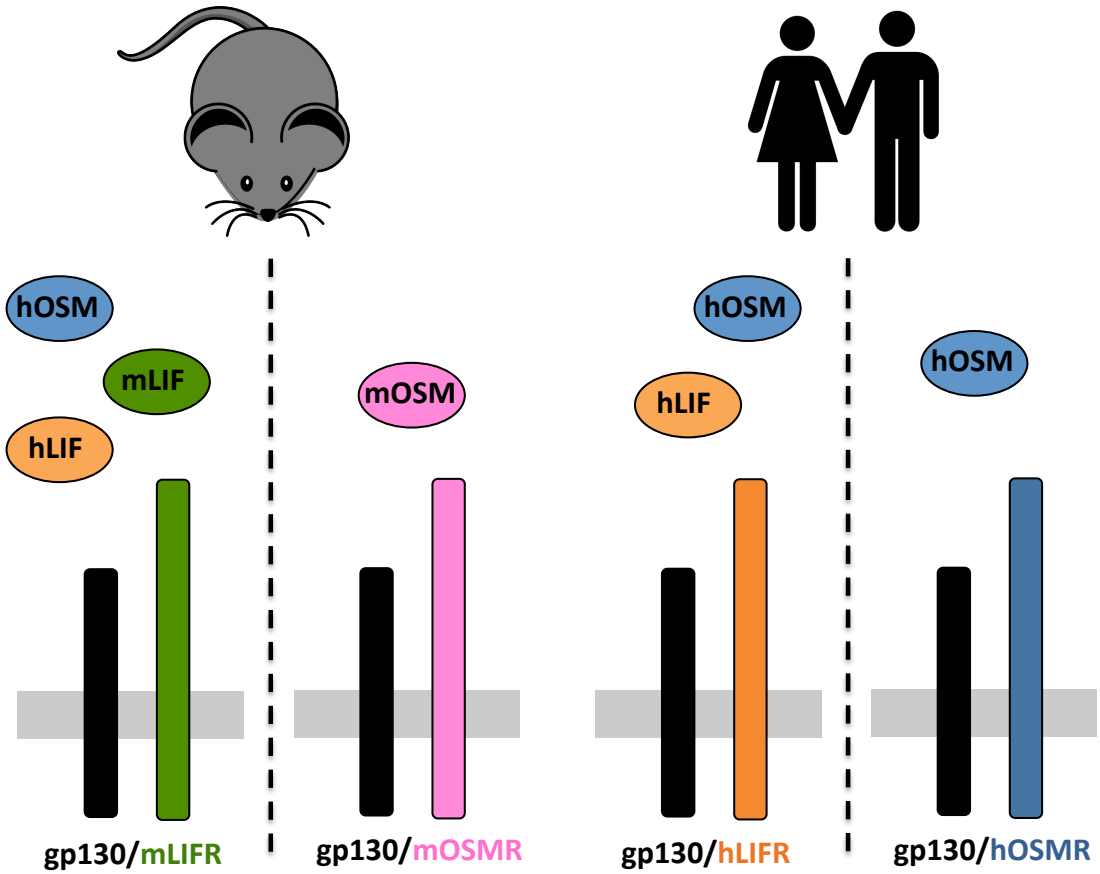

Figure 5: OSM displays species-specific receptor activation abilities. The receptor activation abilities for the human and murine OSM orthologs are shown: mOSM is specific to the mOSMR, while neither of the murine cytokines can bind to the human receptors. On the other hand, hOSM is promiscuous for hLIFR and hOSMR, and both human molecules are able to activate the mLIFR but not the mOSMR.

This difference in behavior is especially problematic given the widespread usage of mouse models in the investigation of OSM functions: unlike rats, mice do not reflect the full physiological response that hOSM would have in humans. (Drechsler et al. 2012) The underlying molecular mechanisms behind this characteristic, however, remain unexplained to date.

2. Goals of the Study

Multiple studies have described the central role of OSM in a variety of physiological and pathological situations, as well as its potential therapeutic applications. These actions are a consequence of OSM recognizing and binding to specific surface receptor complexes, in particular the one formed by OSMR and gp130, which leads to the initiation of downstream signaling events and subsequent changes in gene expression.

However, despite its biological relevance, very little detailed knowledge regarding the interaction between OSM and its receptors is available to date. In contrast to other IL-6 family cytokines, no co-crystal structures involving OSM and either of its receptor complex members have been reported so far. Furthermore, only OSM binding to gp130 has been examined in detail using molecular biology techniques: consequently, the structural features differentiating OSM from other members of the IL-6 family are still unknown.

In addition, the differing receptor specificity between human and mouse OSM also remains unexplained: while hOSM can activate both hOSMR and hLIFR complexes, mOSM is specific for the mOSMR. This is particularly concerning in view of the potential therapeutic applications of OSM, since as of now the results obtained in preclinical murine models cannot be directly translated to the human situation.

In light of these facts, this work had two clearly defined goals: the first of these was to investigate the critical features in hOSM enabling signaling through the specific hOSMR complex, focusing on the comparison with the closely related hLIF to identify exclusive hOSM traits. This could be done through the expression and purification of recombinant cytokines, the identification of specific readout systems for the hOSMR and hLIFR and the generation of mutant hOSM variants. The second goal involved mapping the molecular determinants responsible for the existing divergence in receptor activation profiles between hOSM and mOSM by employing the same techniques, as well as assessing the feasibility of modifying their receptor specificity to improve the translatability of future studies in murine models.

3. Materials and Methods

3.1. Materials

3.1.1. Laboratory equipment

Equipment	Manufacturer
Pipetting equipment	
HandyStep® electronic repeating pipette	BrandTech®
Pipet-Aid® XP	Drummond Scientific®
Pipet-Lite pipettes	Rainin®
Centrifuges	
Galaxy Mini centrifuge	VWR®
Heraeus™ Fresco™ 21	ThermoFisher Scientific™
Heraeus™ Multifuge™ 1 L	ThermoFisher Scientific™
Heraeus™ Multifuge™ 3S-R	ThermoFisher Scientific™
Heraeus™ Biofuge™ Stratos™	ThermoFisher Scientific™
Sorvall® Evolution™ RC superspeed centrifuge	ThermoFisher Scientific™
Mammalian cell culture equipment	
MaxQ 2000 CO_2 Plus digital CO_2 resistant shaker	ThermoFisher Scientific™
Heracell™ 150 CO_2 incubator	ThermoFisher Scientific™
Herasafe™ KS (NSF) Class II, Type A2 Biological Safety Cabinet	ThermoFisher Scientific™
Leica DMi1 inverted microscope	Leica Microsystems®
Neubauer cell counting chamber	Optik Labor®
Molecular cloning equipment	
Heraeus™ microbiological incubator	ThermoFisher Scientific™
Horizontal electrophoresis chambers	Peqlab®
Labcycler thermocycler	Sensoquest®
NanoDrop 2000c UV-Vis spectrophotometer	ThermoFisher Scientific™
New Brunswick™ Innova® 44 incubator shaker	Eppendorf®
UV transilluminator	INTAS Science Imaging Instruments®
Protein electrophoresis and detection	
ChemiDoc™ MP System	Bio-Rad®
Consort EV261 electrophoresis power supply	Sigma-Aldrich®

FLUOstar® Galaxy microplate reader	BMG Labtech®
Odyssey® 9120 imaging system	LI-COR Biosciences®
Sonopuls® HD 2070 ultrasonic homogenizer	Bandelin®
XCell SureLock™ Mini-Cells	Novex™
XCell II™ Blot Modules	Novex™
Assorted laboratory equipment	
Assistent RM5 rotating mixer	Karl Hecht®
BioPhotometer 6131 spectrophotometer	Eppendorf®
Borosilicate flasks and bottles	SCHOTT DURAN®
Dewar Carrying Flask	KGW-Isotherm®
Discovery DV-215CDM analytical balance	Ohaus®
Fridge and -20ºC freezers	Liebherr®
GFL®-3006 laboratory shaker	Gesellschaft für Labortechnik®
HERAfreeze™ HFC Series -86°C Ultra-Low Temperature Chest Freezer	ThermoFisher Scientific™
IKAMAG™ RCT hot plate magnetic stirrer	IKA®
Milli-Q® Integral Water Purification System	Merck Millipore®
pH 211 precision pH meter and HI 1144 Tris buffer pH electrode	Hanna Instruments®
R-202 microwave oven	Sharp®
Rocky® RT-1S rocking platform	Uniequip®
Scotsman AF103 ice flaker	Scotsman® Ice Systems
Stuart™ SB2 tube rotator	Bibby Scientific®
Thermomixer comfort	Eppendorf®
Vortex-Genie 2	Scientific Industries®

3.1.2. Consumables

Consumables	**Manufacturer**
Tubes and flasks	
1 mL CryoTube™ vials	Nunc™
1.5 and 2 mL polypropylene tubes	Eppendorf®
12 mL polypropylene two-position cap tubes	Greiner Bio-One®
15 and 50 mL Cellstar® polypropylene tubes	Greiner Bio-One®
PCR 8er SoftStrips 0.2 mL	Biozym®
Polycarbonate 125 and 250 mL	Corning®

Erlenmeyer cell culture flasks	
Pipettes and tips	
Cellstar® serological pipettes	Greiner Bio-One®
Combitips® Plus electronic pipette tips	Eppendorf®
Disposable pipette tips	Greiner Bio-One®
Fisherbrand™ SureOne™ filter tips	ThermoFisher Scientific™
Dishes and plates	
6-well and 96-well Cellstar® cell culture plates	Greiner Bio-One®
10 cm Cellstar® cell culture dishes	Greiner Bio-One®
10 cm Petri dishes	Greiner Bio-One®
96-well flat bottom microplates	Greiner Bio-One®
Others	
1 mL Omnifix®-R single-use syringes	B. Braun®
Cell scraper 25cm	Sarstedt®
Disposable 10 µL inoculation loops	Roth®
Filtropur S 0.2 syringe filter	Sarstedt®
Mr. Frosty™ Freezing Container	ThermoFisher Scientific™
Parafilm M® All-Purpose laboratory film	Bemis®
Semi-micro cuvette, polystyrene	Sarstedt®
Surgical disposable scalpels	B. Braun®

3.1.3. Chemical reagents

Reagent	Catalog Number	Manufacturer
Acetic acid	3738	Roth®
Ammonium persulfate	A3678	Sigma-Aldrich®
Ampicillin sodium salt	K029	Roth®
Aprotinin	10820	Sigma-Aldrich®
Aqua B. Braun	0082479E	B. Braun®
Benzamidine, hydrochloride	199001	Merck Millipore®
Bicine	B3876	Sigma-Aldrich®
Bis-Tris	A1025	Applichem®
Bromophenol blue	108122	Merck Millipore®
Calcium chloride ($CaCl_2$)	102382	Merck Millipore®
Chloroform	6340	Roth®
D(+)-glucose	X997	Roth®
DEPC	K028	Roth®
Dimethyl sulfoxide (DMSO)	D4540	Sigma-Aldrich®
dNTP set (100 mM)	10297018	Invitrogen™

DTT (1,4-Dithiothreitol)	6908	Roth®
EDTA	1610729	Bio-Rad®
Ethanol ROTIPURAN® ≥ 99.8% purity	9065	Roth®
Ethidium bromide solution 1 % *BioChemica*	A1152	Applichem®
Glycerin ≥ 86% purity	7533	Roth®
Hydrochloric acid fuming 37% (HCl)	4625	Roth®
Imidazole	3899	Roth®
IPTG	2316	Sigma-Aldrich®
Isopropanol ROTIPURAN® ≥ 99.8% purity	6752	Roth®
Kanamycin sulphate	T832	Roth®
Leupeptin	L2884	Sigma-Aldrich®
Magnesium chloride ($MgCl_2$) hexahydrate	2189	Roth®
Magnesium sulfate ($MgSO_4$)	105886	Merck Millipore®
Methanol ROTIPURAN® ≥ 99.9% purity	4627	Roth®
Phenylmethylsulfonylfluorid (PMSF)	6367	Roth®
Polyethylene glycol 6000 (PEG-6000)	81260	Sigma-Aldrich®
Potassium acetate	T874	Roth®
Potassium chloride (KCl)	104933	Merck Millipore®
Potassium phosphate monobasic (KH_2PO_4)	104873	Merck Millipore®
Random Primers	C1181	Promega®
RNasin® Plus RNase Inhibitor	N2611	Promega®
Rotiphorese® Gel 40 (29:1 acrylamide/bisacrylamide)	A515	Roth®
Sodium dodecyl sulfate (SDS) ultra pure ≥ 99.5%	2326	Roth®
Sodium chloride (NaCl)	3957	Merck Millipore®
Sodium fluoride (NaF)	201154	Sigma-Aldrich®
Sodium hydroxide (NaOH)	106498	Merck Millipore®
Sodium orthovanadate (Na_3VO_4)	S6508	Sigma-Aldrich®

Sodium phosphate dibasic (Na_2HPO_4)	4984	Roth®
TEMED	2367	Roth®
TriFast™	30-2010	Peqlab®
Tris	5429	Roth®
Tween® 20	9127	Roth®
Urea	U5378	Sigma-Aldrich®

3.1.4. Ladders and enzymes

Reagent	Catalog Number	Manufacturer
Ladders		
GeneRuler 1 kb DNA ladder	SM0312	ThermoFisher Scientific™
GeneRuler 100 bp DNA ladder	SM0241	ThermoFisher Scientific™
Protein Marker VI (10 - 245) prestained	A8889	AppliChem®
Enzymes		
AscI restriction enzyme	R0558	New England Biolabs®
DNAse I	10104159001	Roche®
DpnI restriction enzyme	R0176	New England Biolabs®
EcoRI restriction enzyme	EN-114	Jena Bioscience®
HindIII restriction enzyme	EN-116	Jena Bioscience®
Lysozyme from chicken egg white	62970	Sigma-Aldrich®
NdeI restriction enzyme	R0111	New England Biolabs®
PacI restriction enzyme	R0547	New England Biolabs®
PfuUltra High Fidelity DNA Polymerase	600380	Agilent®
Phusion Hot Start II DNA Polymerase (2 U/µL)	F-549S	ThermoFisher Scientific™
RNAse A	10109142001	Roche®
RQ1 RNAse-free DNase	M6101	Promega®
SlaI restriction enzyme	EN-134	Jena Bioscience®
SuperScript® II Reverse Transcriptase	18064014	Invitrogen™
T4 DNA ligase	M1804	Promega®
XbaI restriction enzyme	EN-143	Jena Bioscience®

3.1.5. Cell lines, cell culture mediums and reagents

Reagent	Catalog Number	Manufacturer
Mammalian cell lines		
A375 cell line (human malignant melanoma)	88113005	European Collection of Authenticated Cell Cultures (ECACC)
FreeStyle™ 293-F (HEK293 cells adapted to high density, serum-free, suspension growth)	R79007	ThermoFisher Scientific™
HepG2 cell line (human hepatocellular carcinoma)	-	Gift of Dr. Sarah Tonack
JAR cell line (human choriocarcinoma)	ATCC® HTB-144™	American Type Culture Collection (ATCC®)
MH-S cell line (murine monocyte)	-	Gift of Dr. Holger Lörchner
NIH3T3 cell line (murine fibroblast)	-	Gift of Dr. Praveen Gajawada
NIH3T3 cell line (murine fibroblast) stably transfected with empty vector	-	Gift of Dr. Krishnamoorthy Sreenivasan
NIH3T3 cell line (murine fibroblast) stably transfected with anti-mouse LIFR shRNA	-	Gift of Dr. Krishnamoorthy Sreenivasan
Cell culture mediums		
Dulbecco's modified Eagle medium (DMEM) with 4500 mg/L glucose, L-glutamine and sodium bicarbonate	D5796	Sigma-Aldrich®
DMEM with high glucose, HEPES and no phenol red	21063029	Gibco™
DMEM/F-12 with GlutaMAX™ supplement	31331028	Gibco™
FreeStyle™ 293 expression medium	12338001	Gibco™
Opti-MEM® I reduced	31985062	Gibco™

serum medium		
OptiPRO™ SFM	12309019	Gibco™
Roswell Park Memorial Institute (RPMI) 1640 medium with L-glutamine	21875034	Gibco™
Reagents and kits		
Anti-clumping agent	0010057AE	Gibco™
Fetal bovine serum (FBS)	F7524	Sigma-Aldrich®
FreeStyle™ MAX reagent	16447100	Invitrogen™
Lipofectamine® RNAiMAX transfection reagent	13778030	Invitrogen™
Penicillin-streptomycin solution	P4333	Sigma-Aldrich®
Trypsin-EDTA solution 10x (sterile-filtered)	59418C	Sigma-Aldrich®
Vybrant® MTT cell proliferation assay kit	V13154	ThermoFisher Scientific™

3.1.6. Antibodies, recombinant proteins and siRNAs

Reagent	Catalog Number	Manufacturer
Antibodies		
His-Tag (monoclonal mouse Penta-His antibody, BSA-free)	34660	Qiagen®
Goat IgG Horseradish Peroxidase-conjugated antibody	HAF109	R&D Systems®
LIFR alpha antibody (human)	AF-249-NA	R&D Systems®
Mouse IgG (H+L) Alexa Fluor® 680-conjugated	A21057	Invitrogen™
Mouse IgG Horseradish Peroxidase-conjugated antibody	HAF007	R&D Systems®
OSMR beta antibody (human)	AF4389	R&D Systems®
Pan-Actin	4968	Cell Signaling Technology®
Phospho-ERK1/2	9101	Cell Signaling

(Thr202/Tyr204)		Technology®
Phospho-SAP/JNK (Thr183/Tyr185)	9251	Cell Signaling Technology®
Phospho-STAT1 (Tyr701)	9171	Cell Signaling Technology®
Phospho-STAT3 (Tyr705)	9131	Cell Signaling Technology®
Rabbit IgG Horseradish Peroxidase-conjugated antibody	HAF008	R&D Systems®
STAT3 (124H6) mouse monoclonal	9139	Cell Signaling Technology®
TIMP1 (D10E6) rabbit monoclonal	8946	Cell Signaling Technology®
TIMP1 (mouse)	MAB9801	R&D Systems®
Recombinant proteins		
LIF Protein (human)	7734-LF/CF	R&D Systems®
Oncostatin M (OSM) Protein (human)	295-OM-010/CF	R&D Systems®
Oncostatin M (OSM) Protein (mouse)	495-MO-025/CF	R&D Systems®
siRNAs		
5x siRNA Buffer	B-002000-UB-100	Dharmacon®
ON-TARGETplus Non-targeting Control Pool	D-001810-10-05	Dharmacon®
SMARTpool: ON-TARGETplus LIFR siRNA	L-008017-01-0005	Dharmacon®
SMARTpool: ON-TARGETplus OSMR siRNA	L-008050-00-0005	Dharmacon®

3.1.7. Protein Electrophoresis and Detection

Reagent	Catalog Number	Manufacturer
Protein Electrophoresis		
Amersham™ Protran™ 0.45 µm NC nitrocellulose blotting membranes	10600002	GE Healthcare Life Sciences®
Bovine Serum Albumin solution	A7284	Sigma-Aldrich®
DC™ Protein Assay	5000112	Bio-Rad®

Empty Gel Cassettes, mini, 1.0 mm	NC2010	Novex™
NuPAGE™ 4-12% Bis-Tris Protein Gels, 1.0 mm, 17-well	NP0329BOX	Novex™
NuPAGE® 20xMES SDS Running Buffer	NP0002	Novex™
Protein standard for protein quantification	P0834	Sigma-Aldrich®
RedAlert™ 10x Western Blot Stain	71078	Merck Millipore®
Rotilabo®-Blotting Papers, Thickness 0.35 mm	CL66	Roth®
Skim milk powder	70166	Sigma-Aldrich®
Protein Detection		
SuperSignal™ West Femto Maximum Sensitivity Substrate	34095	ThermoFisher Scientific™
InstantBlue™ Coomassie® stain	ISB1L	Expedeon Protein Solutions®
SilverQuest™ Silver Staining Kit	LC6070	Novex™

3.1.8. Molecular cloning, recombinant protein expression and purification

Reagent	Catalog Number	Manufacturer
Molecular cloning		
Human Oncostatin M template vector	-	Gift of Dr. Heike Hermanns
LB Broth (Lennox)	X964	Roth®
LB Agar (Lennox)	X965	Roth®
LE agarose	840004	Biozym®
MGC Human LIF Sequence-Verified cDNA (CloneId: 7939578), glycerol stock	MHS6278-202857165	ThermoFisher Scientific™
NucleoBond® Xtra Maxi kit	740414	Macherey-Nagel®
NucleoSpin® Gel and PCR clean-up kit	740609	Macherey-Nagel®
pCAGGS vector with PacI and AscI restriction sites	-	Gift of Dr. André Schneider

pcDNA™ 3.1(+) vector	-	Gift of Dr. Natalie Al-Furoukh
pET-26b(+) vector	-	Gift of Dr. Natalie Al-Furoukh
pFLAG-CMV-3 vector	E6783	Sigma-Aldrich®
XL-1 Blue competent *E. coli*	-	Gift of Dr. Natalie Al-Furoukh
Recombinant protein expression and purification		
Amicon Ultra-4 10 kDa centrifugal filters	UFC801024	Merck Millipore®
BL21 (DE3) competent *E. coli*	-	Gift of Dr. Natalie Al-Furoukh
HIS-Select® HF nickel affinity gel	H0537	Sigma-Aldrich®
Polypropylene columns (5 ml)	34964	QIAGEN®
Protein Deglycosylation Mix	P6039S	New England Biolabs®
SHuffle® T7 Express competent *E. coli*	C3029H	New England Biolabs®

3.1.9. Primers

All primers were purchased from Sigma-Aldrich®	
Primer Name	**Sequence (5' -> 3')**
Cytokine cloning in pET-26b(+) vector	
NdeI hOSM fw	AAAGGGAAACATATGGCGGCTATAGGCAGCTGCTCGA
hOSM SlaI rev	TTTCCCTTTCTCGAGCCGGCTCCGGTTCGGGCTCTCC
NdeI hLIF fw	AAAGGGAAACATATGAGCCCCCTCCCCATCACCCCTG
hLIF SlaI rev	TTTCCCTTTCTCGAGGAAGGCCTGGGCCAACACGGCG
NdeI mOSM fw	AAAGGGAAACATATGAATCGTGGCTGCTCCAACTCT
mOSM SlaI rev	TTTCCCTTTCTCGAGTCTCCGGCTGCGTGTGGAGCCA
Cytokine cloning in pcDNA 3.1(+) vector	
EcoRI NatSP hOSM fw	AAAGGGAAAGAATTCGCACGGGCACCCAGCATGGGGGTACTGCTCACACAGAGGACG
EcoRI NativeSP hLIF fw	AAAGGGAAAGAATTCGAAGTGCAGCCCATAATGAAGGTCTTGGCGGCAGGAGTTGTG
EcoRI NativeSP mOSM fw	AAAGGGAAAGAATTCGTACCAGGACCCAGTATGCAGACACGGCTTCTAAGAACACTG
NdeI-EcoRI-Koz-PPT fw	AAAGGGAAACATATGGAATTCGCCACCATGTCTGCACTTCTGATCCT

PPT+hOSM fw	GGAGCTGCAGTTGCTGCGGCTATAGGCAGC
PPT+hOSM rev	GCTGCCTATAGCCGCAGCAACTGCAGCTCC
PPT+hLIF fw	GAGCTGCAGTTGCTAGCCCCCTCCCCATCA
PPT+hLIF rev	TGATGGGGAGGGGGCTAGCAACTGCAGCTC
PPT+mOSM fw	GGAGCTGCAGTTGCTAATCGTGGCTGCTCC
PPT+mOSM rev	GGAGCAGCCACGATTAGCAACTGCAGCTCC
Cytokine cloning in pFLAG-CMV-3 vector	
HindIII hOSM fw	AAAGGGAAAAAGCTTCCGGCTCCGGTTCGGGCTCTCCCCCCA
HindIII mOSM fw	AAAGGGAAAAAGCTTAATCGTGGCTGCTCCAACTCTTCCTCT
HindIII hLIF fw	AAAGGGAAAAAGCTTAGCCCCCTCCCCATCACCCCTGTCAAC
HisTag XbaI rev	TTTCCCTTTTCTAGAGTCTCAGTGGTGGTGGTGGTGGTGCTCGAG
Cytokine cloning in pCAGGS vector	
PacI hOSM fw	AAAGGGAAATTAATTAAGCTAGCGCATCGCCACCATGGGGGTACT GCTCACACAGAGGACG
SP+hOSM fw	CAAGCATGGCGAGCATGGCGGCTATAGGCAGCTG
SP+hOSM rev	CAGCTGCCTATAGCCGCCATGCTCGCCATGCTTG
PacI mOSM fw	AAAGGGAAATTAATTAAGCTAGCGCATCGCCACCATGCAGACACG GCTTCTAAGAACACTG
PacI hLIF fw	AAAGGGAAATTAATTAAGCTAGCGCATCGCCACCATGAAGGTCTT GGCGGCAGGAGTTGTG
SP+hLIF fw	GGAAACATGGGGCGGGGAGCCCCCTCCCCATCAC
SP+hLIF rev	GTGATGGGGAGGGGGCTCCCCGCCCCATGTTTCC
AscI HisTag rev	TTTCCCTTTGGCGCGCCGCGGCCGCTATCAGTGGTGGTGGTGGTG GTGCTCGAG
Human OSM - LIF chimeras	
hLIF AB Start fw	AATGCCCTCTTTATTCCCTATATACGTATC
hLIF AB Start rev	GATACGTATATAGGGAATAAAGAGGGCATT
hLIF AB End fw	CTGAGAGAGCACTGCGGCCCCAACGTGACG
hLIF AB End rev	CGTCACGTTGGGGCCGCAGTGCTCTCTCAG
hLIF AB2 fw	TTTATTCTCTATTACCGTATCCAAGGCCTG
hLIF AB2 rev	CAGGCCTTGGATACGGTAATAGAGAATAAA
hLIF AB3 fw	CTCTATTACACAGCCCAAGGCCTGGATGTT
hLIF AB3 rev	AACATCCAGGCCTTGGGCTGTGTAATAGAG
hLIF BC Start fw	AACATCACCCGGGACTTAGAGCAGCGCCTC
hLIF BC Start rev	GAGGCGCTGCTCTAAGTCCCGGGTGATGTT
hLIF BC End fw	GACTTGGAGAAGCTGAACGCCACCGCCGAC
hLIF BC End rev	GTCGGCGGTGGCGTTCAGCTTCTCCAAGTC
hLIF Dhelix rev	GCCCAGCTTCTTCTTCTGGAAGACATCCTTACCCGAGGTGGGGGTG GGCGG
hLIF Dhelix fw	TCGGGTAAGGATGTCTTCCAGAAGAAGAAGCTGGGCTGCAGGTTC

	CTGCAT
hOSM AB Start fw	AGCAGACTCCTGGACCTCTATTACACAGCC
hOSM AB Start rev	GGCTGTGTAATAGAGGTCCAGGAGTCTGCT
hOSM AB End fw	CTGGACAAGCTATGTAGGGAGCGCCCCGGG
hOSM AB End rev	CCCGGGGCGCTCCCTACATAGCTTGTCCAG
hOSM BC Start fw	CACAGACTGGCCGACCAGAAGATCCTCAAC
hOSM BC Start rev	GTTGAGGATCTTCTGGTCGGCCAGTCTGTG
hOSM BC End fw	CTCCACAGCAAGCTCCAGATGGCGAGGCCG
hOSM BC End rev	CGGCCTCGCCATCTGGAGCTTGCTGTGGAG
hOSM Dhelix rev	GCCCTCCAGCTTGCGCTGAAAAGCATCCGAGGCAGGGGTGTCAGG GCCGTA
hOSM Dhelix fw	CCTGCCTCGGATGCTTTTCAGCGCAAGCTGGAGGGCTGTCAACTCC TGGGG
Human OSM point mutants - AB loop	
hOSM P33A fw	CAGCAGACTCCTGGACGCCTATATACGTATCCA
hOSM P33A rev	TGGATACGTATATAGGCGTCCAGGAGTCTGCTG
hOSM Y34A fw	CTCCTGGACCCCGCTATACGTATCCAAGGCCTGGATG
hOSM Y34A rev	CATCCAGGCCTTGGATACGTATAGCGGGGTCCAGGAG
hOSM I35A fw	GACTCCTGGACCCCTATGCACGTATCCAAGGCCTGG
hOSM I35A rev	CCAGGCCTTGGATACGTGCATAGGGGTCCAGGAGTC
hOSM R36A fw	TCCTGGACCCCTATATAGCTATCCAAGGCCTGGATG
hOSM R36A rev	CATCCAGGCCTTGGATAGCTATATAGGGGTCCAGGA
hOSM I37A fw	CTGGACCCCTATATACGTGCCCAAGGCCTGGATGTTCC
hOSM I37A rev	GGAACATCCAGGCCTTGGGCACGTATATAGGGGTCCAG
hOSM Q38A fw	GGACCCCTATATACGTATCGCAGGCCTGGATGTTCCTAAA
hOSM Q38A rev	TTTAGGAACATCCAGGCCTGCGATACGTATATAGGGGTCC
hOSM G39A fw	CCTATATACGTATCCAAGCCCTGGATGTTCCTAAACT
hOSM G39A rev	AGTTTAGGAACATCCAGGGCTTGGATACGTATATAGG
hOSM L40A fw	CCTATATACGTATCCAAGGCGCGGATGTTCCTAAACTGAGAG
hOSM L40A rev	CTCTCAGTTTAGGAACATCCGCGCCTTGGATACGTATATAGG
hOSM D41A fw	CCAAGGCCTGGCTGTTCCTAAACTGAGAGAGCA
hOSM D41A rev	TGCTCTCTCAGTTTAGGAACAGCCAGGCCTTGG
hOSM V42A fw	TATCCAAGGCCTGGATGCTCCTAAACTGAGAGAGC
hOSM V42A rev	GCTCTCTCAGTTTAGGAGCATCCAGGCCTTGGATA
hOSM P43A fw	CCAAGGCCTGGATGTTGCTAAACTGAGAGAGCA
hOSM P43A rev	TGCTCTCTCAGTTTAGCAACATCCAGGCCTTGG
hOSM K44A fw	CTGGATGTTCCTGCACTGAGAGAGCACTGCAGGGAGC
hOSM K44A rev	GCTCCCTGCAGTGCTCTCTCAGTGCAGGAACATCCAG
hOSM L45A fw	GCCTGGATGTTCCTAAAGCGAGAGAGCACTGCAGGG
hOSM L45A rev	CCCTGCAGTGCTCTCTCGCTTTAGGAACATCCAGGC

hOSM R46A fw	CTGGATGTTCCTAAACTGGCAGAGCACTGCAGGGAGC
hOSM R46A rev	GCTCCCTGCAGTGCTCTGCCAGTTTAGGAACATCCAG
hOSM E47A fw	GTTCCTAAACTGAGAGCGCACTGCAGGGAGCG
hOSM E47A rev	CGCTCCCTGCAGTGCGCTCTCAGTTTAGGAAC
hOSM H48A fw	CCTAAACTGAGAGAGGCCTGCAGGGAGCGCC
hOSM H48A rev	GGCGCTCCCTGCAGGCCTCTCTCAGTTTAGG
hOSM C49A fw	AACTGAGAGAGCACGCCAGGGAGCGCCCC
hOSM C49A rev	GGGGCGCTCCCTGGCGTGCTCTCTCAGTT
Human OSM point mutants - D helix	
hOSM P153A fw	GCCGCCCACCGCCACCCCTGC
hOSM P153A rev	GCAGGGGTGGCGGTGGGCGGC
hOSM T154A fw	CGCCCACCCCCGCCCCTGCCTCG
hOSM T154A rev	CGAGGCAGGGGCGGGGGTGGGCG
hOSM P155A fw	CCACCCCCACCGCTGCCTCGGAT
hOSM P155A rev	ATCCGAGGCAGCGGTGGGGGTGG
hOSM S157A fw	CCCCACCCCTGCCGCGGATGCTTTTCA
hOSM S157A rev	TGAAAAGCATCCGCGGCAGGGGTGGGG
hOSM D158A fw	CCTGCCTCGGCTGCTTTTCAGCGCAAGCTG
hOSM D158A rev	CAGCTTGCGCTGAAAAGCAGCCGAGGCAGG
hOSM F160A fw	CTCGGATGCTGCTCAGCGCAAGCTGGAGGGC
hOSM F160A rev	GCCCTCCAGCTTGCGCTGAGCAGCATCCGAG
hOSM Q161A fw	GCCTCGGATGCTTTTGCGCGCAAGCTGGAGGG
hOSM Q161A rev	CCCTCCAGCTTGCGCGCAAAAGCATCCGAGGC
hOSM R162A fw	CAGCCCTCCAGCTTGGCCTGAAAAGCATCCGA
hOSM R162A rev	TCGGATGCTTTTCAGGCCAAGCTGGAGGGCTG
hOSM K163A fw	GATGCTTTTCAGCGCGCGCTGGAGGGCTGCAG
hOSM K163A rev	CTGCAGCCCTCCAGCGCGCGCTGAAAAGCATC
hOSM L164A fw	GCTTTTCAGCGCAAGGCGGAGGGCTGCAGGTT
hOSM L164A rev	AACCTGCAGCCCTCCGCCTTGCGCTGAAAAGC
hOSM E165A fw	CAGCGCAAGCTGGCGGGCTGCAGGTTC
hOSM E165A rev	GAACCTGCAGCCCGCCAGCTTGCGCTG
hOSM G166A fw	CGCAAGCTGGAGGCCTGCAGGTTCCTG
hOSM G166A rev	CAGGAACCTGCAGGCCTCCAGCTTGCG
Mouse OSM sequence optimization and mouse/human chimeras	
mOSM SeqOpt PacI fw	AAAGGGAAATTAATTAAGCTAGCGCATCGCCACCATGCAGACGAG ATTGCTGCGCACCCTG
mOSM SeqOpt AscI rev	TTTCCCTTTGGCGCGCCGCGGCCGCTATCAATGATGATGGTGGTGA TGCTCCAGCCT
mOSM Dlong fw	CAGCCGCCCACCCCCACCCCTGCAAGCGACGCTTTTCAAAG
mOSM Dlong rev	AGGGGTGGGGGTGGGCGGCTGGCTCGCGCCACTGTCGGTTT

mOSM WT 1	ATGCAGACGAGATTGCTGCGC
mOSM WT 2	GTCAGGCTCAGCAGGGTGCGCAGCAATCTCGTCTG
mOSM WT 3	ACCCTGCTGAGCCTGACCCTGTCACTGCTTATCCTTTCT
mOSM WT 4	CGATTGGCAAGGGCCATAGAAAGGATAAGCAGTGACAGG
mOSM WT 5	ATGGCCCTTGCCAATCGCGGGTGCAGCAACAGC
mOSM WT 6	GCTCAACAGTTGGCTGCTGCTGTTGCTGCACCCG
mOSM WT 7	AGCAGCCAACTGTTGAGCCAGCTTCAAAACCAGGCCA
mOSM WT 8	GGTGTTGCCGGTCAGGTTGGCCTGGTTTTGAAGCTG
mOSM WT 9	ACCTGACCGGCAACACCGAGAGCCTTCTTGAGCCCT
mOSM WT 10	GGTTTTGCAGGCGGATGTAGGGCTCAAGAAGGCTCTC
mOSM WT 11	ACATCCGCCTGCAAAACCTCAACACCCCCGACCTT
mOSM WT 12	GTGCACGCAGCGCGAAGGTCGGGGGTGTTGA
mOSM WT 13	CGCGCTGCGTGCACCCAGCACAGCGTGGCT
mOSM WT 14	GGTGTCCTCGCTAGGGAAAGCCACGCTGTGCTGG
mOSM WT 15	TTCCCTAGCGAGGACACCCTGAGGCAGTTGAGCAAGC
mOSM WT 16	CGGTGGACAGGAAGTGTGGCTTGCTCAACTGCCTCAG
mOSM WT 17	CACACTTCCTGTCCACCGTCTACACCACCCTGGACC
mOSM WT 18	TCGAGCTGGTACAGCACTCGGTCCAGGGTGGTGTAGA
mOSM WT 19	GAGTGCTGTACCAGCTCGACGCGCTCCGGCAGAA
mOSM WT 20	GCGGGGGTCTTCAGAAACTTCTGCCGGAGCGCG
mOSM WT 21	GTTTCTGAAGACCCCCGCATTCCCCAAGTTGGACAGC
mOSM WT 22	CAGGATGTTGTGCCTGGCGCTGTCCAACTTGGGGAAT
mOSM WT 23	GCCAGGCACAACATCCTGGGCATCAGGAACAACGTCT
mOSM WT 24	AGAAGCCTAGCCATGCAGAAGACGTTGTTCCTGATGCC
mOSM WT 25	TCTGCATGGCTAGGCTTCTGAACCACAGCCTTGAGATCC
mOSM WT 26	GGTTTGCGTGGGTTCGGGGATCTCAAGGCTGTGGTTC
mOSM WT 27	CCGAACCCACGCAAACCGACAGTGGCGCGAGCA
mOSM WT 28	CGGGCGTAGTGGTAGACCTGCTCGCGCCACTGTC
mOSM WT 29	GGTCTACCACTACGCCCGACGTGTTTAATACCAAGATAGGC
mOSM WT 30	CCACAGAAAGCCGCAAGAGCCTATCTTGGTATTAAACACGT
mOSM WT 31	TCTTGCGGCTTTCTGTGGGGTTACCATCGGTTCATGGG
mOSM WT 32	ACACTCTCCCGACGCTGCCCATGAACCGATGGTAACC
mOSM WT 33	CAGCGTCGGGAGAGTGTTCAGGGAGTGGGACGATG
mOSM WT 34	CCTGCTCCTCGTGGAGCCATCGTCCCACTCCCTGA
mOSM WT 35	GCTCCACGAGGAGCAGGAGGCTGGAGCATCACCA
mOSM WT 36	ATGATGATGGTGGTGATGCTCCAGCCT
mOSM AB 10	GTCCTTGGATGCGGATGTAGGGCTCAAGAAGGCTCTC
mOSM AB 11	ACATCCGCATCCAAGGACTCGATGTGCCCAAGCTT
mOSM ABshort 12	GTGCAATGTTCGCGAAGCTTGGGCACATCGA
mOSM ABshort 13	CGCGAACATTGCACCCAGCACAGCGTGGCT

mOSM ABlong 12	CGGCAGTGTTCGCGAAGCTTGGGCACATCGA
mOSM ABlong 13	CGCGAACACTGCCGGGAACGGCCTGGAGCT
mOSM ABlong 14	GGTGTCCTCGCTAGGGAAAGCTCCAGGCCGTTCC
mOSM D 28	CGCTTGCAGTGGTAGACCTGCTCGCGCCACTGTC
mOSM D 29	GGTCTACCACTGCAAGCGACGCTTTTCAAAGAAAGCTCGAA
mOSM D 30	CCACAGAAAGCCGCATCCTTCGAGCTTTCTTTGAAAAGCGT
mOSM D 31	GGATGCGGCTTTCTGTGGGGTTACCATCGGTTCATGGG
Mouse OSM point mutants - AB loop	
mOSM L35I 10	GGTTTTGGATGCGGATGTAGGGCTCAAGAAGGCTCTC
mOSM L35I 11	ACATCCGCATCCAAAACCTCAACACCCCCGACCTT
mOSM N37G 10	GTCCTTGCAGGCGGATGTAGGGCTCAAGAAGGCTCTC
mOSM N37G 11	ACATCCGCCTGCAAGGACTCAACACCCCCGACCTT
mOSM N39D 11	ACATCCGCCTGCAAAACCTCGACACCCCCGACCTT
mOSM N39D 12	GTGCACGCAGCGCGAAGGTCGGGGGTGTCGA
mOSM T40V 11	ACATCCGCCTGCAAAACCTCAACGTGCCCGACCTT
mOSM T40V 12	GTGCACGCAGCGCGAAGGTCGGGCACGTTGA
mOSM D42K 11	ACATCCGCCTGCAAAACCTCAACACCCCCAAACTT
mOSM D42K 12	GTGCACGCAGCGCGAAGTTTGGGGGTGTTGA
mOSM 35+37 10	GTCCTTGGATGCGGATGTAGGGCTCAAGAAGGCTCTC
mOSM 35+37 11	ACATCCGCATCCAAGGACTCAACACCCCCGACCTT
mOSM 35+39 11	ACATCCGCATCCAAAACCTCGACACCCCCGACCTT
mOSM 35+40 11	ACATCCGCATCCAAAACCTCAACGTGCCCGACCTT
mOSM 35+42 11	ACATCCGCATCCAAAACCTCAACACCCCCAAACTT
mOSM 37+39 11	ACATCCGCCTGCAAGGACTCGACACCCCCGACCTT
mOSM 37+40 11	ACATCCGCCTGCAAGGACTCAACGTGCCCGACCTT
mOSM 37+42 11	ACATCCGCCTGCAAGGACTCAACACCCCCAAACTT
mOSM 39+40 11	ACATCCGCCTGCAAAACCTCGACGTTCCCGACCTT
mOSM 39+40 12	GTGCACGCAGCGCGAAGGTCGGGAACGTCGA
mOSM 39+42 11	ACATCCGCCTGCAAAACCTCGACACCCCCAAACTT
mOSM 39+42 12	GTGCACGCAGCGCGAAGTTTGGGGGTGTCGA
mOSM 40+42 11	ACATCCGCCTGCAAAACCTCAACGTGCCCAAGCTT
mOSM 40+42 12	GTGCACGCAGCGCGAAGCTTGGGCACGTTGA
mOSM 35+37+39 11	ACATCCGCATCCAAGGACTCGACACCCCCGACCTT
mOSM 35+37+40 11	ACATCCGCATCCAAGGACTCAACGTGCCCGACCTT
mOSM 35+37+42 11	ACATCCGCATCCAAGGACTCAACACCCCCAAACTT
mOSM 35+39+40 11	ACATCCGCATCCAAAACCTCGACGTTCCCGACCTT

mOSM 35+39+42 11	ACATCCGCATCCAAAACCTCGACACCCCCAAACTT
mOSM 35+40+42 11	ACATCCGCATCCAAAACCTCAACGTGCCCAAGCTT
mOSM 37+39+40 11	ACATCCGCCTGCAAGGACTCGACGTTCCCGACCTT
mOSM 37+39+42 11	ACATCCGCCTGCAAGGACTCGACACCCCCAAACTT
mOSM 37+40+42 11	ACATCCGCCTGCAAGGACTCAACGTGCCCAAGCTT
mOSM 39+40+42 11	ACATCCGCCTGCAAAACCTCGATGTGCCCAAGCTT
mOSM 39+40+42 12	GTGCACGCAGCGCGAAGCTTGGGCACATCGA
mOSM 35+37+39+40 11	ACATCCGCATCCAAGGACTCGACGTTCCCGACCTT
mOSM 35+37+39+42 11	ACATCCGCATCCAAGGACTCGACACCCCCAAACTT
mOSM 35+37+40+42 11	ACATCCGCATCCAAGGACTCAACGTGCCCAAGCTT
mOSM 35+39+40+42 11	ACATCCGCATCCAAAACCTCGATGTGCCCAAGCTT
mOSM 37+39+40+42	ACATCCGCCTGCAAGGACTCGATGTGCCCAAGCTT
mOSM 5M	ACATCCGCATCCAAGGACTCGATGTGCCCAAGCTT
Human OSM mutants - mouse AB loop	
hOSM AB mO fw	GACTCCTGGACCCCTATATACGTCTGCAAAACCTCAACACCCCCGACCTTCGCGCTGCG
hOSM AB mO rev	AAGGCCCCGGGGCGCTCCCTGCACGCAGCGCGAAGGTCGGGGGTGTTGAGGTTTTGCAG
hOSM G39N fw	ATATACGTATCCAAAACCTGGATGTTCC
hOSM G39N rev	GGAACATCCAGGTTTTGGATACGTATAT
hOSM V42T fw	TCCAAGGCCTGGATACTCCTAAACTGAGAG
hOSM V42T rev	CTCTCAGTTTAGGAGTATCCAGGCCTTGGA
hOSM K44D fw	GCCTGGATGTTCCTGATCTGAGAGAGCACT
hOSM K44D rev	AGTGCTCTCTCAGATCAGGAACATCCAGGC
hOSM 39+42 fw	AACCTGGATACTCCTAAACTGAGAGAGCACTGCA
hOSM 39+42 rev	GTATCCAGGTTTTGGATACGTATATAGGGGTCCA
hOSM 39+44 fw	AACCTGGATGTTCCTGATCTGAGAGAGCACTGCAGGGAGCG
hOSM 39+44 rev	ATCAGGAACATCCAGGTTTTGGATACGTATATAGGGGTCCA

hOSM 42+44 fw	ACTCCTGATCTGAGAGAGCACTGCAGGGAGCG
hOSM 42+44 rev	ATCAGGAGTATCCAGGCCTTGGATACGTATAT
hOSM 39+42+44 fw	AACCTGGATACTCCTGATCTGAGAGAGCACTGCAGGGAGCG
hOSM 39+42+44 rev	ATCAGGAGTATCCAGGTTTTGGATACGTATATAGGGGTCCA
Sequencing primers	
T7 seq fw	TAATACGACTCACTATAGGG
pCAGGS seq fw	GCCTCTGCTAACCATGTTCATGC
pCAGGS seq rev	TCGATACCGTCGATCTCAGTGGTA
pFLAG seq fw	ACGCAAATGGGCGGTAGGCGTGT

3.1.10. Buffers

Bis-Tris buffer (3.5x)
1.25 M bis-Tris, pH 6.4

DNA loading buffer (6x)
20mM Tris, pH 7.8
20mM acetic acid
1mM EDTA
50% glycerol

His-Tag purification binding buffer
50 mM sodium phosphate, pH 7.4
500 mM NaCl
10 mM imidazole

His-Tag purification elution buffer
50 mM sodium phosphate, pH 7.4
500 mM NaCl
250 mM imidazole

His-Tag purification wash buffer
50 mM sodium phosphate, pH 7.4
500 mM NaCl
20 mM imidazole

Miniprep solution A
25 mM Tris, pH 8.0
10 mM EDTA
50 mM D(+)-Glucose
10 µg/mL RNase A

Miniprep solution B
0.2 N NaOH
1% SDS

Miniprep solution C
3 M potassium acetate
8.9% acetic acid

KCM buffer (5x)
0.5 M KCl
150 mM $CaCl_2$
250 mM $MgCl_2$

Phosphate-buffered saline (PBS)
10 mM Na_2HPO_4
1.5 mM KH_2PO_4
137 mM NaCl
2.7 mM KCl
pH adjusted to 7.4 with HCl

Protease/phosphatase inhibitor mix
500 µg/ml benzamidin
2 µg/ml aprotinin
2 µg/ml leupeptin
2 mM PMSF
1 mM sodium orthovanadate
20 mM sodium fluoride

Protein extraction buffer
100 mM Tris, pH 8.8
10 mM EDTA
40 mM DTT
10 % SDS
pH adjusted to 8.0 with HCl

Protein loading buffer (5x)
66.7 mM Tris, pH 6.8
2.2% SDS
27% glycerol

Protein transfer buffer
25 mM bis-Tris
25 mM bicine
1 mM EDTA
20% methanol

Tris-Acetate-EDTA (TAE) buffer
40mM Tris, pH 7.8
40mM acetic acid
2mM EDTA

Tris-buffered saline + Tween-20 (TBS-T) buffer
20 mM Tris
136.9 mM NaCl
0.01% Tween® 20
pH adjusted to 7.6 with HCl

Tris-EDTA (TE) buffer
10 mM Tris, pH 7.4
1 mM EDTA

TSB buffer
5% DMSO
10 mM $MgCl_2$
10 mM $MgSO_4$
10% polyethylene glycol 6000
dissolved in 2xLB broth

Sonication buffer
50 mM Tris, pH 8.0
500 mM NaCl
10 mM imidazole

3.1.11. Software

Software	Version	Manufacturer
ApE - A plasmid Editor	2.0.47	M. Wayne Davis
Clustal Omega	1.2.2	European Molecular Biology Laboratory - European Bioinformatics Institute (EMBL-EBI)
DNAWorks	3.2.3	National Institutes of Health (NIH)
Image Lab	5.0 build 18	Bio-Rad®
Image Studio	4.0.21	LI-COR Biosciences®
MacPyMOL	1.7.2.1	Schrödinger LLC®
MetaPIGA	3.100	Đorđe Grbić, Michel C. Milinkovitch and Raphaël Helaers
QuikChange® Primer Design Program	-	Agilent®
R	3.0.3	The R Foundation for Statistical Computing
RStudio	0.98.1062	RStudio®
SWISS-MODEL	-	Swiss Institute of Bioinformatics

3.2. Methods

3.2.1. Cell line culture conditions

Cell lines were cultured under 37ºC and 8% CO_2 in the recommended medium supplemented with 10% FBS: A375 and NIH3T3 cells were grown in DMEM medium, HepG2 cells in DMEM/F12 medium, JAR cells in RPMI 1640 medium and FreeStyle™ 293-F cells in FreeStyle™ 293 Expression Medium. DMEM, DMEM/F12 and RPMI 1640 mediums were additionally supplemented with penicillin/streptomycin.

Adherent cell lines (A375, NIH3T3, HepG2 and JAR) were grown in 10 cm cell culture dishes and passaged at 80-90% confluence. First the medium was aspirated, the plate was washed once with 5 mL of PBS buffer and 5 mL of a 2xTrypsin-EDTA solution diluted in PBS was added. The plate was incubated for 5-10 minutes at 37ºC until the cell layer was dispersed, after which addition of 5 mL of growth medium stopped trypsin digestion. Cells were subsequently pelleted by centrifugation for 5 minutes at 200 g, followed by aspiration of the supernatant, resuspension of the cell

pellet in fresh growth medium and plating in new cell culture dishes/plates at a 1:4 to 1:10 ratio.

Cryopreservation of adherent lines was achieved by resuspension of the cell pellet after trypsinization in FBS, to which an equal volume of medium supplemented with 20% DMSO was slowly added. The resulting cell solution was aliquoted in CryoTube™ vials, and cooled down in the -80ºC freezer inside a Mr. Frosty™ freezing container.

The suspension cell line FreeStyle™ 293-F was grown in 125 or 250 mL disposable cell culture Erlenmeyer flasks, employing a CO_2-resistant incubator at 150-160 rpm. Passage of these cells was performed upon reaching a density of 1 to $3x10^6$ cells/mL, by dilution of the cells to 0.1-0.2$x10^6$ cells/mL in in fresh medium pre-warmed to 37ºC. Anti-clumping agent was added to the medium during the first few passages after initially thawing the cryostocks to prevent clump formation.

Cryopreservation of the FreeStyle™ 293-F was achieved in cultures at $1x10^6$ cells/mL by centrifugation for 5 minutes at 350 g. The supernatant was aspirated and the cell pellet resuspended at a density of 10^7 cells/mL in ice-cold sterile-filtered FreeStyle™ 293 Expression Medium supplemented with 10% DMSO. 1 mL aliquots were placed into CryoTube™ vials, and a Mr. Frosty™ freezing container was used to slowly cool down the cells inside the -80ºC freezer.

3.2.2. Cell stimulation assays

Cell stimulation was performed in 6-well cell culture plates with 80-90% confluent cells for 10-minute stimulation assays, and 50-60% confluent cells for 24-hour stimulation assays. 25 ng/mL of the desired cytokine was added into each well, after which the plate was incubated at 37ºC and 8% CO_2 for the specified amount of time.

The medium was removed after stimulation, wells were washed once with PBS and proteins were harvested by addition of 100 µL of a 3:2 solution of protein extraction buffer and protein loading buffer (5x) supplemented with protease/phosphatase inhibitors. After a brief sonication (6-7 pulses of 0.5 seconds at 20% power using a Sonopuls® HD 2070 ultrasonic homogenizer), 2-5 µL of the sample were used to measure protein concentration with the DC™ Protein Assay and a FLUOstar® Galaxy microplate reader following the manufacturer's instructions.

To prepare the remainder of the sample for protein electrophoresis DTT was added to a final concentration of 0.04 M, samples were boiled at 99ºC for 2 minutes and diluted to a concentration of 1 µg/µL.

3.2.3. Protein electrophoresis

Protein electrophoresis was carried out with either 10% polyacrylamide bis-Tris gels polymerized with ammonium persulfate and TEMED or 17-well NuPAGE™ 4-12% Bis-Tris Protein Gels. SDS-polyacrylamide gel electrophoresis (SDS-PAGE) was then performed in XCell SureLock™ Mini-Cells with NuPAGE™ MES buffer. 2 µL of Protein Marker VI or 10 µg of sample protein were loaded into the wells, after which the Mini-Cells were put in ice and connected to an electrophoresis power supply.

Protein electrophoresis was performed at 75V for the initial 10 minutes, after which the voltage was increased to 165V until reaching the desired separation. Once protein electrophoresis was completed, the cassette encasing the SDS-PAGE gel was removed and protein detection was performed through western blotting, Coomassie blue staining or silver staining.

3.2.4. Western blotting

XCell II™ Blot Modules were used to transfer the proteins from SDS-PAGE gels to Amersham™ Protran™ 0.45 µm NC nitrocellulose blotting membranes. The gel was placed in direct contact with a nitrocellulose membrane pre-soaked in protein transfer buffer, and gel and membrane were sandwiched by pre-soaked filter paper and blotting sponges inside the blotting module.

The module was inserted into an XCell SureLock™ Mini-Cell, protein transfer buffer was added to the mini-cell's inside chamber and cold tap water to the outer chamber. The mini-cell was then connected to an electrophoresis power supply, and protein transfer was carried out for 2 hours at 30V.

After the 2 hours had passed, membranes were taken out of the blotting modules and incubated with RedAlert™ Western Blot Stain to verify the protein transfer had been successful. In the cases in which multiplexing was necessary the membrane was cut into different sections, in accordance to the expected molecular weight of the proteins to be detected. RedAlert™ stain was subsequently removed by a first incubation with distilled water followed by incubation in TBS-T buffer; these and all subsequent steps were performed under gentle shaking.

Membranes were then transferred to a solution of 5% skim milk powder in TBS-T and incubated at room temperature (RT) for 1 hour, in order to prevent unspecific protein binding to the membrane. Afterwards membranes were washed five times with TBS-T, waiting for 5 minutes at RT between each wash. The desired primary antibody was diluted following the manufacturer's instructions into a solution of

either 3% skim milk powder or 3% BSA in TBS-T, added to the membrane and incubated overnight at 4ºC.

On the following day the antibody solution was removed and the membranes were washed 5 times with TBS-T, followed by a 1-hour incubation at RT with the corresponding secondary antibody in a solution of 3% skim milk powder in TBS-T. Removal of the secondary antibody was followed by an additional 5 washes with TBS-T. Detection was performed with an Odyssey® 9120 imaging system in the case of fluorescently labeled secondary antibodies, while horseradish peroxidase-conjugated secondary antibody detection was performed using SuperSignal™ West Femto substrate and a ChemiDoc™ MP System.

3.2.5. Coomassie blue and silver staining

Coomassie blue staining to visualize total protein in an SDS-PAGE gel was carried out using InstantBlue™ Coomassie® stain. After protein separation by electrophoresis the gel cassette was removed, the gel was transferred to the InstantBlue™ solution and kept shaking for 1 hour at RT. Removal of the InstantBlue™ solution was followed by 3-5 washes with distilled water, after which the gel was scanned using the ChemiDoc™ MP System.

Silver staining was performed with the SilverQuest™ Silver Staining Kit. After cassette removal gels were incubated in the kit's fixing solution for a minimum of 1 hour in a rocking platform, then transferred first to the sensitizing solution for 30 minutes and washed 3 times with distilled water. The silver solution was added and incubated for 20 minutes, after which the gel was washed briefly and incubated with developing solution. Once the bands reached the desired intensity the gel was transferred to the stopping solution and kept shaking for 10 minutes, after which it was washed 3 additional times with distilled water and scanned with the ChemiDoc™ MP System.

3.2.6. Cell proliferation assays

Cell proliferation assays were performed in 96-well cell culture plates, in which A375 cells were seeded at a density of 5000 cells/well in DMEM medium without phenol red, stimulated with 10 ng/mL of the desired cytokine and grown for 5 days before performing an MTT proliferation assay following the manufacturer's instructions.

Briefly, the medium was changed and MTT reagent was added to the wells. After an incubation of 4 hours at 37ºC degrees, a 10% SDS solution in 0.01 M HCl was added and incubated overnight at 37ºC and 8% CO_2, after which the absorbance of each sample at 570 nm was measured by a FLUOstar® Galaxy microplate reader.

3.2.7. DNA electrophoresis

To cast an agarose gel for DNA electrophoresis, 1% agarose was added into TAE buffer and the mixture was heated in a microwave oven until the agarose was completely dissolved. Once it had cooled down to 55ºC a small amount (4 µL per 100 mL of solution) of 1% ethidium bromide was mixed in, and the resulting solution was poured into a horizontal electrophoresis chamber with appropriate combs to form the desired wells.

After solidification of the solution into a gel the combs were removed, the chamber was filled with TAE buffer and the DNA was loaded into the wells along with the appropriate GeneRuler DNA ladder. The chamber was then connected to an electrophoresis power supply, and electrophoresis was carried out for 20-30 minutes at 100-160V depending on the size of the gel and of the DNA bands of interest. Afterwards DNA bands were visualized employing an UV transilluminator.

3.2.8. Standard molecular cloning

Genes selected for recombinant protein expression in *E. coli* were cloned into the pET-26b(+) vector, while expression in mammalian cells was achieved via the pCAGGS vector. Primers complementary to the 5' and 3' ends of the gene's coding region and including specific restriction enzyme sites were designed and purchased from Sigma-Aldrich®.

Amplification of the gene of interest by polymerase chain reaction (PCR) was performed by following the manufacturer's instructions: for a 25 µL reaction mixture Phusion HF buffer was supplemented with 0.5 µM of the desired primers, 200 µM dNTPs, 3% DMSO, 0.5 units of Phusion Hot Start II DNA Polymerase and either 1-5 ng of plasmid DNA or 2.5 µL of cDNA as template.

After carefully mixing the different reagents in ice, the tubes were transferred to a thermocycler in which the PCR reaction was performed. An initial denaturation step (98ºC, 30 seconds) was followed by 23-25 cycles of denaturation (98ºC, 10 seconds), annealing (68ºC, 25 seconds) and extension (72ºC, 30 seconds/kilobase), after which a final extension step (72ºC, 5 minutes) concluded the amplification.

The resulting PCR product was supplemented with 5 µL of DNA loading buffer and subjected to DNA electrophoresis, after which the band corresponding to the gene of interest was excised using a disposable scalpel and purified using the NucleoSpin® Gel and PCR clean-up kit according to the manufacturer's instructions.

After purification the PCR products were eluted in 30 µL of distilled water and subjected to restriction enzyme digestion. 1 µL of the selected restriction enzymes, able to recognize and cut restriction sites in the sequence of the employed primers, was mixed with their recommended buffer and the purified DNA in a total volume of 50 µL, and incubated for 4 hours at 37ºC. In parallel, 1 µg of the desired plasmid was subjected to restriction enzyme digestion with identical enzymes and conditions.

After 4 hours, 10 µL of DNA loading buffer was added to the digestion mixture and DNA electrophoresis was performed. The bands corresponding to the vector and the gene of interest were excised and purified using the NucleoSpin® Gel and PCR clean-up kit, and eluted in 20-30 µL of distilled water. DNA concentration of these samples was measured by a NanoDrop 2000c UV-Vis spectrophotometer, and ligation reactions were performed with a 3:1 molar ratio between the gene to be inserted and the vector.

For the ligation, 40 ng of vector and the corresponding amount of insert were diluted in distilled water, and 2 µL of T4 DNA ligase and ligase buffer were added for a total volume of 20 µL. This ligation mixture was then incubated overnight at 16ºC before being transformed into chemically competent XL-1 Blue *E. coli*.

3.2.9. Molecular cloning by gene synthesis

Codon-optimization of the amino acid sequence of the genes to be cloned and the design of the overlapping oligonucleotides covering the optimized gene sequence was done with DNAWorks. (Hoover & Lubkowski 2002) Default options were used except in two cases: the first concerned the selection of the option 'no gaps in assembly', which facilitates the generation of subsequent mutants reusing most of the original set of oligonucleotides. Additionally, the planned restriction sites to be used in the cloning procedure were excluded from the protein-coding region of the synthetic gene. Oligonucleotides were acquired from Sigma-Aldrich®.

Assembly of the synthetic genes required a nested PCR protocol. (Varadarajan et al. 2009) In the first PCR amplification procedure, 50 µL of Phusion HF buffer was supplemented with 2 pM of each of the designed oligonucleotides, 200 µM dNTPs and 1 unit of Phusion Hot Start II DNA Polymerase. The oligonucleotides were assembled in a thermocycler by means of an initial denaturation step (95ºC, 2 minutes) followed by 40 cycles of denaturation (95ºC, 30 seconds), annealing (52ºC, 30 seconds) and extension (72ºC, 30 seconds).

The product of this first reaction was directly used as DNA template in a second PCR amplification step, in which 1 µM of the outermost forward and reverse primers, 200 µM dNTPs and 1 unit of Phusion Hot Start II DNA Polymerase was added to 50 µL of Phusion HF buffer. The PCR conditions were similar to the first, but the annealing temperature was increased to 58ºC, the number of cycles was reduced to 30 and a final extension step (72ºC, 5 minutes) was included.

The result of the second PCR amplification was a single band that could be separated by DNA electrophoresis, purified, digested with restriction enzymes and ligated into a vector by following the procedure detailed in section 3.2.8.

3.2.10. Molecular cloning by overlap extension PCR

Chimeric cytokines were generated by overlap extension PCR, employing the same general procedures detailed in section 3.2.8. In a first PCR amplification step, primers complementary to the sequences to be joined were designed so that the amplified fragments would have an overlapping 30 base pair sequence covering the chimeric region.

These PCR products were purified and used together as DNA templates in a second PCR reaction, along with the primers corresponding to the 5' and 3' ends of the full cytokine sequence. The resulting full-length product was purified, subjected to restriction enzyme digestion and ligated into the vector of interest.

3.2.11. Site-directed mutagenesis

Point mutants were created by different procedures, including gene synthesis and overlap extension PCR, but most of the variants used in this work were generated by site-directed mutagenesis. Overlapping forward and reverse primers including the desired mutation were generated with the QuikChange® Primer Design Program and used to amplify a template vector containing the gene to be mutated.

Full-length plasmid amplification was achieved by PCR reaction, using a 25 µL mixture containing PfuUltra buffer, 0.25 µM of each primer, 200 µM dNTPs, 1.25 units of PfuUltra High Fidelity DNA Polymerase and 20 ng of template plasmid DNA. The reaction conditions involved a first denaturation step (95ºC, 1 minute) followed by 30 cycles of denaturation (95ºC, 30 seconds), annealing (68ºC, 30 seconds) and extension (72ºC, 1 minute/kilobase), as well as a final extension step (72ºC, 10 minutes).

The resulting PCR product was purified by addition of 400 µL isopropanol, 80 µL of distilled water and 100 µL of ammonium acetate 4M to 20 µL of the PCR mixture. After a 15-minute incubation at RT the solution was centrifuged for 15 minutes at 21000 g and the supernatant was discarded. The pellet was washed with 500 µL of 70% ethanol and centrifuged again (10 minutes, 21000 g), the supernatant was discarded and the pellet was allowed to dry for 10-15 minutes to remove any residual ethanol.

The pellet was then resuspended in water and digested with DpnI for 4 hours at 37ºC in order to remove the original plasmid employed as DNA template. Since DpnI is only able to cut methylated DNA the template vector isolated from *E. coli* will be degraded, while the unmethylated PCR product will not be affected. After 4 hours the digestion mixture can be directly used to transform chemically competent XL-1 Blue *E. coli*, since the PCR product generated is able to re-circularize and form a doubly nicked plasmid that can be transformed into the bacteria.

3.2.12. Generation of chemically competent *E. coli*

In order to generate chemically competent bacteria for transformation, 1 mL of LB broth without antibiotics was first inoculated with 10 µL of XL1 Blue *E. coli* under sterile conditions. After incubation for 1 hour at 37ºC and 700-800 rpm, 50-100 µL of the solution was plated into an LB-Agar plate without antibiotics and allowed to grow overnight in a bacterial incubator at 37ºC.

The following day 5 mL of LB broth were inoculated with a single clone from the plate under sterile conditions, and kept overnight in a bacterial incubator at 37ºC shaking at 180-200 rpm. This starter culture was then used to inoculate 100 mL of LB broth, which was incubated shaking at 37ºC until its optical density measurement at 600 nm (OD_{600}) reached a value of 0.5-0.6.

The culture was harvested by centrifugation for 15 minutes at 2500 g and 4ºC and the supernatant was discarded. The bacterial pellet was immediately resuspended in 7.5 mL of TSB buffer and incubated for 1 hour on ice, after which the cell suspension was aliquoted, frozen in liquid nitrogen and stored at -80ºC.

3.2.13. Chemical Transformation of competent *E. coli*

50 µL of transformation mixture was made up with 5 µL of the ligation product from the molecular cloning protocol in KCM buffer, or 20-100 ng of purified DNA plasmid. An aliquot of chemically competent XL1 Blue *E. coli* was allowed to thaw in ice, 50 µL

were added to the transformation mixture and the resulting solution was incubated on ice for 10 minutes, followed by a 20-minute incubation at RT.

Afterwards 1 mL of LB broth without antibiotics pre-warmed to 37ºC was added, and the sample was incubated for 60-90 minutes at 37ºC and 700-800 rpm. Bacterial cells were pelleted by centrifugation for 1 minute at 2000 g, 1 mL of supernatant was discarded and the pellet was resuspended in the remaining solution. Samples were then plated on LB-Agar plates supplemented with appropriate antibiotics, and incubated overnight at 37ºC.

3.2.14. Plasmid DNA isolation and purification

Plasmid DNA was amplified in transformed XL1 Blue *E. coli*. For the isolation of a small amount of plasmid DNA after molecular cloning (miniprep), 3 mL of LB broth with the adequate selection antibiotic was inoculated with a single colony from a plate of transformed *E. coli* and incubated overnight at 37ºC and 180-220 rpm.

On the following day, bacteria were pelleted by centrifugation of 2 mL of the overnight culture for 5 minutes at 21000 g. The supernatant was discarded and the pellet resuspended in 150 µL of miniprep solution A, after which 200 µL of miniprep solution B was added to lysate the bacteria for 10 minutes at RT. The lysis reaction was stopped and the proteins and genomic DNA were precipitated by adding 175 µL of miniprep solution C and incubating for 10 minutes on ice.

This step was followed by centrifugation at 21000 g and 4ºC for 15 minutes to pellet the genomic DNA. The supernatant containing plasmid DNA was transferred to another tube containing 500 µL of isopropanol and subsequently precipitated by centrifugation at 21000 g and 4ºC for 20 minutes. After washing the pellet with 500 µL of 70% ethanol by centrifugation at 21000 g and 4ºC for 10 minutes, the supernatant was decanted and the pellet was allowed to dry for 10-15 minutes to remove residual ethanol. Finally, the pellet was resuspended in TE buffer and the plasmid DNA was verified by DNA sequencing (performed by Seqlab Sequence Laboratories Göttingen) and/or restriction enzyme digestion.

For the isolation of large amounts of plasmid DNA after plasmid verification, the NucleoBond® Xtra Maxi kit was used according to the manufacturer's instructions. A starter culture of 3 mL of LB broth supplemented with the selection antibiotic was inoculated with a single colony and grown for 8 hours at 37ºC and 180-220 rpm, after which a larger culture of 300 mL of LB broth with antibiotic was inoculated 1:1000 with the starter culture and grown overnight at 37ºC and 180-220 rpm.

On the following day the bacteria were pelleted by centrifugation at 5000 g and 4ºC for 10 minutes, resuspended in the kit's re-suspension buffer and lysed for 5 minutes by addition of lysis buffer. Protein and chromosomal DNA was precipitated with the neutralization buffer, after which the lysate was loaded into previously equilibrated NucleoBond® Xtra Maxi columns with filters.

The columns were then washed first with the kit's equilibration buffer, the filter was removed and a second wash was performed with wash buffer, followed by elution of plasmid DNA with elution buffer. Isopropanol was added at RT to precipitate the eluted plasmid DNA, which was then pelleted by centrifugation at 10000 g and 4ºC for 30 minutes. The supernatant was discarded and the pellet washed with RT 70% ethanol and centrifuged at 5000 g for 5 minutes.

Finally the ethanol was discarded and the pellet was allowed to dry at room temperature for 15 minutes, before re-suspension in 300 µL of TE buffer. Plasmid DNA concentration was measured with a NanoDrop 2000c UV-Vis spectrophotometer and verified by DNA sequencing (Seqlab Sequence Laboratories Göttingen).

3.2.15. RNA isolation and purification

3 mL of TriFast™ was added to a 10 cm cell culture dish of 80-90% confluent monolayer cells, the cells were harvested with the help of a pipette and incubated at RT for 5 minutes. The solution was supplemented with 600 µL of chloroform, vortexed for 15 seconds, incubated at RT for 3 minutes and centrifuged at 12000 g and 4ºC for 20 minutes.

The upper aqueous fresh was recovered after centrifugation, 500 µL of isopropanol was added and incubated at RT for 10 minutes, after which it was centrifuged at 12000 g and 4ºC for 15 minutes to enable RNA precipitation. The supernatant was discarded and the pellet washed twice with 1 mL of 75% ethanol (in 0.1% DEPC water) by centrifugation at 7500 g and 4 ºC for 5 minutes.

Finally, the supernatant was discarded and the pellet allowed to dry for 5-10 minutes before re-suspension in RNAse-free water (Aqua B. Braun). Optimal re-suspension of the RNA was ensured by an incubation at 56ºC and 850 rpm for 10 minutes, after which the RNA concentration was measured with a NanoDrop 2000c UV-Vis spectrophotometer.

3.2.16. Reverse Transcription PCR

Purified RNA was employed for complementary DNA (cDNA) synthesis using random primers: 1 µg of the RNA to be retro-transcribed, along with 1 µL of RQ1 DNase and 0.1 µL of RNasin plus in 10 µL of RQ1 DNase reaction buffer, were incubated at 37ºC for 30 minutes to degrade any DNA remnants.

1 µL of 25 mM EDTA was then added, the sample was heated to 65ºC and incubated for 10 minutes before addition of 0.5 µL random primers and 1 µL of 10 mM dNTPs. After 5 more minutes of incubation at 65ºC the solution was cooled down on ice, 4 µL of Superscript® II buffer and 2 µL of 0.1M DTT were supplemented and a 2-minute incubation at 25ºC was performed.

Immediately after this step 1 µL of Superscript® II reverse transcriptase was added and the mixture was incubated at 25ºC for an additional 10 minutes, followed by an incubation at 42ºC for 50 minutes and a final incubation at 70ºC for 15 minutes to inactivate the reverse transcriptase. Distilled water was added to make the final volume 50 µL, in order to obtain a 20 ng/µL cDNA solution.

3.2.17. Soluble recombinant protein expression in a prokaryotic system

A pET-26b(+) plasmid containing the gene to be expressed followed by a C-terminal hexahistidine tag (His-tag) was transformed in SHuffle® T7 Express competent *E. coli* following the general protocol detailed in section 3.2.13, except for the final incubation being performed at 30ºC instead of 37ºC, plated in LB-agar plates with 50 µg/mL of kanamycin and incubated overnight at 30ºC.

A single colony from the plate was then used to inoculate a starter culture of 3 mL of LB broth with kanamycin, which was grown overnight at 30ºC and 180-220 rpm. On the following day the starter culture was diluted into 200 mL of LB broth with kanamycin, and the resulting solution incubated at 30ºC and 180-220 rpm until reaching an OD_{600} value of 0.5-0.7.

At this point the culture was supplemented with 0.1 mM of IPTG to induce recombinant protein expression and allowed to grow for an additional 4-6 hours. Finally, the bacterial cells were harvested by centrifugation at 5000 g and 4ºC for 10-15 minutes, at which point the pellets could either be stored at -20ºC for several days or immediately processed.

In order to release the produced recombinant protein from the bacterial cytoplasm, cell pellets were resuspended in 9 mL of cold sonication buffer and a first lysis step

was performed by incubation for 30 minutes on ice with 1 mg/mL of lysozyme along with a protease inhibitor (1 mM PMSF).

Afterwards the bacterial cell wall was thoroughly ruptured by 10 rounds of 30 seconds of sonication on ice, interspersed with 30 second breaks to avoid excessive heating of the samples. 1 mM $MgCl_2$ and 0.1 mg/mL DNase I were then added to the sample to degrade bacterial and plasmid DNA, and the solution was centrifuged at 21000 g and 4ºC for 30-40 minutes to separate the insoluble fraction. The supernatant containing the soluble recombinant protein of interest was then collected and purified by using the protocol detailed in section 3.2.20.

3.2.18. Soluble recombinant protein expression in a mammalian system

A pcDNA 3.1(+), pFLAG-CMV-3 or pCAGGS plasmid containing the gene to be expressed followed by a C-terminal hexahistidine tag (His-tag) was transfected into FreeStyle™ 293-F cells at a density of 10^6 cells/mL according to the manufacturer's instructions. First, purified plasmids were diluted to a concentration of 1 µg/mL and filter-sterilized with a 0.22 µm filter.

To transfect a 30 mL flask of 293-F cells, 37.5 µL of plasmid per mL was diluted into 0.6 mL of OptiPro™ SFM kept at RT in a sterile tube and mixed by inversion. In a second tube 37.5 µL of FreeStyle™ MAX Reagent was also diluted in 0.6 mL of OptiPro™ SFM at RT and mixed by inversion.

Immediately afterwards the OptiPro™ SFM medium with the MAX reagent was added to the medium with the plasmid, mixed by inversion 15-20 times and incubated for 10-20 minutes at RT. Finally, the medium was added dropwise to the cell culture flask while gently swirling the flask, and the cells were allowed to grow under normal culturing conditions for an additional 3 to 7 days.

After the desired amount of time, the cell solutions were centrifuged at 4000 g and 4ºC for 15 minutes to pellet cells and insoluble debris. The supernatant containing the soluble recombinant protein was collected, supplemented with 300 mM NaCl and 10 mM imidazole and used for his-tagged protein purification according to the procedure in section 3.2.20.

3.2.19. His-tagged protein purification

All purification steps were performed at 4ºC. 0.75-1 mL of HIS-Select® HF nickel affinity gel slurry, containing nickel-nitrilotriacetic acid (Ni-NTA) chelate groups able to bind to histidine residues, was transferred to a 5 mL polypropylene column. An

initial wash by gravity flow with 2 column volumes of distilled water was performed to remove the ethanol in which the gel is preserved, followed by 3 column volumes of His-tag purification binding buffer to equilibrate the affinity gel.

The column was then capped and supernatant containing C-terminal his-tagged recombinant proteins added. An incubation step at 4ºC in an end-over-end tube rotator for 20-30 minutes was carried out in order to allow the recombinant protein to bind to the affinity gel, after which the column was placed vertically and the gel became packed again at the bottom.

The next step comprised uncapping the column and discarding the flow through by gravity flow, followed by washing with 10 column volumes of His-tag purification wash buffer. To elute the recombinant protein from the affinity gel, the column was capped and 1 mL of His-tag purification elution buffer added. After a 10-minute incubation the cap was removed, the buffer collected and the elution repeated 3 additional times.

Finally, the eluted product was concentrated in centrifugal filters with a 10 kDa molecular weight cutoff by centrifugation at 4000g and 4ºC for 30 minutes, and collected in PBS buffer before measuring protein concentration and assessing purity.

3.2.20. siRNA transfection

A reverse transfection protocol was employed according to the manufacturer's instructions. 500 µL of OptiMEM® medium was added to each well of a 6-well cell culture plate, supplemented with 7.5 µL of the desired siRNA 20 µM stock and 7.5 µL of Lipofectamine® RNAiMAX and incubated for 10-20 minutes at RT.

Immediately after this step, $2.5x10^5$ cells resuspended in 2.5 mL of antibiotic-free growth medium supplemented with 10% FCS were added to each well and incubated overnight under 37ºC and 5-8% CO_2 conditions. On the following day the medium was exchanged to growth medium with antibiotics and FCS, and cells were allowed to grow for an additional 24-48 hours before performing the desired stimulation assays.

3.2.21. Deglycosylation assay

Deglycosylation assays were performed using the Protein Deglycosylation Mix kit under denaturing reaction conditions. 18 µL of recombinant protein in PBS was supplemented with 2 µL of the glycoprotein denaturing buffer provided in the kit,

denatured by heating at 100ºC for 10 minutes, chilled on ice and centrifuged for 10 seconds.

5 µL of glycobuffer 2, 5 µL of 10% NP-40 and 15 µL of distilled water were then added to the solution, followed by 5 µL of deglycosylation enzyme cocktail. The reaction was incubated at 37ºC overnight, and samples were subjected to SDS-PAGE and western blotting.

3.2.22. Statistical analysis

Statistical analysis was performed and graphical representations were created in R and Rstudio. The existence of statistically significant differences between groups was assessed through a two-tailed Welch's T-test, considering p-values below 0.05 to be significant. Welch's T-test is a variant of Student's T-test recommended for small sample sizes and/or unequal group variances; as is the case for other parametric tests, it is relatively insensitive to deviations from normality. (McDonald 2014) Graphical representation of the data is based on the mean value of the group, with error bars corresponding to the standard error of the mean (s.e.m.).

3.2.23. Structural modeling and visualization

Visualization of protein structures was carried out with MacPyMOL. Structures derived from crystallization data were employed for human OSM (Protein Data Bank ID: 1EVS) and human LIF (Protein Data Bank ID: 2Q7N). (Deller et al. 2000) (Huyton et al. 2007) A homology model for mouse OSM based on the available human structure was generated with SWISS-MODEL. (Biasini et al. 2014)

3.2.24. Phylogeny inference

Protein sequences were retrieved from the Reference Sequence (RefSeq) database of NCBI and aligned by Clustal Omega. (Maglott et al. 2000) (Sievers et al. 2011) The aligned protein sequences were then used to construct a phylogenetic tree by stochastic heuristics, applying the metapopulation genetic algorithm (metaGA) implemented in MetaPIGA. (Lemmon & Milinkovitch 2002) (Helaers & Milinkovitch 2010)

4. Results

4.1. Structural determinants of human Oncostatin M activity

4.1.1. Readout systems to assess human receptor complex activation

The first step in order to study receptor complex activation required establishing reliable systems to monitor this event. Unfortunately, there are no tools available to track activation of these receptors directly, such as antibodies specifically raised against the phosphorylated forms of OSMR and LIFR.

As a result, studies on OSM signaling have had to rely on indirect measurements of receptor activation. One of the most common approaches is to monitor the phosphorylation of downstream signaling mediators after cytokine stimulation: the most common target has been STAT3, which is tyrosine phosphorylated in response to IL-6 family cytokines. (Akira et al. 1994)

Different human cell lines have been identified that exclusively express either the OSMR/gp130 complex (A375 human melanoma cell line, Fig. 6A) or the LIFR/gp130 complex (JAR human choriocarcinoma cell line, Fig. 6C). (Auguste et al. 1997) By performing cytokine stimulations in parallel in two such cell lines, it becomes then possible to assess the activation of each of the receptors through the comparison of the STAT3 phosphorylation pattern 10 minutes after stimulation. (Chollangi et al. 2012)

To further validate this readout system, siRNA experiments were performed to confirm that the observed STAT3 phosphorylation in A375 and JAR cell lines is a product of the activation of their respective specific receptors. As expected, only siRNA-mediated knockdown of the hOSMR affected STAT3 phosphorylation in A375 cells (Fig. 6B). In a similar fashion, only siRNA directed against hLIFR impaired STAT3 phosphorylation in JAR cells (Fig. 6D).

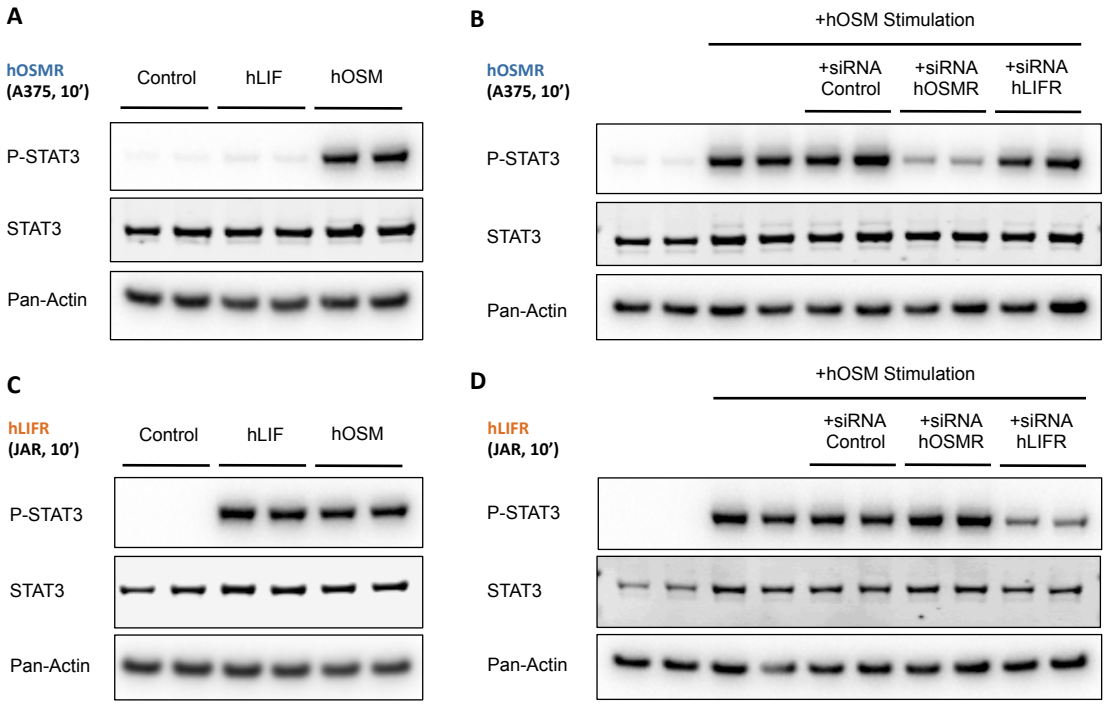

Figure 6: STAT3 phosphorylation reflects hOSMR activation in A375 cells, and hLIFR activation in JAR cells. (A) STAT3 phosphorylation pattern in A375 cells stimulated for 10 minutes with hLIF and hOSM. **(B)** STAT3 phosphorylation pattern in A375 cells treated for 72 hours with the indicated siRNAs, and stimulated for 10 minutes before sample harvesting. **(C)** STAT3 phosphorylation in JAR cells after a 10-minute stimulation with hLIF and hOSM. **(D)** STAT3 phosphorylation in JAR cells incubated for 72 hours after siRNA transfection and subjected to 10-minute cytokine stimulation prior to harvesting.

To corroborate that the variations potentially observed in STAT3 phosphorylation are not just due to a delay in signaling, but a consequence of differential receptor activation properties, a second readout system based on longer-term (24 hour) stimulation experiments was established. Tissue inhibitor of metalloproteinase 1 (TIMP1) upregulation is a well-known target of OSMR activation in different cell types, including hepatic cells, so the HepG2 human hepatoma cell line was selected to monitor hOSMR activation through TIMP1 expression (Fig. 7A). (Richards et al. 1993) (Bugno et al. 1995) Additionally, since STAT3 levels after 24 hours are markedly increased in response to its activation via phosphorylation, long-term hLIFR activation was assessed through measurement of STAT3 expression levels in the JAR human choriocarcinoma cell line (Fig. 7C). (Bugno et al. 1995)

Once again siRNA-mediated knockdown experiments were performed to confirm that TIMP1 expression in HepG2 cells is exclusively due to hOSMR signaling (Fig. 7B),

while STAT3 upregulation in JAR cells upon stimulation is mediated by the hLIFR (Fig. 7D).

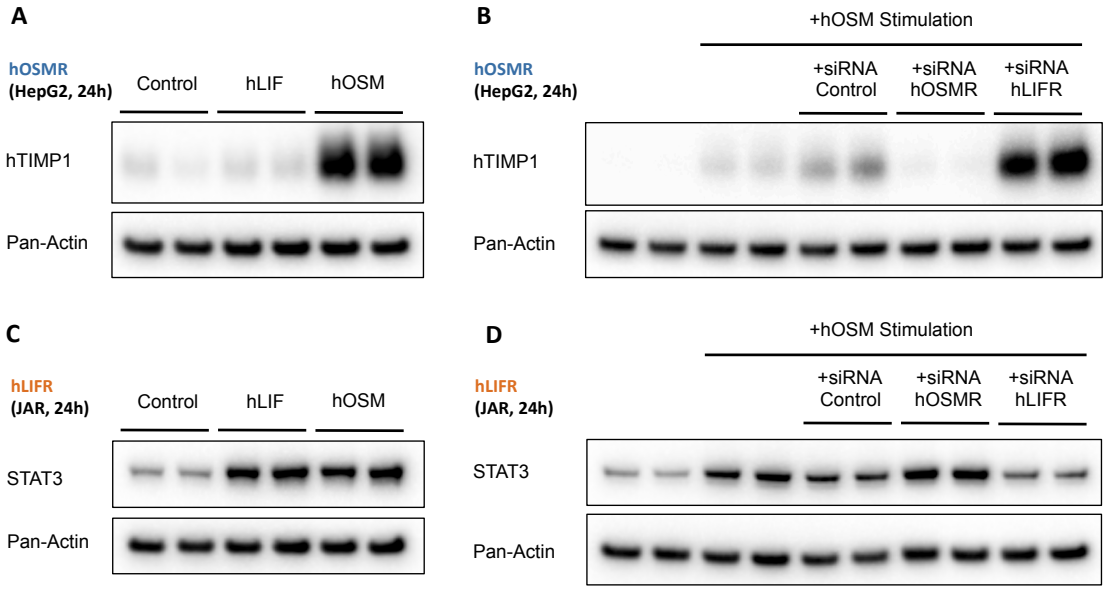

Figure 7: TIMP1 expression after 24 hours reflects hOSMR activation in HepG2 cells, while STAT3 upregulation is a consequence of hLIFR activation in JAR cells. **(A)** TIMP1 expression levels in HepG2 cells stimulated for 24 hours with hLIF and hOSM. **(B)** TIMP1 expression in HepG2 cells treated for 48 hours with the indicated siRNAs, and subsequently stimulated for an additional 24 hours before sample harvesting. **(C)** Total STAT3 levels in JAR cells after a 24-hour stimulation with hLIF and hOSM. **(D)** Total STAT3 expression levels in JAR cells incubated for 48 hours after siRNA transfection before being subjected to an additional 24-hour cytokine stimulation treatment prior to harvesting.

In addition, a non-Western blot based assay system was implemented to confirm long-term biological activity caused by hOSMR activation. OSM was first described as a growth regulator of human tumor cells, inhibiting the proliferation of A375 melanoma cells as well as other tumor-derived cell lines. (Zarling et al. 1986) This ability was apparent after seeding A375 cells at low density and stimulating them with either hOSM or hLIF: after 5 days, only hOSM proved capable of inhibiting cell growth (Fig. 8A).

One of the most popular methods to easily monitor cellular growth is the MTT assay, a colorimetric assay employed to detect living cells. (Mosmann 1983) By means of this method the effect of different treatments on cell proliferation could be quantified, evidencing the growth inhibition caused by hOSM (Fig. 8B).

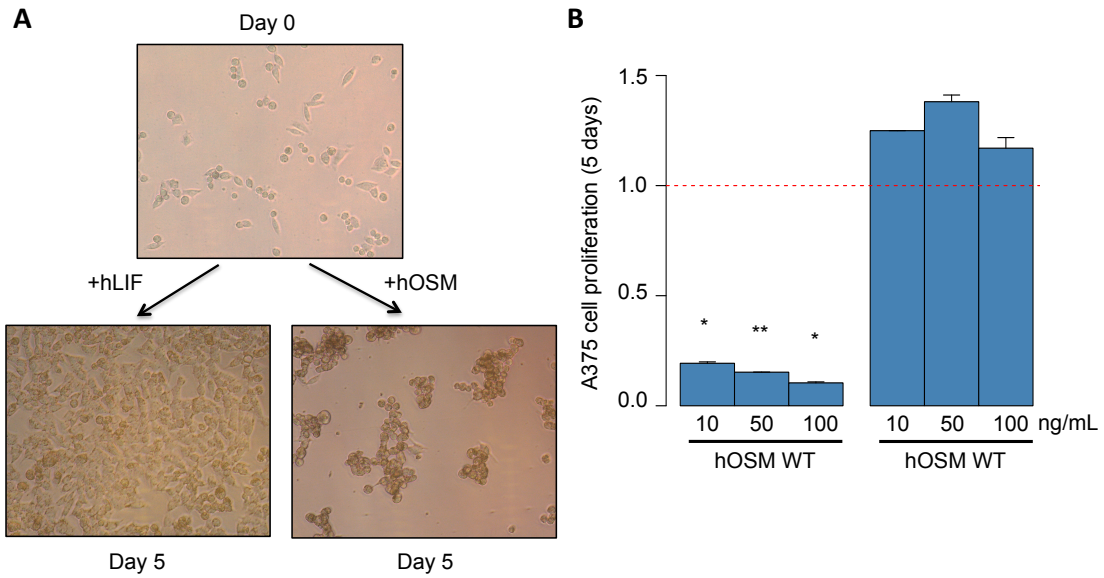

Figure 8: A375 cell line proliferation reflects hOSMR activation after 5 days. (A) Proliferation of A375 cells after 5 days is inhibited by stimulation with 10 ng/mL of hOSM, but unaffected by treatment with equal amounts of hLIF. **(B)** Quantification of A375 cell proliferation via MTT assay, 5 days after plating and stimulation with the indicated concentrations of either hOSM or hLIF (n=3 for each group).

4.1.2. Production of recombinant human Oncostatin M

Initially, the nucleotide sequence of hOSM flanked by NdeI and SlaI restriction sites was amplified by PCR and cloned in a pET-26b(+) vector. This vector contains a C-terminal His-tag and a T7 promoter, which enables recombinant protein expression upon IPTG induction in *Escherichia coli* (*E. coli)*. The resulting plasmid was then transformed in the BL21 (DE3) *E. coli* strain, commonly used for recombinant protein production due to its high protein yield.

However, when expressed in BL21 (DE3) hOSM tended to misfold and aggregate into insoluble inclusion bodies: while expression in the insoluble fraction was very robust, little soluble protein could be detected 2 hours after IPTG induction (Fig. 9A). This particularity had forced past studies on OSM and mutant OSM variants to apply a variety of strategies to obtain these recombinant proteins in soluble form. Successful OSM purification methods include its recovery and refolding from inclusion bodies (Sporeno et al. 1994), its fusion and subsequent cleavage to a solubility tag such as GST (Deller et al. 2000) (Chollangi et al. 2012) or its expression in eukaryotic systems such as *Picchia pastoris* (Kong et al. 2009) or Chinese hamster ovary cells. (Kallestad et al. 1991)

Since most of these approaches require additional time-consuming steps, an effort to establish a protocol for production of soluble hOSM in *E. coli* was made to facilitate the generation of the cytokine variants to be studied in this project. Given that disulfide bonds had been shown to be critical for proper OSM folding and function, (Kallestad et al. 1991) it appeared likely that OSM aggregation might be a consequence of the reducing redox state of the prokaryotic cytoplasm preventing disulfide bond formation. (Baneyx & Mujacic 2004)

In order to test this hypothesis, the same hOSM plasmid was transformed into SHuffle® T7 Express competent *E. coli.* This is a modified BL21 (DE3) strain expressing DsbC, a chaperone/disulfide bond isomerase that catalyzes disulfide bond formation and promotes proper folding of disulfide bond-containing proteins. (de Marco 2009) When expressed in this strain hOSM was detected in the soluble fraction as early as 2 hours after induction (Fig. 9B).

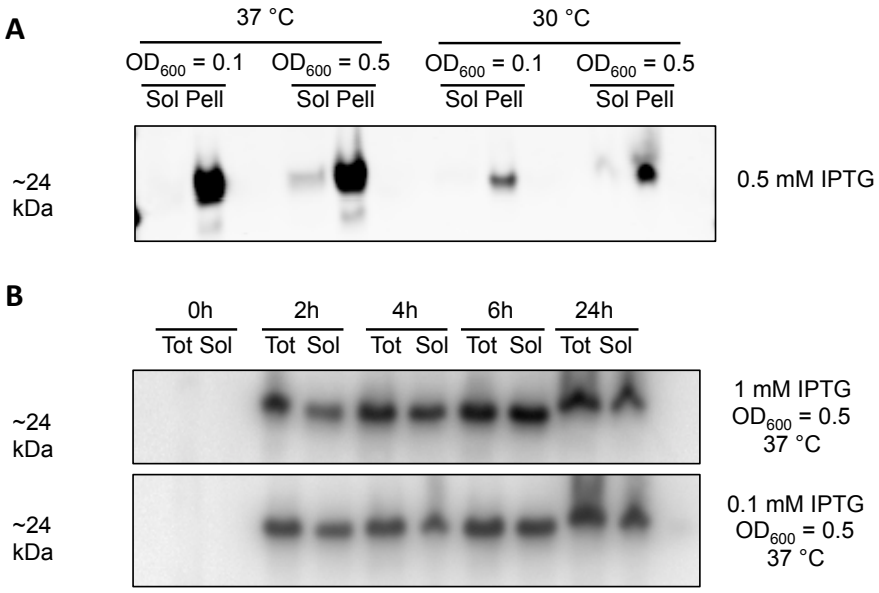

Figure 9: The presence of DsbC, a chaperone/disulfide bond isomerase, enables soluble recombinant hOSM expression in *E. coli.* Western blots using penta-His antibody to detect recombinant His-tagged hOSM production are shown. **(A)** Expression of hOSM in BL21 (DE3) *E. coli* 2 hours after induction with 0.5 mM IPTG at different temperatures and densities, as measured by OD_{600}. The soluble (Sol) and insoluble (Pell) protein fractions are compared, with very little soluble OSM in evidence. **(B)** Expression of hOSM in SHuffle® T7 Express *E. coli* at 30ºC after induction at an OD_{600} of 0.5-0.7. Comparing soluble (Sol) and total (Tot) protein fractions, the majority of OSM produced by this strain appears to be soluble.

Having achieved soluble hOSM expression, the next step was to establish a protocol for purification of the recombinant protein out of the bacterial cell lysate. The

inclusion of a C-terminal His-tag greatly facilitated this task, enabling most of the bacterial contaminants to be washed away out of a Ni-NTA affinity gel column by gravity flow before eluting the recombinant protein with increasing amounts of imidazole (Fig. 10).

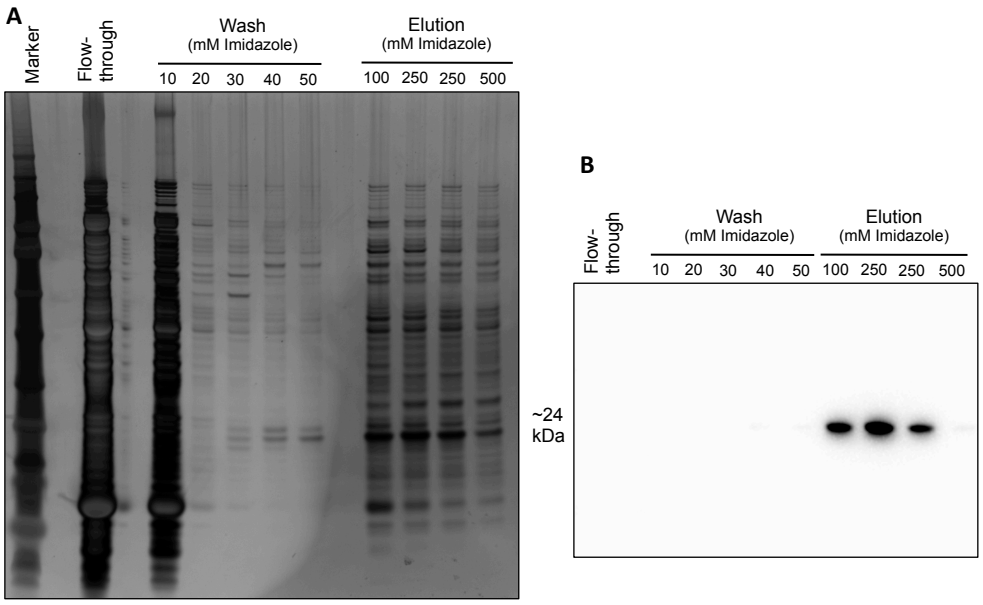

Figure 10: Effective recovery of recombinant His-tagged hOSM by Ni-NTA purification. (A) Silver staining reveals most of the bacterial proteins in the soluble fraction are eliminated during the purification procedure. Strong bands at approximately 24 kDa in the first three elution steps correspond to the eluted recombinant hOSM. **(B)** Western blotting of the same samples using penta-His antibody to detect recombinant His-tagged hOSM indicates that the protein is retained in the affinity gel during the washing steps, and efficiently eluted through increasing imidazole concentrations.

The eluted recombinant hOSM was concentrated by using a centrifugal filter with a molecular weight cutoff of 10 kDa, which also enabled the removal of imidazole from the solution. This led to a recombinant protein solution comparable to the commercially available cytokine in terms of purity, as assessed by silver staining: 83.2% purity was estimated for the commercial recombinant hOSM, and 74.6% for the His-tagged recombinant hOSM (Fig. 11).

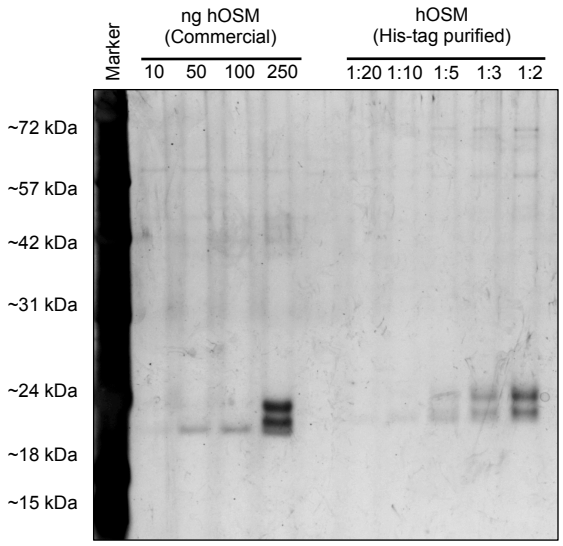

Figure 11: Recovered recombinant His-tagged hOSM is highly pure. Silver staining of increasing concentrations of commercial hOSM and His-tagged recombinant hOSM is shown, proving both preparations to be similarly devoid of bacterial-derived contaminating proteins.

Finally, biological activity of soluble hOSM produced in this manner was compared to commercially available human LIF (hLIF) and hOSM by stimulation of HepG2 cells for 15 minutes (Fig. 12A) and 24 hours (Fig. 12B). Phosphorylation patterns of known downstream mediators of OSMR activation after 10 minutes were identical for both preparations. The same trend was observed when examining the upregulation of hOSM targets genes after 24 hours, confirming the validity of the method for soluble active hOSM production in *E. coli*.

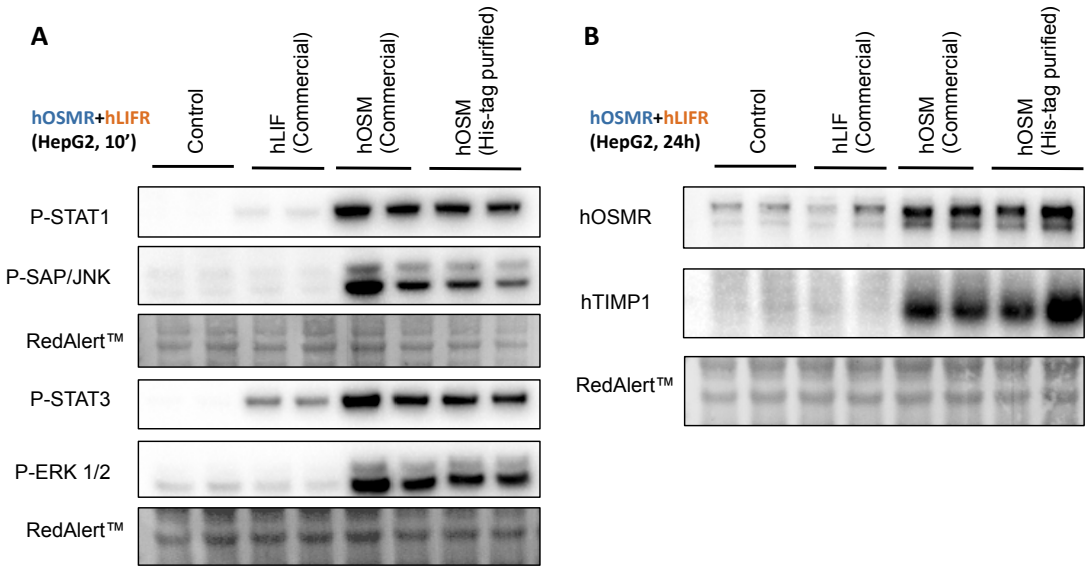

Figure 12: Recombinant His-tagged hOSM displays biological activity comparable to the commercially available cytokine. (A) Western blots of HepG2 cell samples harvested after a 10-minute stimulation with 20 ng/mL of the cytokines show comparable phosphorylation patterns for commercial and His-tag purified hOSM. **(B)** Western blots of HepG2 cells harvested after a 24-hour stimulation with the indicated cytokines evidence similar upregulation of hOSMR and TIMP1 expression for commercial and His-tag purified hOSM.

However, not all the modified protein variants described in the following sections could be successfully expressed in a prokaryotic system (data not shown). To address this issue a mammalian-based expression system had to be established, employing human FreeStyle™ 293-F cells adapted to suspension growth in serum-free medium. In the first place, the nucleotide sequences for wild-type (WT) hOSM and hLIF were cloned into three different mammalian expression vectors (pcDNA™ 3.1(+), pFLAG-CMV-3 and pCAGGS), preceded by a Kozak consensus sequence and either their native signal peptide or the signal peptide from pre-pro-trypsin (PPT) to ensure secretion of the recombinant cytokines into the medium.

FreeStyle™ 293-F cells were then transfected with the different plasmids according to the manufacturer's instructions. A comparison of the expression levels 3 days after transfection showed robust secretion of recombinant hOSM in the supernatant, but much lower production of human LIF (Fig. 13A). Since the pCAGGS plasmid with native signal peptide evidenced the highest level of expression for hOSM, constructs using this plasmid were employed for all further experiments.

A deglycosylation test confirmed that the apparent smearing and differences in molecular weight in comparison to the bacterial-derived cytokines are caused by glycosylation, a post-translational modification exclusive of eukaryotic cells (Fig. 13B). These initial tests were followed by the assessment of the expression over time for both cytokines, in order to determine the optimal incubation time after transfection. While hOSM expression reached maximum levels as little as 3 days after transfection and plateaued afterwards, hLIF expression markedly increased during the first week and did not peak until days 7-8 (Fig. 13C).

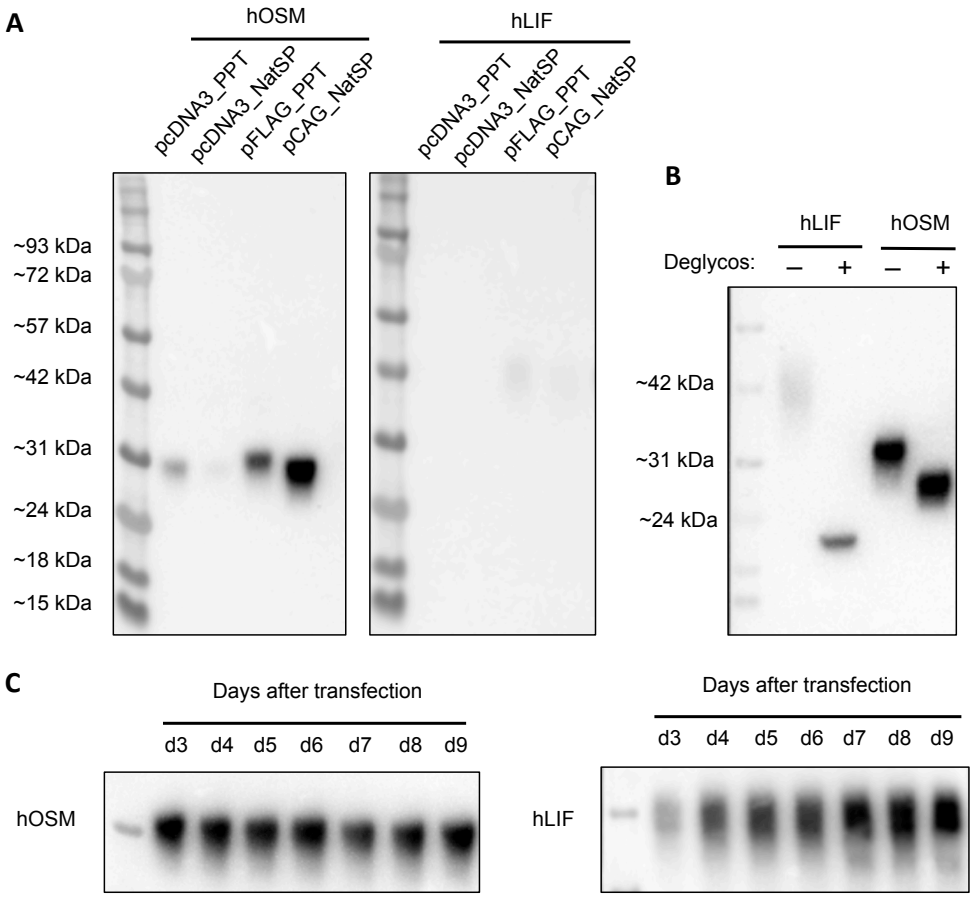

Figure 13: Optimization of recombinant protein expression in mammalian cells. (A) Western blot of FreeStyle™ 293-F cell medium 3 days after transfection with the indicated vectors, using penta-His antibody to detect recombinant protein expression, reveals strong expression of hOSM cloned into the PCAGGS vector. **(B)** Western blot of untreated (-) and deglycosylated (+) mammalian-derived hLIF and hOSM after purification demonstrates the occurrence of post-translational modifications. **(C)** Western blot of FreeStyle™ 293-F cell medium collected 3 to 9 days after transfection with either hOSM or hLIF in the pCAGGS vector indicates different peak production times for each cytokine.

Despite the additional post-translational modifications, cytokines produced in this way evidenced equivalent biological activity when compared to commercial bacterial-derived proteins (Fig. 14A-B). Importantly, both hOSM-based and hLIF-based variant cytokines could be efficiently expressed by the FreeStyle™ 293-F cells and recovered by His-tag purification (Fig. 14C), permitting a detailed examination of the interaction between hOSM and its receptors.

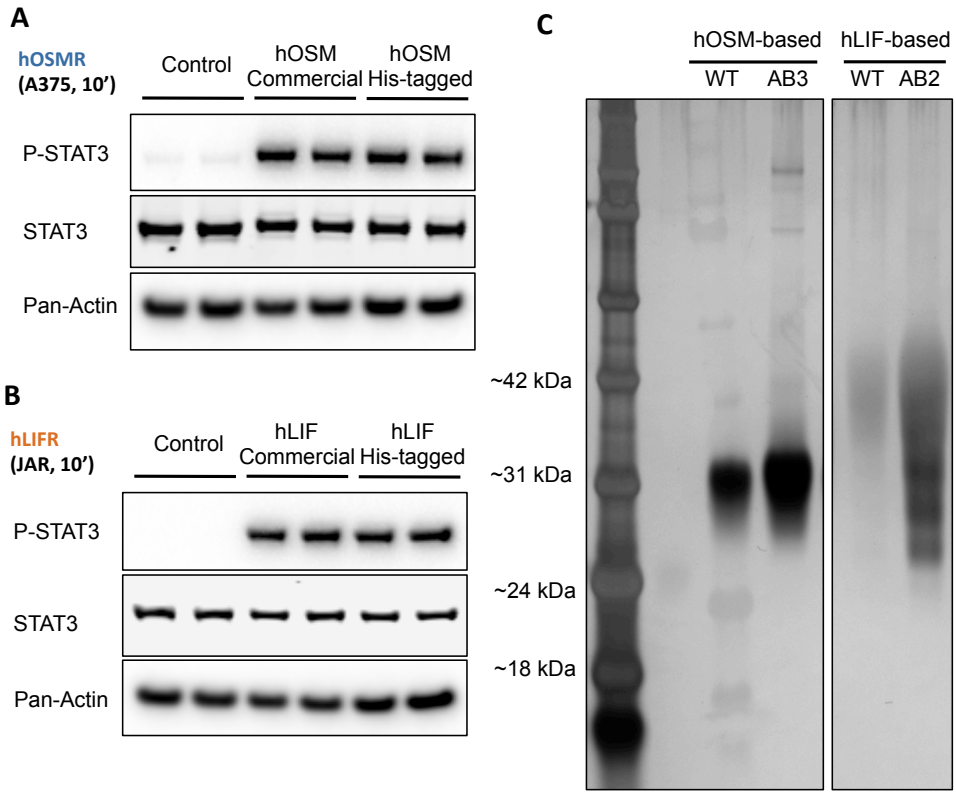

Figure 14: Recombinant protein expression in mammalian cells results in highly pure, active cytokines. (A) Western blot of A375 cell samples collected after a 10-minute stimulation with hOSM shows similar biological activity between bacterial-derived (commercial) and mammalian-derived cytokines. **(B)** Western blot of JAR cell samples subjected to a 10-minute stimulation with hLIF evidences comparable biological activity for bacterial-derived (commercial) and mammalian-derived cytokines. **(C)** Silver staining of purified hOSM-based and hLIF-based chimeric cytokines.

4.1.3. Human Oncostatin M-based chimeric proteins identify a critical binding region for human receptor complex activation

Despite the fact that binding site III of hOSM is a relatively large region of the cytokine, composed by the N-terminal part of the AB loop, the whole BC loop and the N-terminal part of helix D (Fig. 15A-B), very few details about its interaction with both OSMR and LIFR are known so far. It has been proved that the presence of an FXXK motif in the N-terminal D-helix, which is conserved in all LIFR-binding cytokines and corresponds to phenylalanine 160 (F160) and lysine 163 (K163) in hOSM, is critical for both LIFR and OSMR activation. (Hudson et al. 1996) (Deller et al. 2000) Additionally, it was recently shown that shortening the length of the BC loop had positive effects on receptor affinity. (Chollangi et al. 2012)

Given the scarcity of information available, one of the starting goals of this project was to explore whether any of the regions in binding site III could explain the unique ability of hOSM to activate the hOSMR/gp130 complex. To this end chimeric cytokines combining different regions of hOSM and hLIF were designed (Fig. 15C), created by overlap extension PCR and cloned into the pCAGGS mammalian expression vector through PacI and AscI restriction sites.

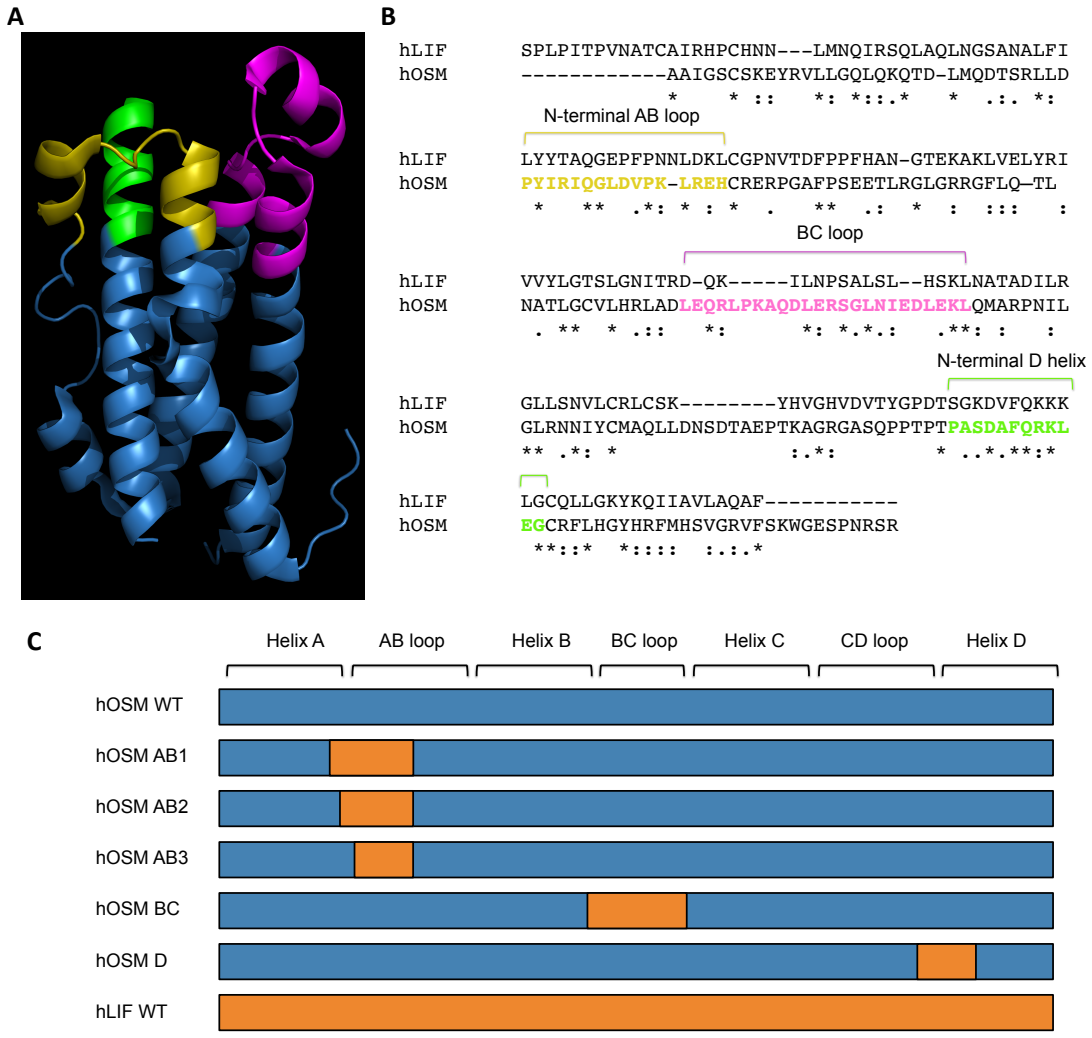

Figure 15: Design of human OSM/LIF chimeric cytokines. (A) Three-dimensional model of human OSM. The N-terminal AB loop region is shown in yellow, the BC loop in purple and the N-terminal D-helix in green. **(B)** Alignment of mature hLIF and hOSM amino acid sequences with Clustal Omega. Residues forming binding site III of hOSM, corresponding to the N-terminal AB loop, the BC loop and the N-terminal part of helix D, are highlighted. Asterisks (*) denote fully conserved residues, colons (:) indicate groups with strongly similar properties and periods (.) are used for groups with weakly similar properties. **(C)** Schematic representation of the constructed chimeric cytokines for hOSM, in which different parts of binding site III were replaced by the equivalent amino acid sequences from hLIF.

Replacements of three different lengths were made for the AB loop: the longest one, termed AB1, involved the substitution of the region between residues proline 33 (P33) to histidine 48 (H48) of hOSM by residues leucine 43 (L43) to leucine 59 (L59) of hLIF, or vice versa. For the shorter AB2 chimeras the replaced region started with arginine 36 (R36) in hOSM and threonine 46 (T46) in hLIF, while the AB3 chimeras started at leucine 40 (L40) of hOSM and the glutamic acid at position 50 (E50) of hLIF.

A single replacement length was chosen for both the BC loop chimera and the N-terminal D-helix chimera. The BC loop substitution involved the region between leucine 88 (L88) and glutamic acid 109 (E109) in hOSM and between glutamine 122 (Q122) and serine 134 (S134) in hLIF. Finally, the D-helix chimera replaced the amino acids from proline 155 (P155) to glutamic acid 165 (E165) of hOSM with serine 151 (S151) to leucine 161 (L161) of hLIF.

After expression and purification of these variants in a mammalian expression system, the impact of the different binding site III regions in receptor activation ability was investigated through cell stimulation assays with the purified hOSM-based chimeric cytokines.

Receptor activation was first monitored indirectly after a 10-minute stimulation by measuring the phosphorylation levels of STAT3, as previously detailed. In A375 cells, which lack hLIFR expression, it became clear that replacements of any length in the AB loop of hOSM abrogated OSMR activation (Fig. 16A). Substituting the N-terminal region of the D helix led to a decrease in receptor activation, while a BC loop had no measurable effect.

Conversely, stimulation of the hOSMR-deficient JAR cells showed normal STAT3 phosphorylation patterns for every variant except for the AB1 chimera, indicating that the secondary structure of the chimeras remains stable. This observation also suggests that the differences in amino acid composition between the AB loops of hOSM and hLIF only appear to be critical for hOSMR activation (Fig. 16B-C).

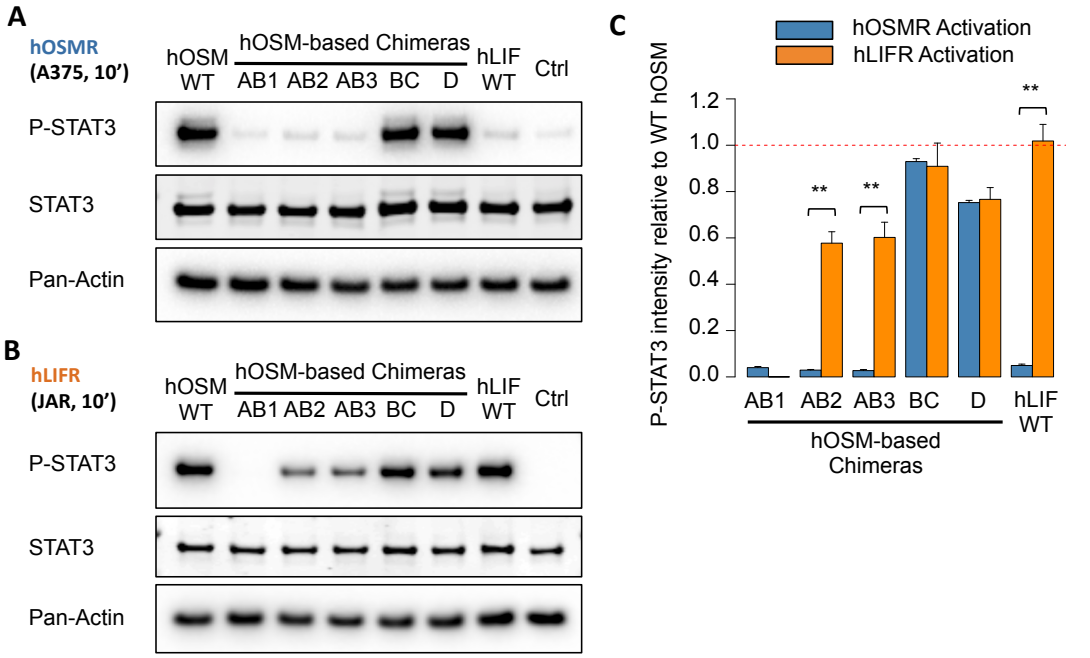

Figure 16: Short-term receptor activation ability of hOSM-based chimeric cytokines identifies the AB loop as critical for hOSMR activation. (A) Western blot of A375 cell samples after a 10-minute stimulation with 25 ng/mL of WT hOSM, WT hLIF and the different hOSM-based chimeric cytokines created. STAT3 phosphorylation reflects hOSMR activation, while total STAT3 and pan-Actin serve as loading controls. **(B)** Western blot of JAR cell samples after a 10-minute stimulation with 25 ng/mL of the indicated cytokines. STAT3 phosphorylation reflects hLIFR activation, while total STAT3 and pan-Actin serve as loading controls. **(C)** Quantitative analysis of hOSMR and hLIFR activation levels after a 10-minute stimulation treatment with the indicated chimeric cytokines, relative to the observed activation for WT hOSM. Values were normalized against total STAT3 levels and presented as mean ± s.e.m. (n=5). Statistical significance was determined by Welch's T-test, with (**) indicating p-values < 0.01.

A second set of 24-hour cell stimulation experiments confirmed that replacing the AB loop of hOSM leads to a complete loss of hOSMR activation, as reflected by the expression levels of TIMP1 in HepG2 cells (Fig. 17A). In comparison, the upregulation of total STAT3 in JAR cells is consistent with normal hLIFR activation by either hOSM or hLIF (Fig. 17B-C). The differing biological activity of the AB loop hOSM chimeras was further proved by a 5-day proliferation assay. While WT hOSM and the BC loop and N-terminal D-helix chimeras proved able to activate the hOSMR and thus inhibit cell proliferation of A375 cells, none of the AB loop chimeras or WT hLIF impaired cell growth (Fig. 17D).

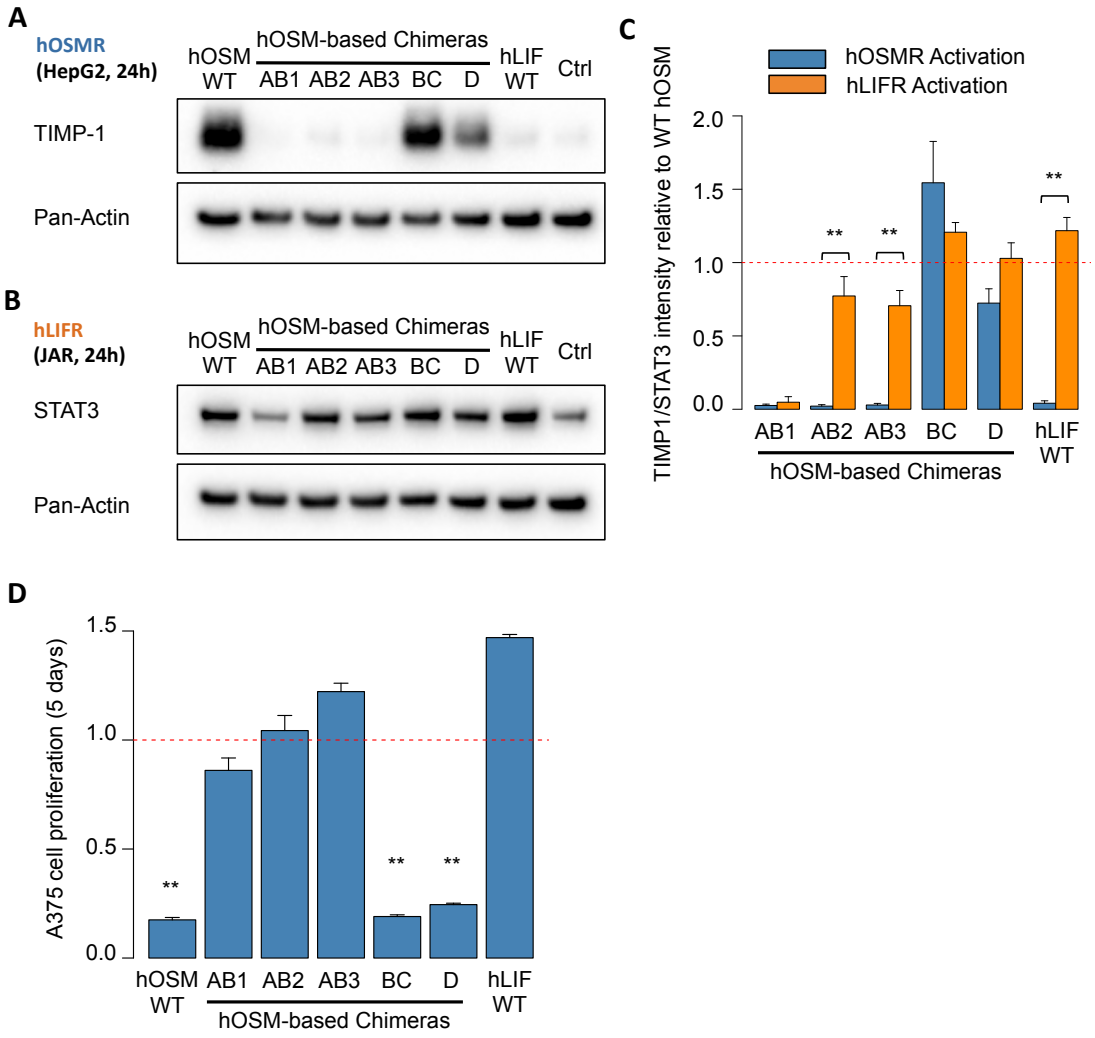

Figure 17: Long-term receptor activation ability of hOSM-based chimeric cytokines confirms the importance of the AB loop in hOSMR activation. (A) Western blot of HepG2 cell samples after a 24-hour stimulation with 25 ng/mL of the specified cytokines. TIMP1 expression reflects hOSMR activation, while pan-Actin levels serve as loading control. **(B)** Western blot of JAR cell samples after a 24-hour stimulation with 25 ng/mL of WT hOSM, WT hLIF and the different hOSM-based chimeric cytokines created. Total STAT3 levels reflect hLIFR activation, while pan-Actin serves as loading control. **(C)** Quantitative analysis of hOSMR and hLIFR activation levels after a 10-minute stimulation treatment with the indicated chimeric cytokines, relative to the observed activation for WT hOSM. Values were normalized against pan-Actin levels and presented as mean ± s.e.m. (n=5). **(D)** A375 proliferation levels after a 5-day stimulation treatment with 10 ng/mL of the indicated chimeric cytokines, relative to the proliferation of the control group. Values are given as mean ± s.e.m. (n=3). Statistical significance was determined by Welch's T-test, with (**) indicating p-values < 0.01.

4.1.4. Leukemia Inhibitory Factor-based chimeric proteins acquire the ability to activate the human Oncostatin M Receptor

These experiments indicate that the amino acid sequence of the AB loop within binding site III of hOSM is key to explain its unique receptor activation profile within the IL-6 cytokine family. However, they did not rule out the existence of other differentiating features outside site III that may also be required for hOSMR activation. To address this question a number of hLIF-based chimeric cytokines with different regions of site III replaced by their hOSM equivalents were created: these include the individual replacements of the N-terminal AB loop, BC loop and N-terminal helix D regions, as well as the combined substitution of the two regions (AB loop and helix D) influencing hOSM-hOSMR binding (Fig. 18).

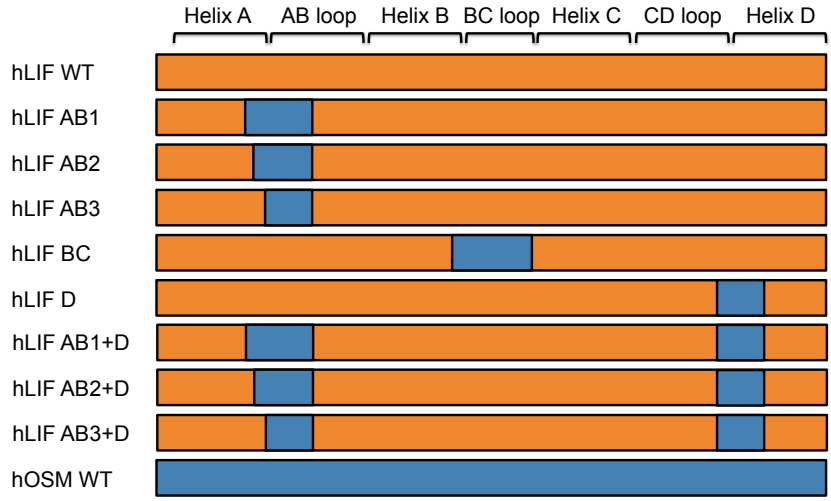

Figure 18: Design of human LIF/OSM chimeric cytokines. Schematic representation of the hLIF-based chimeric cytokines created, with different regions in the N-terminal AB loop, the BC loop and the N-terminal part of helix D substituted by their hOSM counterparts.

Mirroring in the previous set of experiments, receptor activation was first assessed through the comparison of STAT3 phosphorylation levels after a 10-minute stimulation. All the chimeras were still able to signal through the hLIFR, but replacing the N-terminal region of the AB loop alone was not enough for the hLIF-based chimera to activate the hOSMR. On the other hand, the combined replacement of the N-terminal AB loop and helix D regions was sufficient to achieve hOSMR stimulation, albeit always at lower levels than WT hOSM (Fig 19A-C).

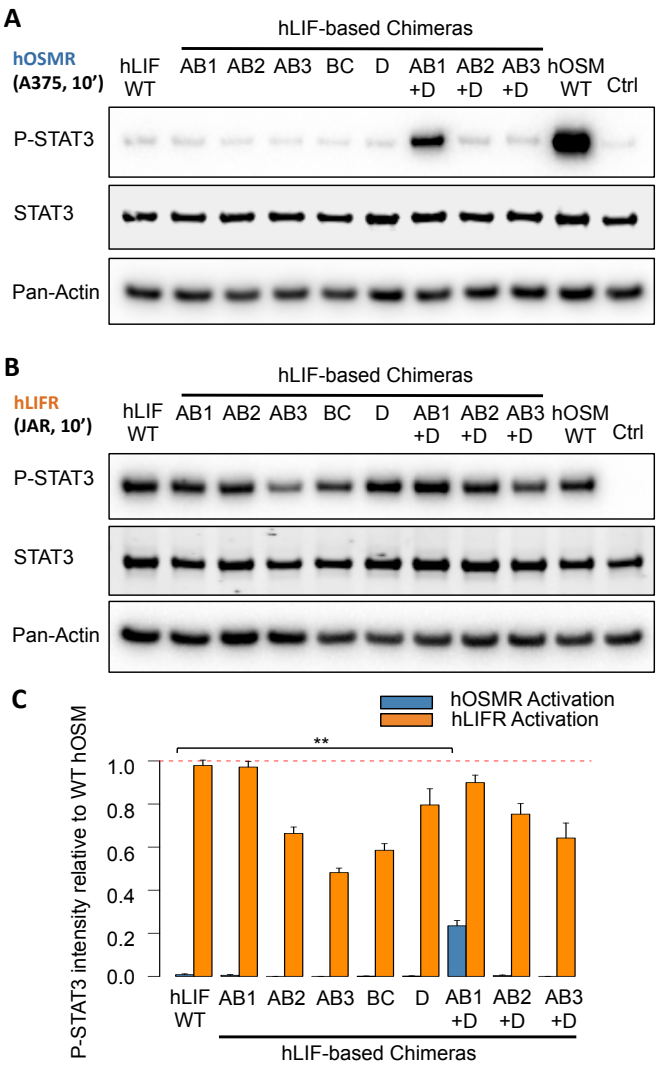

Figure 19: Short-term receptor activation ability of hLIF-based chimeric cytokines indicates the importance of site III regions in receptor interaction. (A) Western blot of 10-minute stimulation of A375 cells with 25 ng/mL of WT hOSM, WT hLIF and the different hLIF-based chimeric cytokines. STAT3 phosphorylation reflects hOSMR activation, with total STAT3 and pan-Actin serving as loading controls. **(B)** Western blot of JAR cell samples stimulated for 10 minutes with 25 ng/mL of WT hOSM, WT hLIF and the indicated hLIF-based chimeras. STAT3 phosphorylation is an indication of hLIFR activation, while total STAT3 and pan-Actin serve as loading controls. **(C)** Quantitative analysis of hOSMR and hLIFR activation levels for the different cytokines tested, relative to WT hOSM. Values were normalized against total STAT3 levels and presented as mean ± s.e.m. (n=5). Statistical significance was determined by Welch's T-test, with (**) indicating p-values < 0.01.

24-hour stimulation experiments confirmed these findings, with all cytokines tested again activating the hLIFR but only the combined AB loop + D-helix hLIF-based chimera being able to stimulate hOSMR-dependent TIMP1 expression in HepG2 (Fig

20A-C). Additional evidence that the differential structural features leading to hOSMR specificity are contained within site III of hOSM could be provided by a longer-term biological assay based on A375 cell proliferation. After 5 days of stimulation, only WT hOSM and the AB1 + D hLIF-based chimera were able to inhibit cell growth (Fig. 20D).

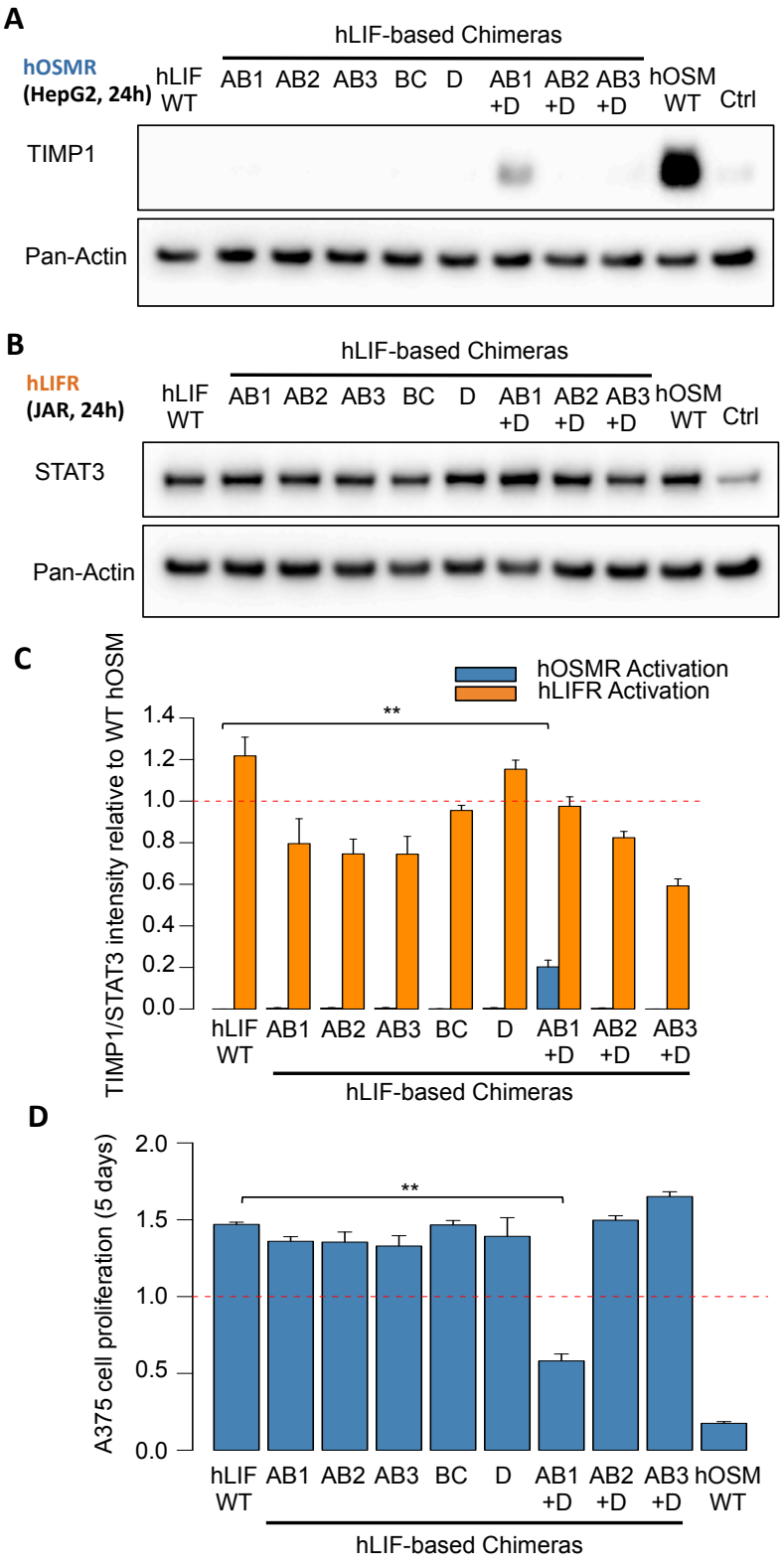

Figure 20: Long-term receptor activation ability of hLIF-based chimeric cytokines confirms the importance of binding site III region for hOSMR interaction. (A) Western blot of HepG2 cell samples collected after a 24-hour stimulation with 25 ng/mL of the indicated cytokines. TIMP1 expression reflects hOSMR activation, with pan-Actin serving as loading control. **(B)** Western blot of JAR cell samples stimulated with 25 ng/mL of WT hOSM, WT hLIF and the indicated hLIF-based chimeras for 24 hours. Total STAT3 expression is an indication of hLIFR activation, while pan-Actin is used as a loading control. **(C)** Quantitative analysis of hOSMR and hLIFR activation levels for the different cytokines tested, relative to WT hOSM. Values were normalized against pan-Actin levels and presented as mean ± s.e.m. (n=5). **(D)** A375 proliferation levels after stimulation for 5 days with 10 ng/mL of the indicated chimeric cytokines, relative to the proliferation observed for the control group. Values are presented as mean ± s.e.m. (n=3). Statistical significance was determined by Welch's T-test, with (**) indicating p-values < 0.01.

4.1.5. Alanine scanning of human Oncostatin M highlights specific residues involved in human receptor complex activation

To assess the relative importance of each residue composing the N-terminal AB loop and the N-terminal helix D regions of hOSM in receptor activation, point mutants were created by site-directed mutagenesis, transformed into SHuffle® T7 Express competent *E. coli*, expressed and His-tag purified as previously detailed.

For each mutant a single amino acid within the region was replaced by alanine, thus removing all side chain atoms past the β-carbon. The biological function of each of these mutants gives then an indication of the importance of its original side chain functional group: mutations in functional epitopes should lead to a loss of function for the variant protein, while mutations in residues that hinder binding will result in increased function instead. (Cunningham & Wells 1989)

In the first place, alanine mutants for the AB loop region between proline 33 (P33) and cysteine 49 (C49) were assessed for their short-term hOSMR/hLIFR activation ability (Fig 21A-B). Several of these residues specifically abrogated hOSMR activation, including glutamine 38 (Q38), glycine 39 (G39), leucine 45 (L45) and to a lesser extent tyrosine 34 (Y34) and valine 42 (V42), while mutations of leucine 40 and cysteine 49 also had a large impact on the activation of the hLIFR (Fig 21C).

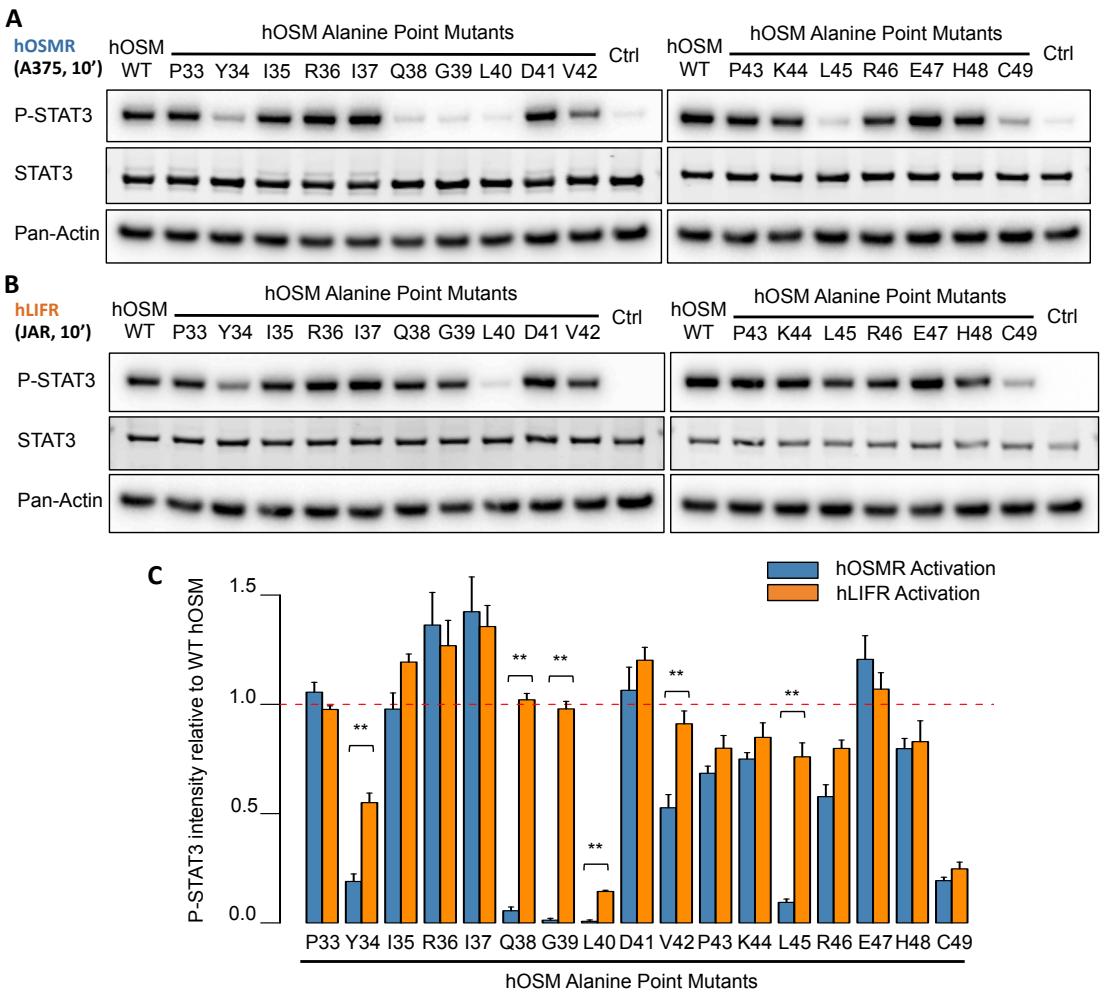

Figure 21: Short-term receptor activation ability of hOSM AB loop point mutants identifies critical amino acids for receptor activation. (A) Western blot of 10-minute stimulation of A375 cells with 25 ng/mL of WT hOSM and the indicated point mutants. STAT3 phosphorylation was used to monitor hOSMR activation, with total STAT3 and pan-Actin serving as loading controls. **(B)** Western blot of JAR cell samples stimulated for 10 minutes with 25 ng/mL of WT hOSM and the different AB loop point mutants shown. STAT3 phosphorylation measures hLIFR activation, while total STAT3 and pan-Actin are included as loading controls. **(C)** Quantitative analysis of hOSMR and hLIFR activation levels for the different point mutants tested, relative to WT hOSM. Values were normalized against total STAT3 levels and presented as mean ± s.e.m. (n=5). Statistical significance was determined by Welch's T-test, with (**) indicating p-values < 0.01.

The crucial role of these residues in receptor activation was confirmed by 24-hour stimulation experiments (Fig. 22A-C), with the detailed amino acid replacements displaying the same effects observed after 10 minutes except for V42. These results were further reinforced by a 5-day cell proliferation assay on A375 cells. In accordance with the shorter-term stimulation experiments, all of the mutants

identified as playing an important role in the interaction between hOSM and the hOSMR showed impaired inhibition of cell growth when compared to the WT cytokine (Fig. 22D).

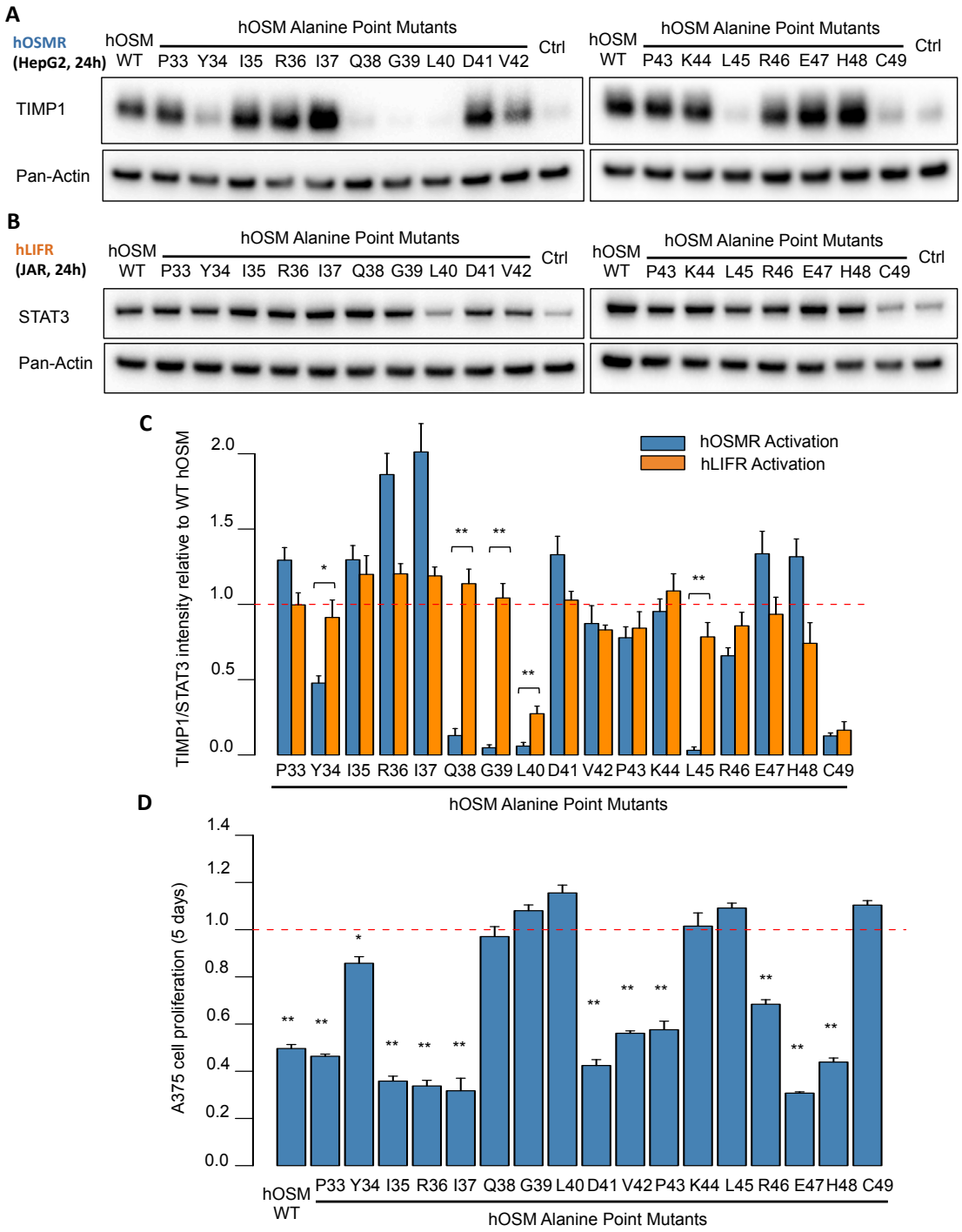

Figure 22: Long-term receptor activation ability of human OSM AB loop point mutants validates critical cytokine residues. (A) Western blot of HepG2 cell samples stimulated for 24 hours with 25 ng/mL of WT human OSM and the detailed point mutants. TIMP1 expression reflects human OSMR activation, with pan-Actin serving as loading control. **(B)** Western blot of JAR cell samples harvested after a 24-hour

stimulation with 25 ng/mL of WT human OSM and the different AB loop point mutants indicated. STAT3 phosphorylation measures human LIFR activation, with pan-Actin included as loading control. **(C)** Quantitative analysis of OSMR and LIFR activation levels for the different point mutants tested, relative to WT hOSM. Values were normalized against pan-Actin levels and presented as mean ± s.e.m. (n=5). **(D)** A375 proliferation was measured by an MTT assay after stimulation for 5 days with 10 ng/mL of the indicated point mutants, relative to the proliferation observed for the control group. Values are presented as mean ± s.e.m. (n=3). Statistical significance was determined by Welch's T-test, with (*) corresponding to p-values < 0.05 and (**) indicating p-values < 0.01.

Interestingly, most of these residues appear to be conserved among OSM orthologs from several different species, hinting at the existence of a shared mechanism for OSMR activation among mammalians (Fig. 23).

```
Mus.musculus              54   PYIRLQNLNTPDLRAAC   70
Rattus.norvegicus         55   PYILHQNLNTLTLRAAC   71
Homo.sapiens              57   PYIRIQGLDVPKLREHC   73
Pan.troglodytes           57   PYIRIQGLDVPKLREHC   73
Gorilla.gorilla           57   PYIRIQGLDVPKLREHC   73
Macaca.mulatta            57   PYIRIQGLDIPKLREHC   73
Bos.taurus                54   PYIHLQGLHSPVLQEHC   70
Capra.hircus              54   PYIRFQGLESPKLQEHC   70
Ovis.aries                54   PYIRFQGLESPKLQEHC   70
Sus.scrofa                54   PYIRMQGLDTPGLKEHC   70
Canis.lupus               54   LYIRSQGLDKNGLKEHC   70
Felis.catus               54   PYISIQGLDKDGLKEHC   70
                                     **  *.*.       *
```

Figure 23: Critical AB loop residues are conserved in mammalians. The equivalent residues to Y34, Q38, G39, L40 and L45 in human OSM are present in most mammalian OSM orthologs compared, with the exception of G39 in mouse and rat OSM. Sequence alignment was performed with Clustal Omega, with amino acid sequence numbers corresponding to the precursor proteins in all species studied.

Since the replacement of the N-terminal region of helix D, in addition to the AB loop, was necessary before the hLIF-based chimera was able to activate the hOSMR, alanine scanning of this region was also performed. As expected the two critical residues forming the conserved FXXK motif, phenylalanine 160 (F160) and lysine 163 (K163), proved to be crucial for activating both hOSMR and hLIFR in a 10-minute stimulation assay. Additionally, substitution of the proline at the start of the helix (P153) specifically impaired hOSMR activation (Fig. 24A-C).

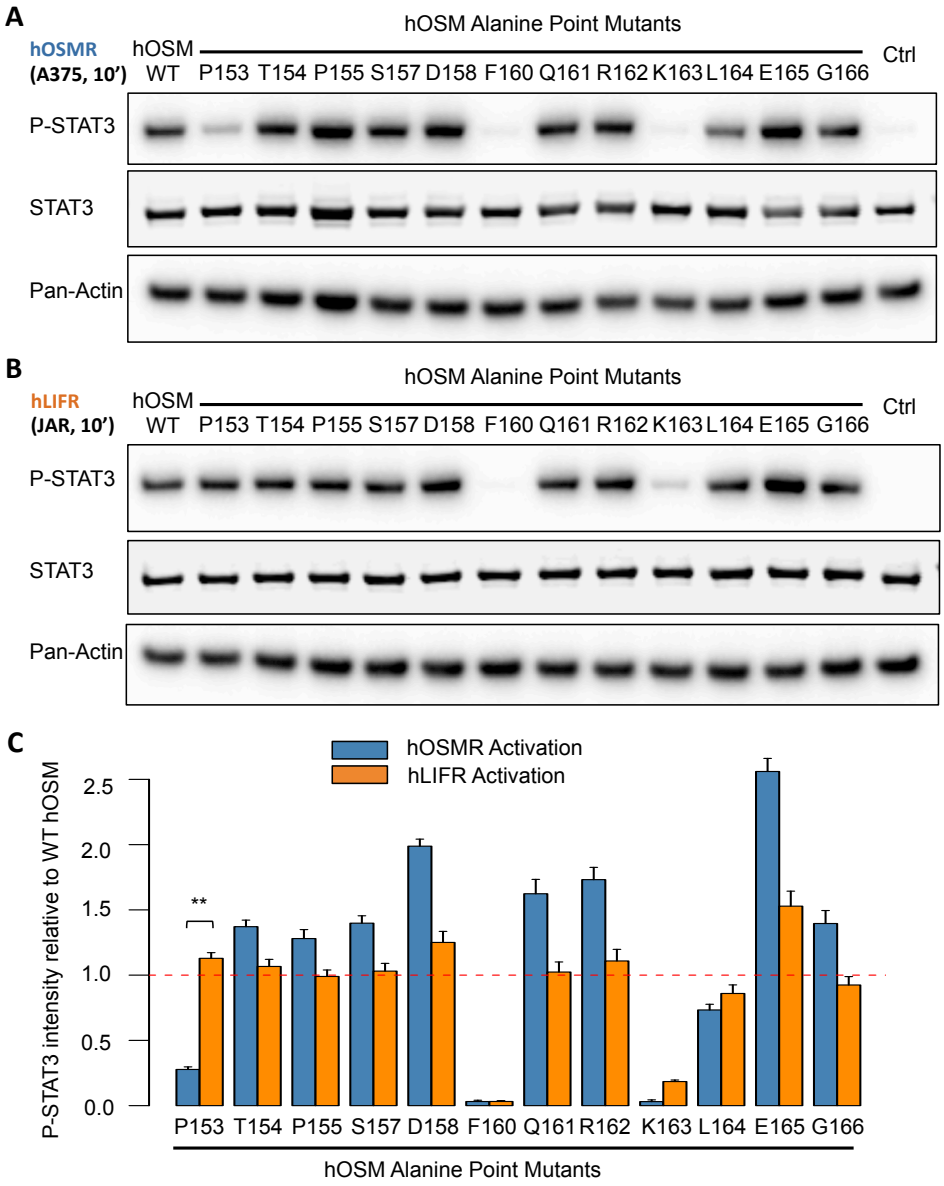

Figure 24: Short-term receptor activation ability of hOSM N-terminal helix D point mutants assesses individual residue involvement. (A) Western blot of A375 cell samples collected after a 10-minute stimulation with 25 ng/mL of WT hOSM and the different helix D point mutants. STAT3 phosphorylation is a sign of hOSMR activation, with total STAT3 and pan-Actin serving as loading controls. **(B)** Western blot of JAR cell samples harvested after stimulation for 10 minutes with 25 ng/mL of WT hOSM and the helix D point mutants shown. STAT3 phosphorylation measures hLIFR activation, while total STAT3 and pan-Actin are included as loading controls. **(C)** Quantitative analysis of hOSMR and hLIFR activation levels for the mutants tested, relative to WT hOSM. Values were normalized against total STAT3 levels and presented as mean ± s.e.m. (n=5). Statistical significance was determined by Welch's T-test, with (**) indicating p-values < 0.01.

24-hour stimulation experiments confirmed the specific importance of P154 for hOSMR activation, with the alanine mutant showing normal hLIFR activation but impaired hOSMR-dependent activity (Fig. 25A-C). Final proof of the requirement of proline 154 for hOSMR activation was given by a 5-day cell proliferation assay, in which the P154 point mutant is shown to lack the growth inhibition activity derived from hOSMR activation in A375 cells (Fig. 25D).

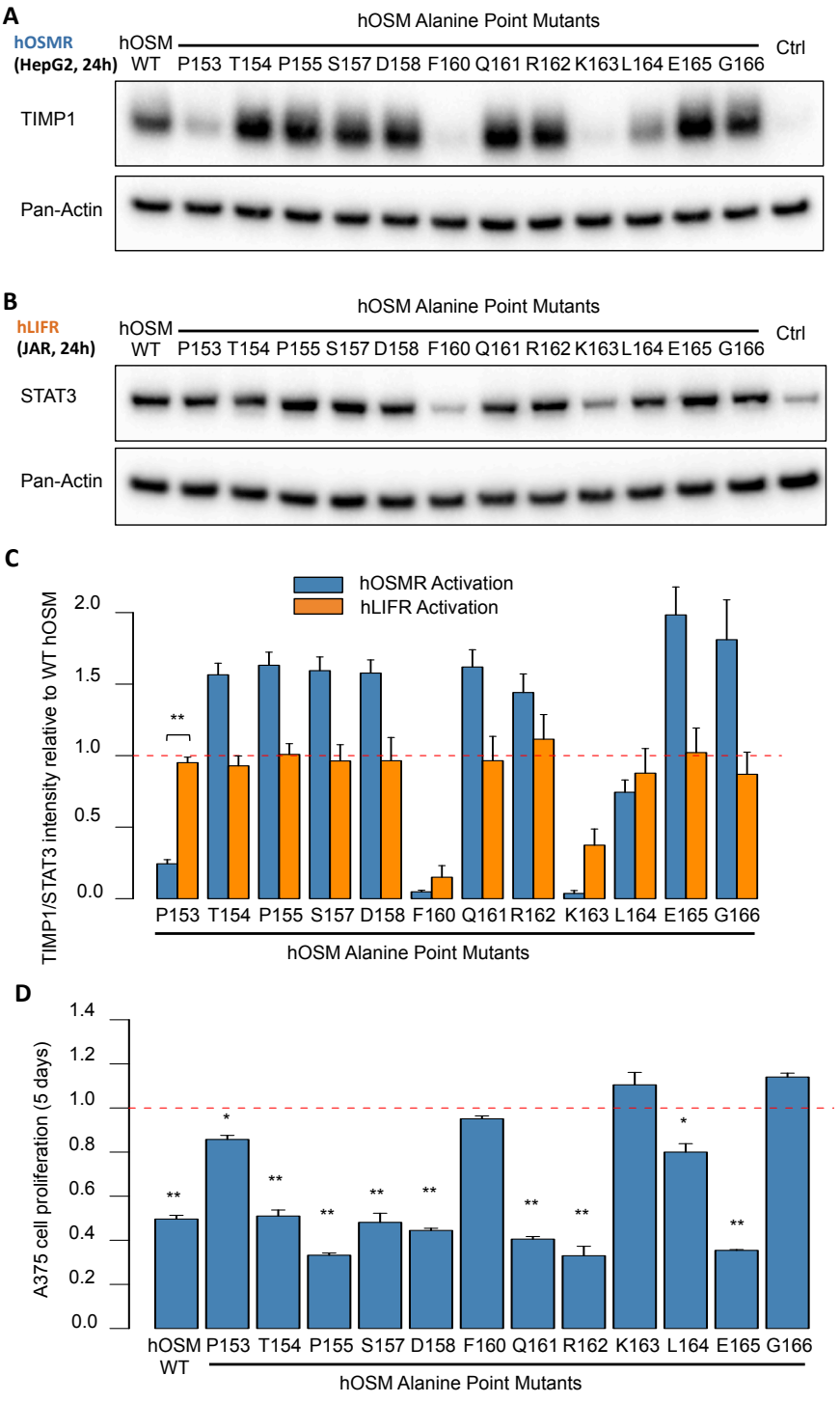

Figure 25: Long-term receptor activation ability of hOSM N-terminal helix D point mutants confirms critical amino acids in the region. (A) Western blot samples of HepG2 cells subjected to a 24-hour stimulation with 25 ng/mL of WT hOSM and the helix D point mutants shown. TIMP1 expression derives from hOSMR activation, with pan-Actin serving as loading control. **(B)** Western blot of JAR cell samples harvested after a 24-hour stimulation with 25 ng/mL of WT hOSM and the D-helix point mutants indicated. Increased STAT3 levels are a consequence of hLIFR activation, while pan-Actin is used as a loading control. **(C)** Quantitative analysis of hOSMR and hLIFR activation levels relative to WT hOSM. Values were normalized against pan-Actin levels and presented as mean ± s.e.m. (n=5). **(D)** A375 proliferation levels were assessed by an MTT assay after 5-day stimulation with 10 ng/mL of the indicated cytokines, relative to the proliferation observed for the unstimulated control group. Values are presented as mean ± s.e.m. (n=3). Statistical significance was determined by Welch's T-test, with (*) corresponding to p-values < 0.05 and (**) indicating p-values < 0.01.

4.2. Structural basis for the species-dependent receptor complex activation properties of human and murine Oncostatin M

4.2.1. Design and production of chimeric mouse/human Oncostatin M cytokines

Besides the unique OSMR/gp130 activation ability explored in the first part of this work, perhaps the most intriguing characteristic of OSM is the widely divergent receptor activation abilities of the human and mouse cytokines. This difference may be reflecting the natural evolutionary process of new cytokines, as will be discussed in more detail in section 5.4: phylogenetic analyses reveal both mOSM and mOSMR to be more distant from their common ancestor proteins, in comparison to other mammalian orthologs (Fig. 26A-C).

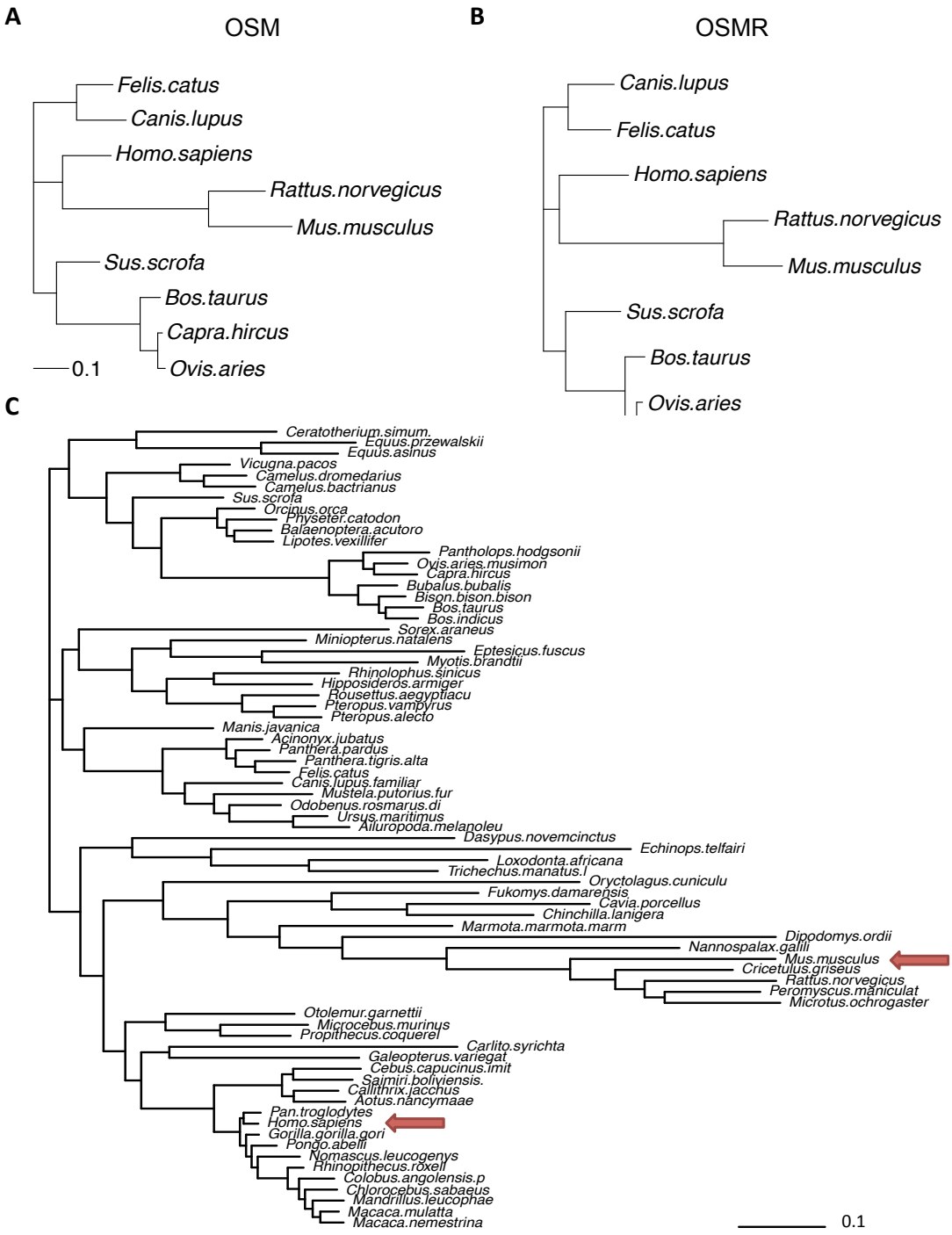

Figure 26: Murine OSM and OSMR orthologs are more evolutionarily distant from the ancestral state. (A) Phylogenetic analysis of 9 selected OSM orthologs evidences a higher degree of deviation from the common ancestor for the murine protein. **(B)** Phylogenetic distances of the OSMR follow the same pattern detected for its ligand among 9 selected mammal species. **(C)** Unbiased phylogenetic analysis of every OSM protein sequence contained in the RefSeq database confirms the evolutionary divergence of the murine ortholog. Phylogenetic analyses were performed by stochastic heuristics in MetaPIGA. (Helaers & Milinkovitch 2010)

Perhaps as a result of this evolutionary process, the murine protein is unable to activate any of the human receptor complexes and appears to act specifically through mOSMR/gp130, while hOSM cannot activate mOSMR and only signals through the mLIFR/gp130 complex in murine cells. (Ichihara et al. 1997) (Lindberg et al. 1998)

Despite this marked difference in their receptor activation abilities, both cytokines are surprisingly similar in terms of amino acid composition: when the mature sequences of hOSM and mOSM were aligned, 48.89% of their residues turned out to be completely conserved and an additional 17.78% had strongly similar properties (Fig. 27B). In contrast hLIF and hOSM, despite sharing a common receptor, only show 24.39% identity when the same comparison is made (Fig. 15B).

This fact suggests that the differing specificity between human and mouse OSM might be explained by just a small number of variations, possibly in the regions required for hOSMR interaction identified in the first section of this work. In order to test this hypothesis, chimeric proteins based on mOSM were designed in which the two main regions influencing OSMR binding within site III, the AB loop and the N-terminal D-helix, had been replaced by their hOSM counterparts (Fig. 27A-C).

In this occasion two different replacement lengths were selected for both the N-terminal AB loop and the N-terminal helix D constructs. In the shortest AB loop chimera, termed AB1, the fragment from leucine 35 (L35) to alanine 46 (A46) of mOSM was replaced by residues isoleucine 37 (I37) to histidine 48 (H48) of hOSM. In the AB2 chimera the region replaced was extended to valine 52 (V52) of mOSM and glycine 54 (G54) of hOSM, respectively.

For the N-terminal helix D chimeras, the shortest modification (chimera D1) consisted of residues threonine 142 (T142) to serine 152 (S152) of mOSM being replaced by residues alanine 156 (A156) to glycine 166 (G166) of hOSM. In the longest version the replacement started with arginine 138 (R138) of the murine cytokine instead, while the hOSM fragment being inserted commenced in glutamine 149 (Q149).

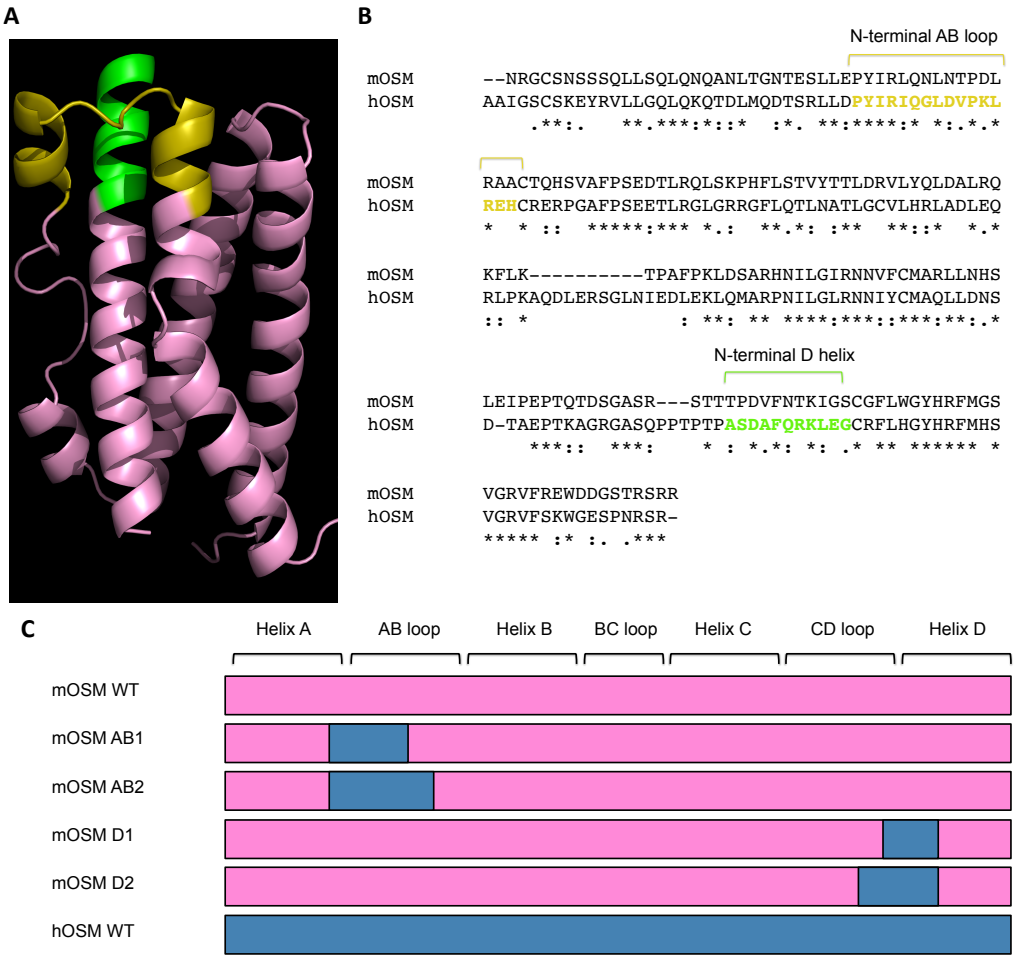

Figure 27: Design of human/mouse OSM chimeric cytokines. (A) Three-dimensional model of mouse OSM. The N-terminal AB loop region is depicted in yellow, and the N-terminal D-helix is shown in green. **(B)** Alignment of mature mouse and human OSM amino acid sequences with Clustal Omega. Residues forming binding site III of OSM, corresponding to the N-terminal AB loop and the N-terminal part of helix D, are highlighted. Asterisks (*) denote fully conserved residues, colons (:) indicate groups with strongly similar properties and periods (.) are used for groups with weakly similar properties. **(C)** Schematic representation of the constructed chimeric cytokines based on mOSM, in which different lengths of the N-terminal AB loop and the N-terminal helix D were replaced by the equivalent amino acid sequences from hOSM.

Considering the difficulties faced in expressing the previous hOSM/hLIF chimeras in a prokaryotic system, a mammalian expression system was selected from the start for the production of mOSM variants. Accordingly, the WT mOSM sequence was cloned from NIH3T3 cDNA into pcDNA™ 3.1(+), pFLAG-CMV-3 and pCAGGS mammalian expression vectors with a Kozak consensus sequence and either the signal peptide from pre-pro-trypsin (PPT) or its native signal peptide.

After transfection of the different constructs into FreeStyle™ 293-F cells, expression and secretion of the cytokine was assessed after three days (Fig. 28A). Both pFLAG and pCAGGS vectors led to robust expression, but due to the presence of additional modifications in the pFLAG construct (an N-terminal FLAG tag and PPT signal peptide) the pCAGGS construct was employed for all subsequent experiments.

Recombinant mOSM produced after transfection was then purified and subjected to a deglycosylation assay, which confirmed that the observed smearing of the purified protein after SDS-PAGE separation is due to post-translational glycosylation and not degradation (Fig. 28B). A time-course experiment monitoring recombinant protein expression in FreeStyle™ 293-F cells showed peak levels of mOSM production 4-5 days after transfection, so all mOSM-derived proteins were harvested at this time point (Fig. 28C).

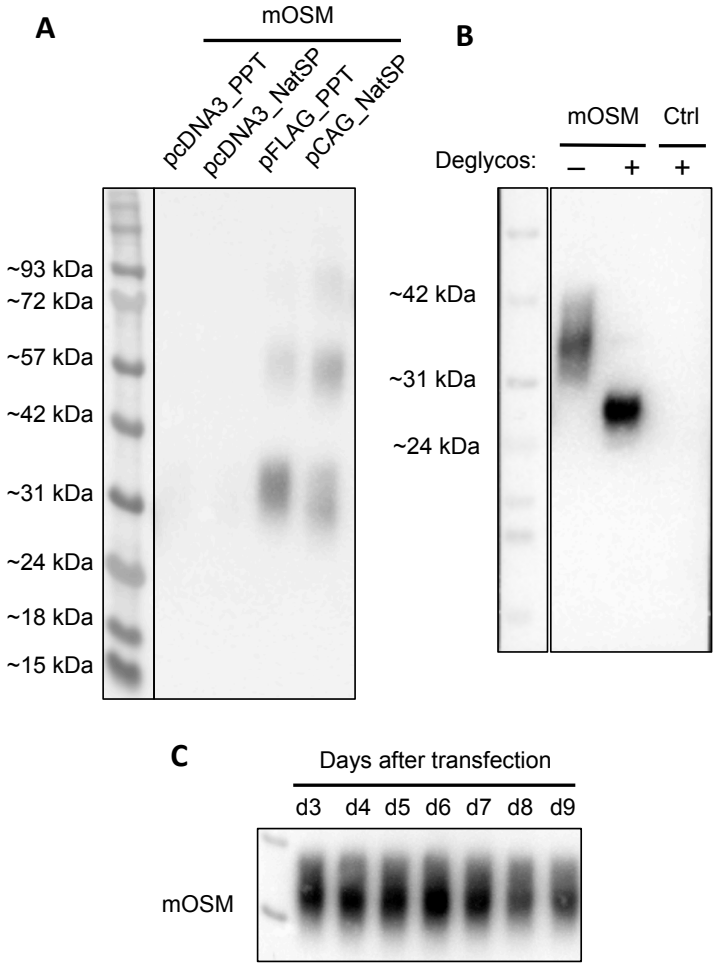

Figure 28: Expression of recombinant mOSM in a mammalian system. (A) Western blot of FreeStyle™ 293-F cell medium 3 days after transfection with the indicated vectors containing the mature mOSM sequence, using penta-His antibody to detect recombinant protein expression. **(B)** Western blot of FreeStyle™ 293-F cell medium samples collected 3 to 9 days after transfection with mOSM in the pCAGGS vector

indicates a peak production time after 4-5 days. **(C)** Western blot of untreated (-) and deglycosylated (+) mammalian-derived mOSM after purification indicates the presence of post-translational modifications.

The biological activity of the purified mOSM was also tested, and proved comparable to a commercial bacterial-derived cytokine in a short-term NIH3T3 murine fibroblast cell stimulation assay (Fig. 29A). In light of these results the different chimeric proteins, along with the WT mOSM version, were sequence-optimized for expression in mammalian cells and constructed from overlapping nucleotides designed with DNAWorks. (Hoover & Lubkowski 2002) The different synthetic genes were assembled through PCR and cloned into the pCAGGS mammalian expression vector via PacI and AscI restriction enzyme sites inserted at the 5' and 3' ends, respectively. After verification of the constructs by DNA sequencing, they were transfected into FreeStyle™ 293-F cells and His-tag purified, resulting in strong expression for the sequence-optimized (SO) WT and all of the mouse/human chimeras created (Fig. 29B).

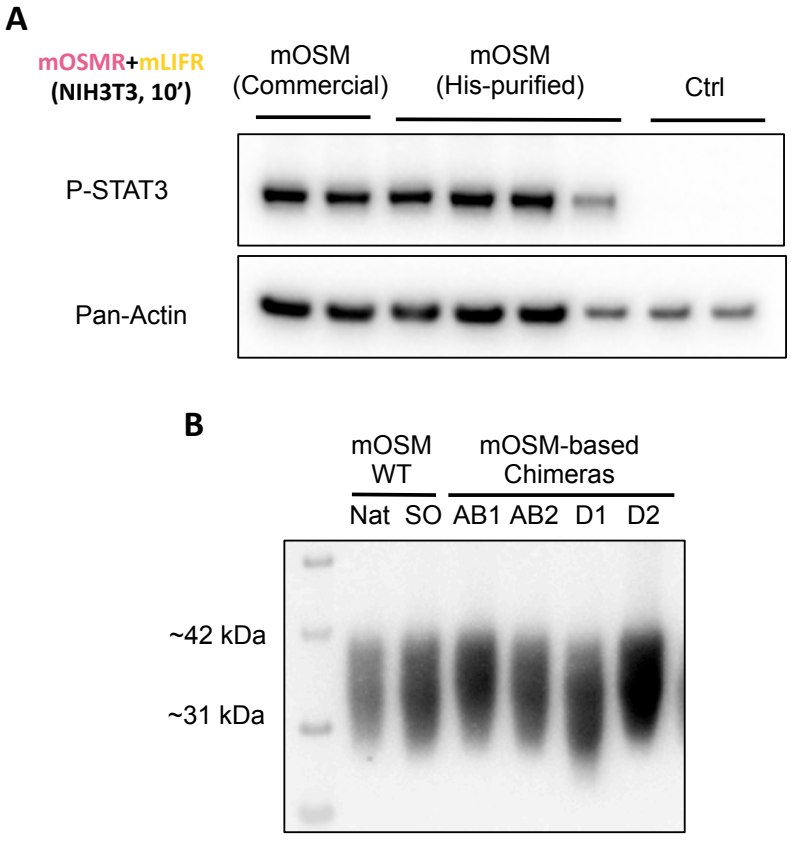

Figure 29: Activity of recombinant mOSM and production of mOSM-based chimeras. (A) Western blot of NIH3T3 cell samples subjected to a 10-minute stimulation with mOSM shows comparable biological activity for the bacterial-derived (commercial) and mammalian-derived cytokine. **(B)** Western blot of purified

mOSM, comparing native (Nat) and sequence-optimized (SO) expression in the WT and confirming expression of all the constructed chimeras.

4.2.2. Murine Oncostatin M-based chimeric proteins identify a critical region for species-specific receptor complex activation

Once purified, the ability of the murine-based OSM chimeras to activate the human receptor complexes was tested first in a short-term stimulation assay. Interestingly, even the shortest exchange in the AB loop of mOSM proved sufficient to enable hOSMR activation, reinforcing the importance of this region for hOSMR interaction (Fig. 30A). hLIFR activation was also clearly within the ability of the AB loop chimeras, and very low levels were also observed for the N-terminal helix D chimeras (Fig 30B-C). As expected, WT mOSM showed a complete lack of activation for either of the human receptors.

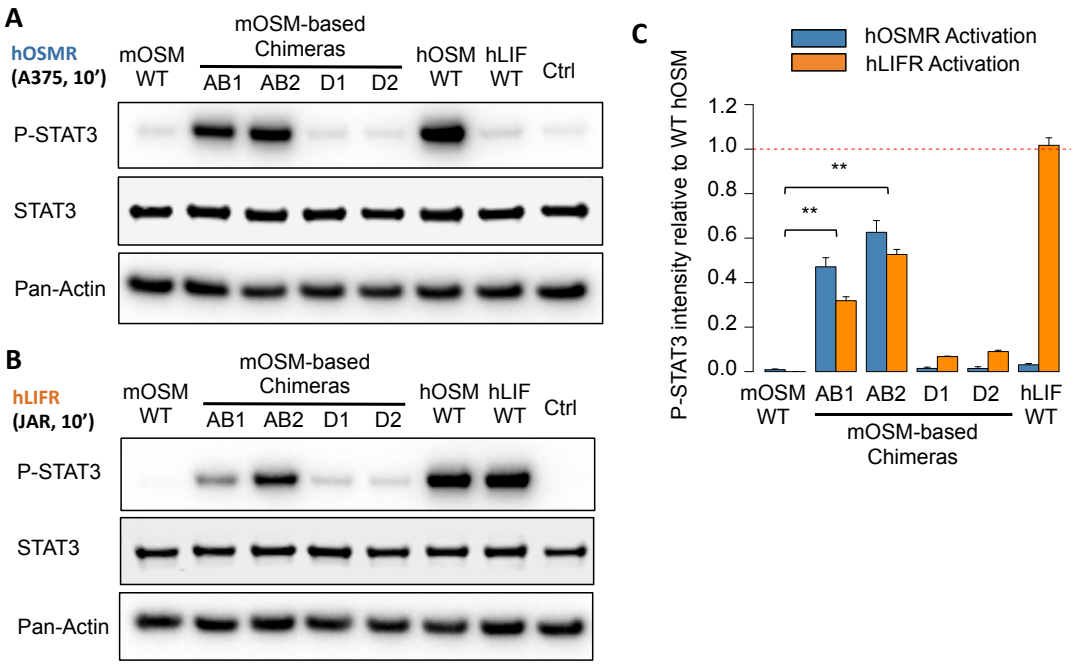

Figure 30: Short-term receptor activation ability of mOSM-based chimeric cytokines identifies the AB loop as a differential feature between human and murine OSM. (A) Western blot of A375 cell samples after a 10-minute stimulation with 25 ng/mL of WT mOSM, WT hOSM, WT hLIF and the four mOSM-based chimeric cytokines created. STAT3 phosphorylation reflects hOSMR activation, while total STAT3 and pan-Actin serve as loading controls. **(B)** Western blot of JAR cell samples after a 10-minute stimulation with 25 ng/mL of the detailed cytokines. In this case STAT3 phosphorylation reflects hLIFR activation, while total STAT3 and pan-Actin serve as loading controls. **(C)** Quantitative analysis of hOSMR and hLIFR activation levels after a 10-minute stimulation treatment with the indicated cytokines, relative to the observed activation for WT hOSM. Values were normalized against total

STAT3 levels and presented as mean ± s.e.m. (n=5). Statistical significance was determined by Welch's T-test, with (**) indicating p-values < 0.01.

The same activation pattern was observed after 24-hour stimulation experiments. Expression levels of hOSMR and hLIFR target genes confirm the affinity of the AB loop mOSM-based chimeras for both receptor complexes, as well as an apparent low-level binding of the D helix chimeras to the hLIFR complex (Fig. 31A-C). Long-term activation of the hOSMR/gp130 complex was further assessed with the same results: only stimulation with the WT hOSM or the murine AB loop chimeras led to hOSMR-mediated inhibition of cell proliferation in A375 cells after 5 days (Fig. 31D).

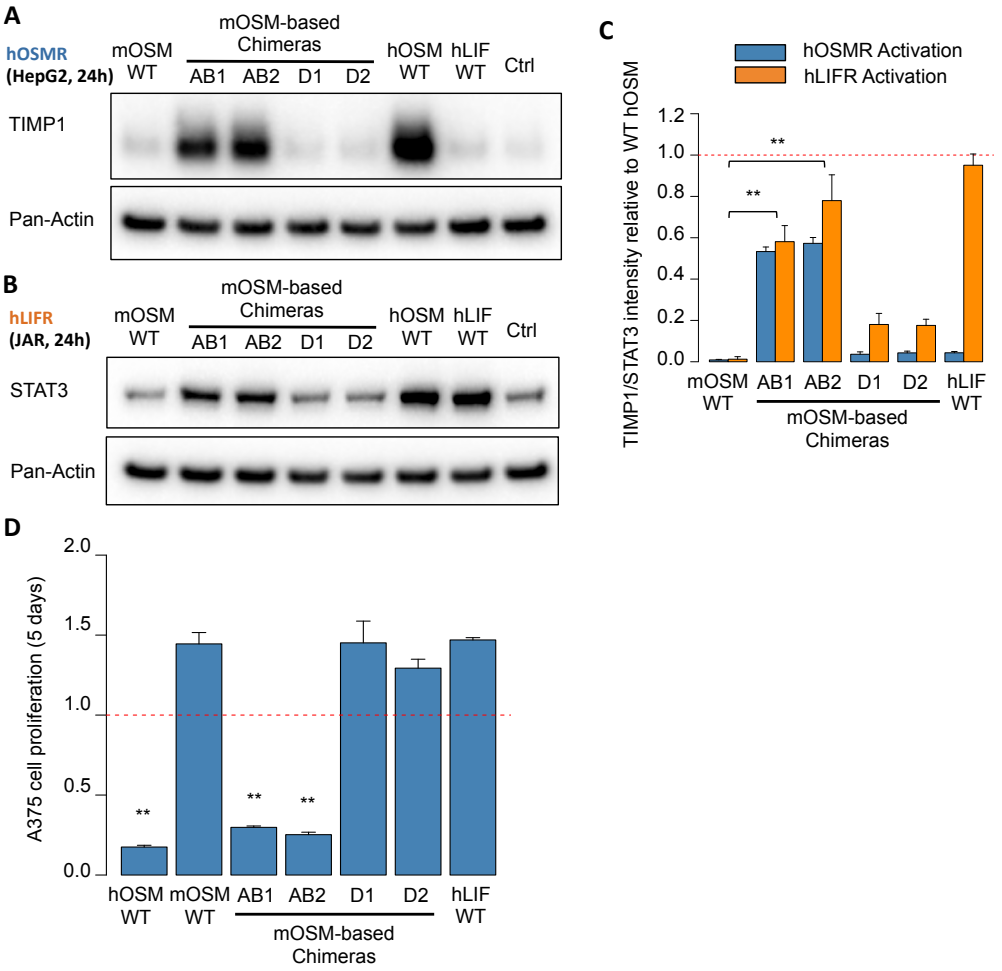

Figure 31: Long-term receptor activation ability of mOSM-based chimeric cytokines confirms AB loop importance. (A) Western blot of HepG2 cell samples after stimulation for 24 hours with 25 ng/mL of WT mOSM, WT hOSM, WT hLIF and the different mOSM-based chimeras. TIMP1 expression reflects hOSMR activation, while pan-Actin levels serve as loading control. **(B)** Western blot of JAR cell samples after a 24-hour stimulation with 25 ng/mL of the indicated cytokines created. Total STAT3 levels reflect hLIFR activation, while pan-Actin serves as loading control. **(C)**

Quantitative analysis of hOSMR and hLIFR activation levels after a 24-hour stimulation treatment with the detailed chimeric cytokines, relative to the observed activation for WT hOSM. Values were normalized against pan-Actin levels and presented as mean ± s.e.m. (n=5). **(D)** A375 proliferation levels 5 days after stimulation with 10 ng/mL of the indicated cytokines, relative to the proliferation of the control group. Values are given as mean ± s.e.m. (n=3). Statistical significance was determined by Welch's T-test, with (**) indicating p-values < 0.01.

4.2.3. Site-directed mutagenesis of murine Oncostatin M pinpoints specific residues responsible for species-specific receptor activation

Since the AB loop in mOSM had been found to be a differentiating factor in respect to the human cytokine, site-directed mutagenesis was employed to clarify exactly which substitutions within the AB loop were responsible to enable human receptor activation.

The AB1 mOSM chimera was selected as the starting point for this approach, since the region replaced in this construct is limited to just twelve amino acids (Fig. 27A). Five of them (Q36, L38, P41, L43 and R44 in mOSM) are conserved in both cytokines, which left seven candidate residues. Given that the alanine scanning experiment described in section 4.1.6 showed no effects of the hOSM mutants E47A and H48A on their receptor activation ability, the analogous A45 and A46 residues on mOSM were judged unlikely to impact hOSMR activation and the five remaining substitutions became the focus of this study.

Thus the mOSM mutant containing these five mutations (L35I, N37G, N39D, T40V and D42K), as well as all single, double, triple and quadruple mutant combinations, were created by assembly PCR and cloned through PacI and AscI restriction sites into the pCAGGS mammalian expression vector.

In first place the quintuple mutant, plus the five different quadruple mutants, were expressed in FreeStyle™ 293-F cells and His-tag purified. Subsequent 10-minute stimulation experiments revealed that the presence of the selected five mutations in mOSM is sufficient to enable both hOSMR and hLIFR activation by the cytokine (Fig. 32A-C).

Quadruple mutants were able to supplement additional information on the individual impact of these five substitutions. The loss of activity of the variant lacking the N37G replacement, and to a lesser extent of T40V and D42K, indicated the importance of these three mutations to enable human receptor activation, while the

L35I and N39D substitutions had very little effect on downstream signaling through the human receptors (Fig. 32A-C).

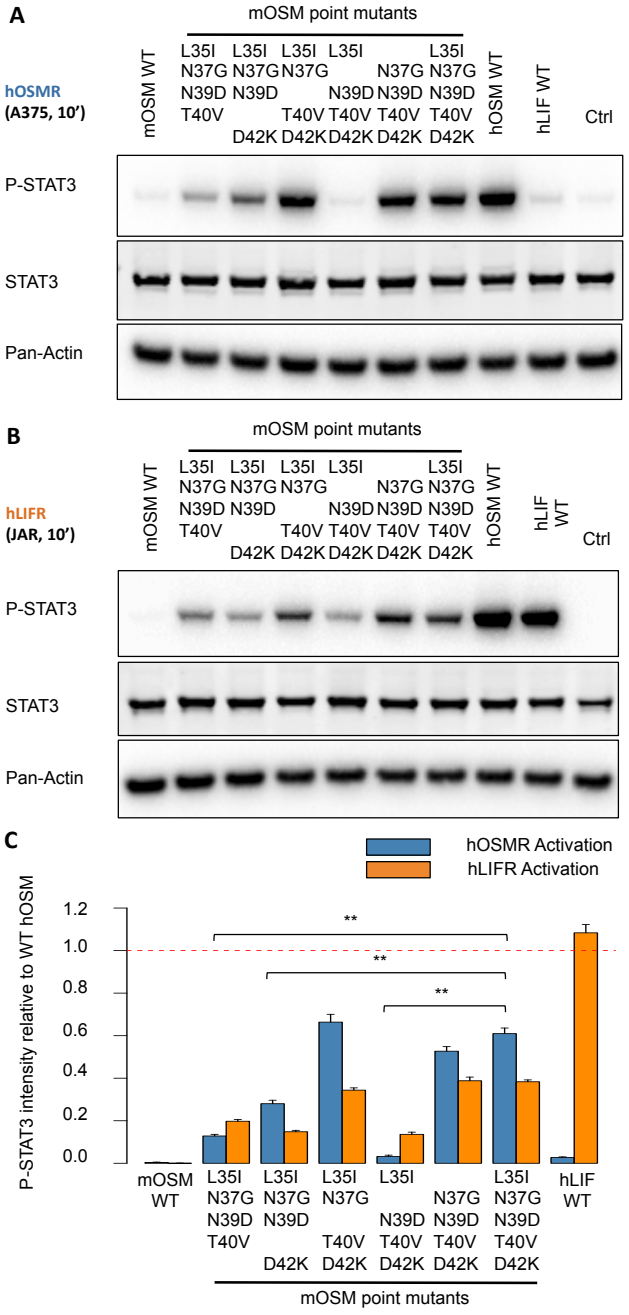

Figure 32: Short-term receptor activation ability of mOSM point mutants suggests residues determining species specificity within the AB loop. (A) Western blot of A375 cell samples after a 10-minute stimulation with 25 ng/mL of WT mOSM, WT hOSM, WT hLIF and the quadruple and quintuple mOSM point mutants detailed. STAT3 phosphorylation reflects hOSMR activation, while total STAT3 and pan-Actin serve as loading controls. **(B)** Western blot of JAR cell samples after a 10-minute stimulation with 25 ng/mL of the indicated cytokines. In this case STAT3 phosphorylation reflects hLIFR activation, while total STAT3 and pan-Actin serve as loading controls. **(C)** Quantitative analysis of hOSMR and hLIFR activation levels after

treatment with the detailed cytokines, relative to WT hOSM. Values were normalized against total STAT3 levels and presented as mean ± s.e.m. (n=5). Statistical significance was determined by Welch's T-test, with (**) indicating p-values < 0.01.

Findings from the 10-minute experiments were confirmed by a 24-hour stimulation experiment in HepG2 and JAR cells (Fig. 33A-C), and in the case of hOSMR activation by the inhibition of A375 cell proliferation after 5 days (Fig. 33D).

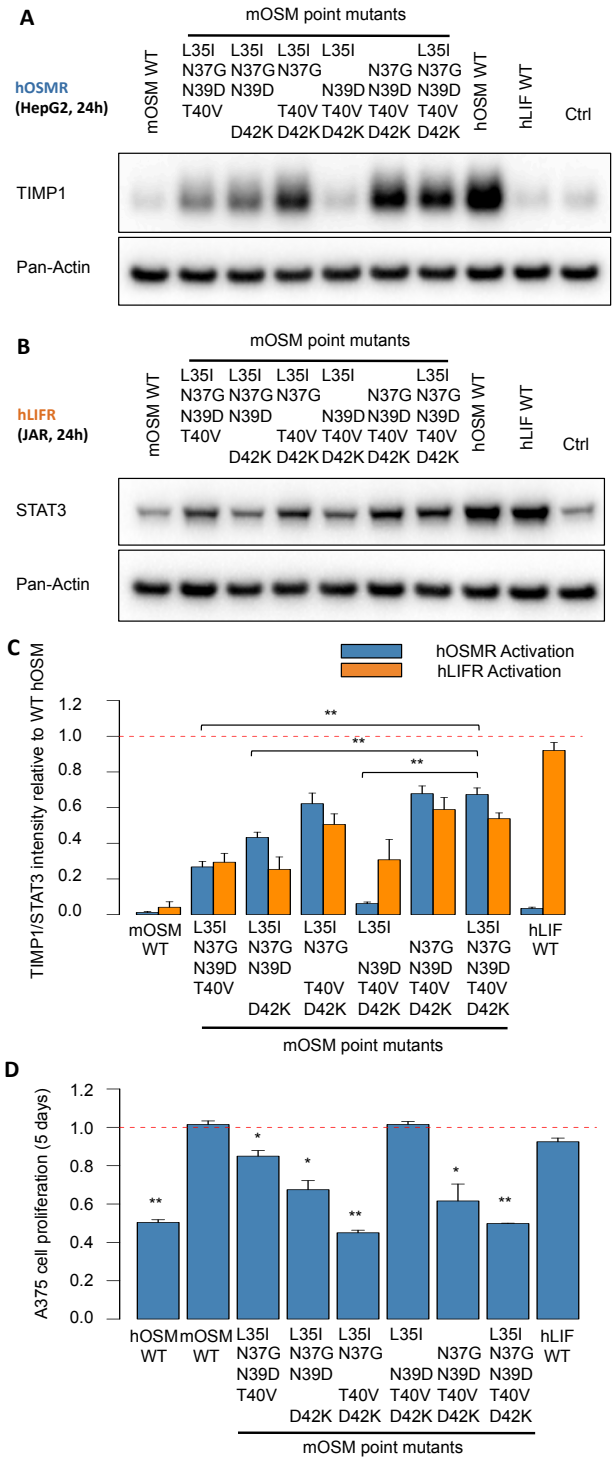

Figure 33: Long-term receptor activation ability of mOSM point mutants suggests residues determining species specificity within the AB loop. (A) Western blot of HepG2 cell samples after a 24-hour stimulation with 25 ng/mL of WT mOSM, WT hOSM, WT hLIF and the quadruple and quintuple mOSM point mutants. TIMP1 levels reflect hOSMR activation, while total pan-Actin levels serve as loading control. **(B)** Western blot of JAR cell samples after a 24-hour stimulation with the indicated cytokines. In this case STAT3 levels reflect hLIFR activation, while pan-Actin level is used as a loading control. **(C)** Quantitative analysis of hOSMR and hLIFR activation levels after the 24-hour stimulation treatment, relative to the observed activation for WT hOSM. Values were normalized against pan-Actin levels and presented as mean ± s.e.m. (n=5). **(D)** A375 proliferation levels 5 days after stimulation with 10 ng/mL of the indicated cytokines, relative to the proliferation of the control group. Values are given as mean ± s.e.m. (n=3). Statistical significance was determined by a Welch's T-test, with (**) indicating p-values < 0.01.

Short-term stimulation experiments employing the single mutant constructs, as well as the double and triple mutants for the relevant residues identified by the quadruple mutants (N37G, T40V and D42K), were then carried out to provide further evidence of the role of these three substitutions in enabling mOSM signaling through the human receptor complexes (Fig. 34A-C).

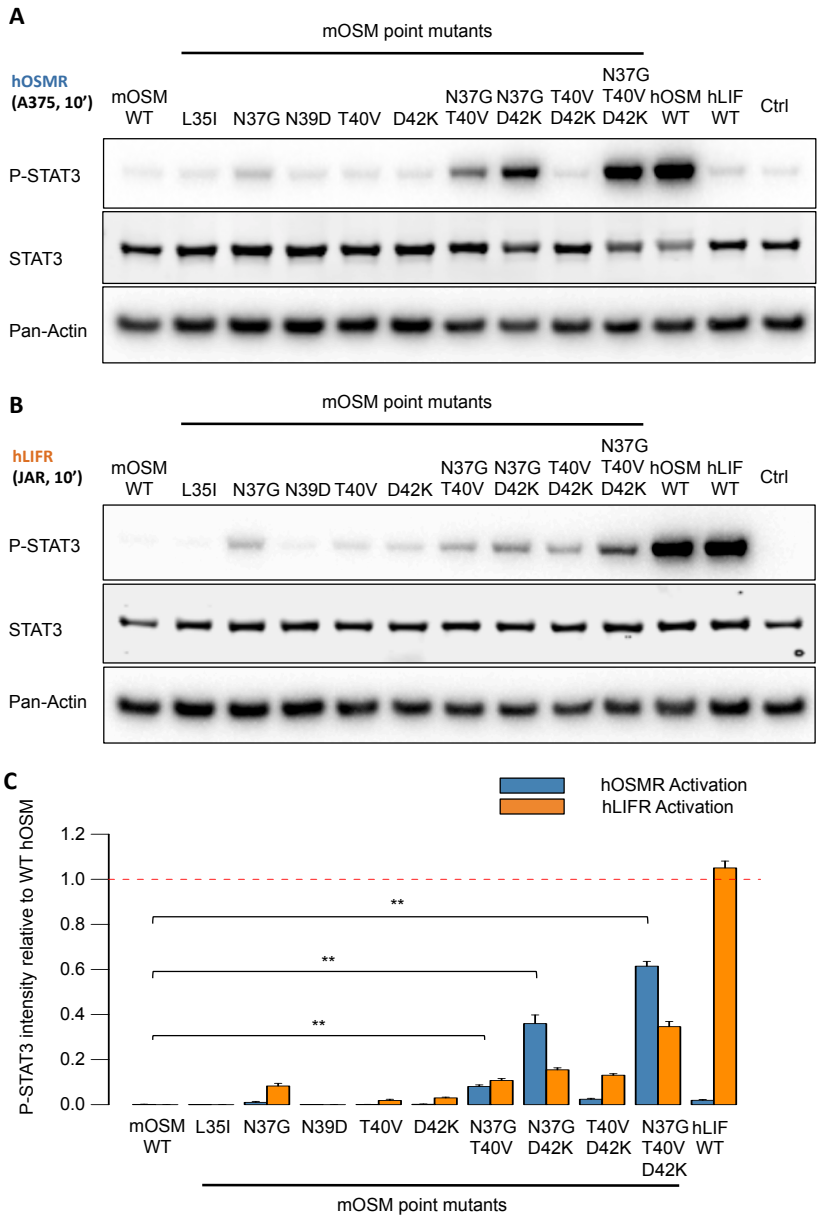

Figure 34: Short-term receptor activation ability of mOSM point mutants identifies residues determining species specificity within the AB loop. (A) Western blot of A375 cell samples after a 10-minute stimulation with 25 ng/mL of WT mOSM, WT hOSM, WT hLIF and the mOSM point mutants detailed. STAT3 phosphorylation reflects hOSMR activation, while total STAT3 and pan-Actin serve as loading controls. **(B)** Western blot of JAR cell samples after a 10-minute stimulation with 25 ng/mL of the detailed cytokines. In this case STAT3 phosphorylation reflects hLIFR activation, while total STAT3 and pan-Actin serve as loading controls. **(C)** Quantitative analysis of hOSMR and hLIFR activation levels after a 10-minute stimulation treatment with the indicated cytokines, relative to the observed activation for WT hOSM. Values were normalized against total STAT3 levels and presented as mean ± s.e.m. (n=5). Statistical significance was determined by Welch's T-test, with (**) indicating p-values < 0.01.

These results point to two substitutions in particular, N37G and D42K, as playing a pivotal role in permitting hOSMR activation. The 24-hour and 5-day stimulation experiments reproduced the pattern observed in the 10-minute readout system, reinforcing this conclusion (Fig. 35A-D).

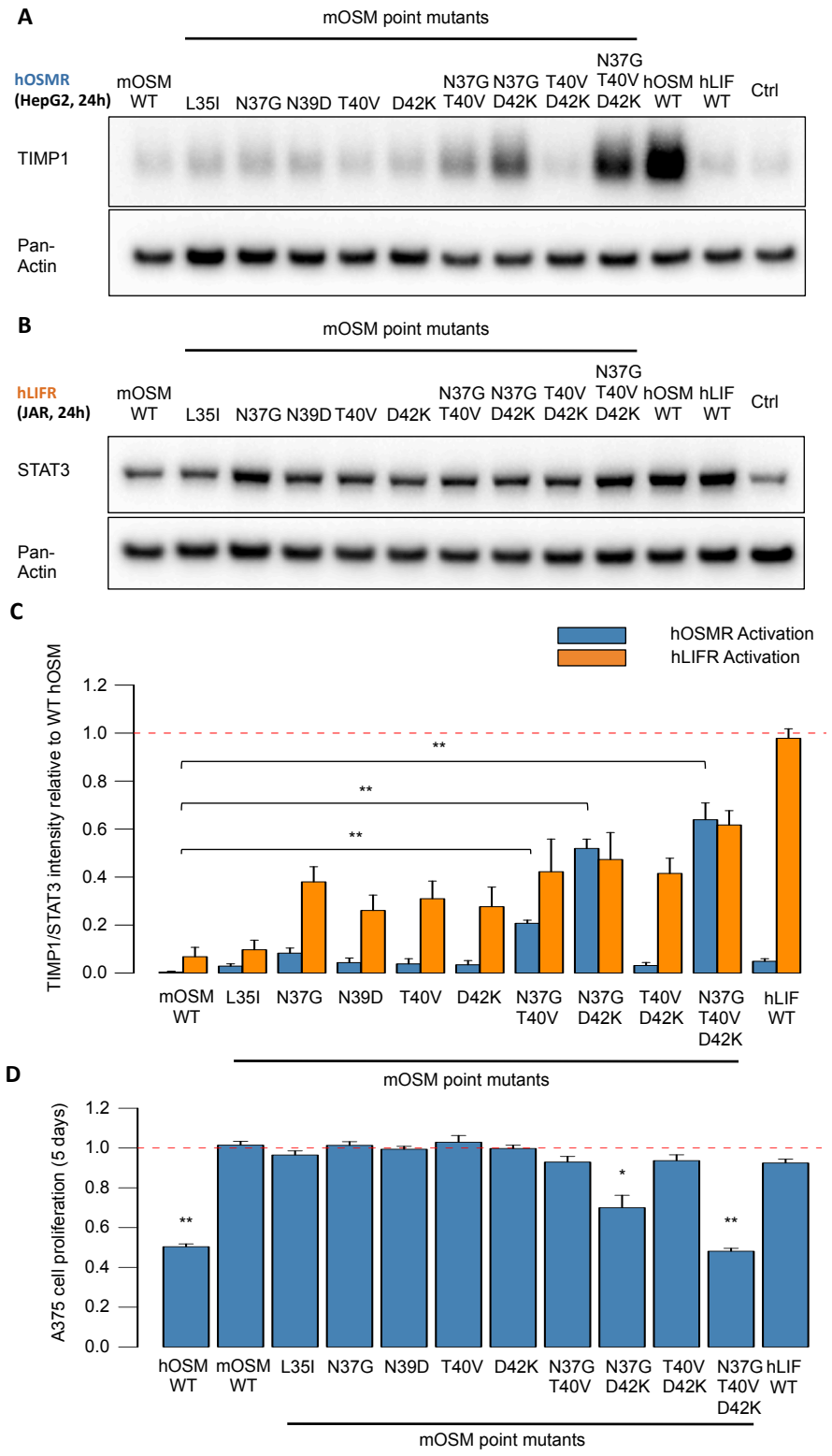

Figure 35: Long-term receptor activation ability of mOSM point mutants confirms residues determining species specificity within the AB loop. (A) Western blot of HepG2 cell samples after a 24-hour stimulation with 25 ng/mL of WT mOSM, WT hOSM, WT hLIF and the mOSM point mutants detailed. TIMP1 levels reflect hOSMR activation, while total pan-Actin levels serve as loading control. **(B)** Western blot of JAR cell samples after a 24-hour stimulation with the indicated cytokines. In this case STAT3 levels reflect hLIFR activation, while pan-Actin level is used as a loading control. **(C)** Quantitative analysis of hOSMR and hLIFR activation levels after the 24-hour stimulation treatment, relative to the observed activation for WT hOSM. Values were normalized against pan-Actin levels and presented as mean ± s.e.m. (n=5). **(D)** A375 proliferation levels 5 days after stimulation with 10 ng/mL of the indicated cytokines, relative to the proliferation of the control group. Values are given as mean ± s.e.m. (n=3). Statistical significance was determined by Welch's T-test, with (**) indicating p-values < 0.01.

4.2.4. Mutations in the residues defining species specificity in murine Oncostatin M result in promiscuous mouse receptor activation

After examining the ability of the created mutant mOSM cytokines to activate the human receptor, the next logical step was to examine whether human and mouse OSMR are mutually exclusive by assessing the mOSMR activation ability of these variants. To this end, a suitable readout system had first to be developed to investigate the activation of the different murine receptors.

In contrast to the human situation, the available information regarding specific mLIFR- or mOSMR-expressing murine cell lines is very limited: the NIH3T3 murine fibroblast cell line had been reported in the past to be responsive to mOSM but not hOSM or hLIF, which would indicate lack of mLIFR expression, although later publications appear to contradict this observation. (Ichihara et al. 1997) (Gyotoku et al. 2001)

To ascertain whether NIH3T3 cells could be used as a suitable readout system for mOSMR activation, we first compared downstream STAT3 phosphorylation after a 10-minute stimulation with both mLIFR- and mOSMR-activating cytokines (Fig. 36A). The presence of both receptor types was quite apparent, so to obtain a more specific readout NIH3T3 cells were stably transfected with an shRNA construct directed against mLIFR (Fig. 36B). By comparing the phosphorylation pattern of these knockdown cells against NIH3T3 cells stably transfected with an empty plasmid, it can then be determined whether a cytokine in question signals through the mLIFR.

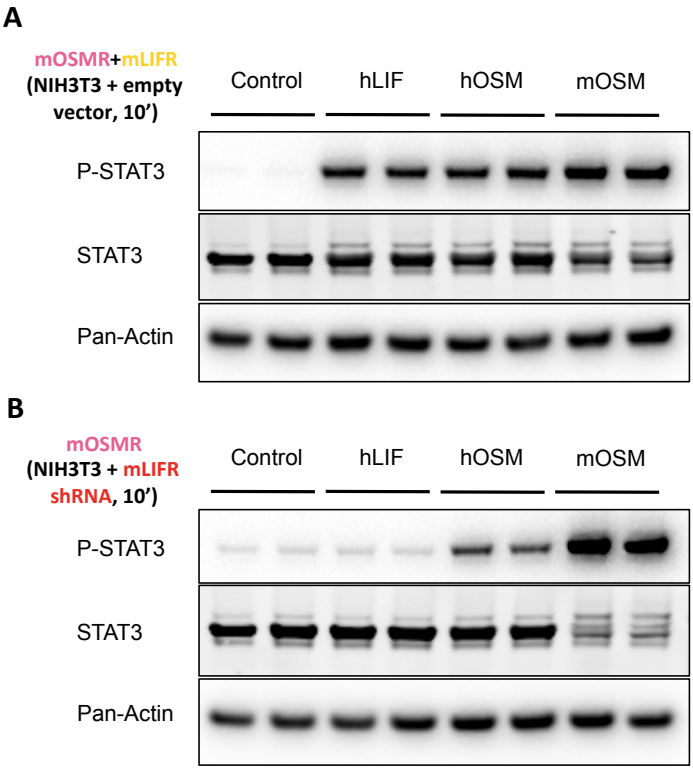

Figure 36: STAT3 phosphorylation after 10 minutes can be used to distinguish mOSMR and mLIFR activation in stably transfected NIH3T3 cells. (A) Western blot of STAT3 phosphorylation levels in NIH3T3 cells stimulated for 10 minutes with 25 ng/mL of hLIF, hOSM and mOSM. Total STAT3 and pan-Actin levels serve as loading controls. **(B)** Western blot showing STAT3 phosphorylation levels in NIH3T3 cells stably transfected with shRNA directed against mLIFR after a 10-minute stimulation with 25 ng/mL of hLIF, hOSM and mOSM. Total STAT3 and pan-Actin expression levels were used as loading controls.

Efforts were also made to establish a second readout system to reliably confirm murine receptor activation. In the case of mOSMR, Richards and colleagues had reported murine TIMP1 (mTIMP1) transcript levels to be upregulated in NIH3T3 cells in response to mOSMR activity, but not mLIFR. (Richards et al. 1993) This observation was confirmed at the protein level after 24 hours of stimulation, with a Western blot against mTIMP1 reflecting the expected receptor activation profile for mOSM, hOSM and hLIF (Fig. 37A).

Regarding mLIFR activation, murine hematopoietic cell lines had been claimed to be responsive to mLIF but not mOSM, which would hint at exclusive expression of the mLIFR. (Ichihara et al. 1997) Given that hematopoietic stem cells give rise to every type of blood cell (reviewed in (Schroeder 2010)), it appeared possible that some of these descendant cell lineages might also share the same mOSMR/mLIFR expression traits. Indeed, when the murine monocyte cell line MH-S was tested for

responsiveness to mOSMR- and mLIFR-activating cytokines, after 10 minutes only those signaling through the mLIFR evidenced strong STAT3 phosphorylation (Fig. 37B). In this manner, 10-minute stimulation experiments in MH-S cells proved suitable as specific readouts for mLIFR activation in subsequent experiments.

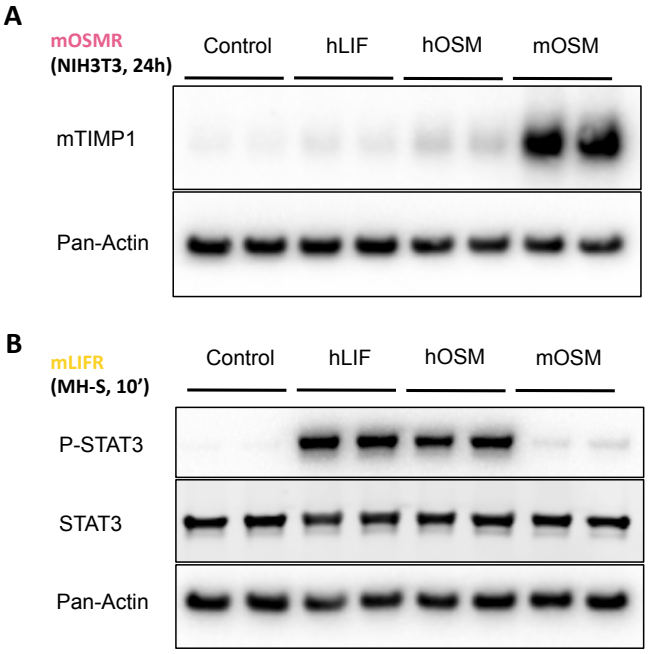

Figure 37: TIMP1 expression after 24 hours indicates mOSMR activation in NIH3T3 cells, while STAT3 phosphorylation reflects mLIFR activation in MH-S cells. (A) Western blot reflecting TIMP1 expression levels in NIH3T3 cells stimulated for 24 hours with 25 ng/mL of hLIF, hOSM and mOSM. Pan-Actin levels serve as a loading control. **(B)** Western blot showing STAT3 phosphorylation levels in MH-S after a 10-minute stimulation with hLIF, hOSM and mOSM. Total STAT3 and pan-Actin expression levels were used as loading controls.

Once the appropriate readout systems had been established, the mOSMR activation ability of the quadruple and quintuple mOSM mutants, as well as the AB loop and N-terminal D-helix chimeras, could be assessed. In first place, the STAT3 phosphorylation pattern in shRNA-mediated mLIFR knockdown (KD) NIH3T3 cells was unchanged in respect to the control cell line, suggesting that even the mOSM variants with the largest replacements retain the ability to signal through the mOSMR (Fig. 38A-C).

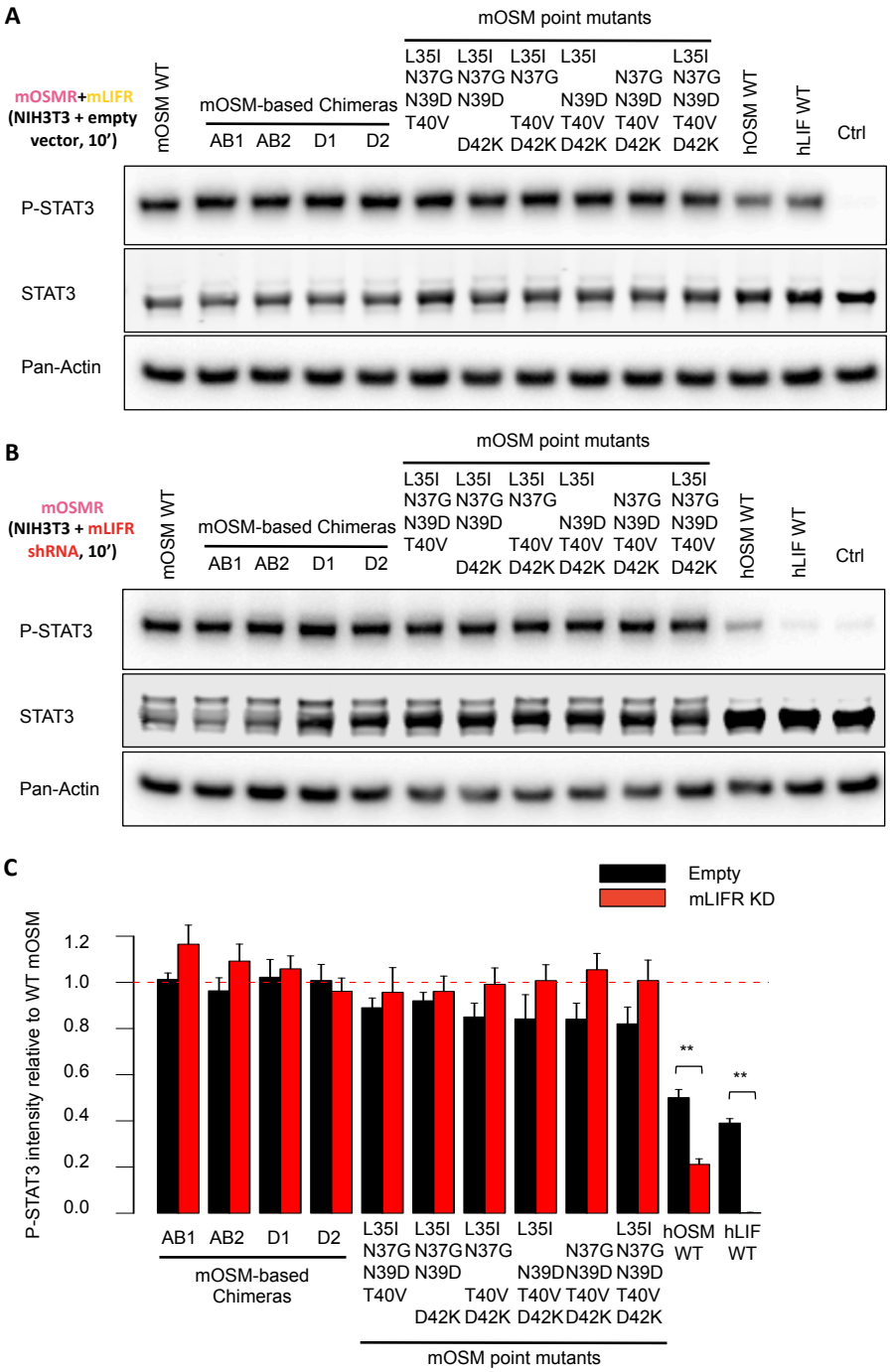

Figure 38: Short-term stimulations with mOSM chimeras point at preserved mOSMR activation abilities. (A) Western blot of NIH3T3 cell samples stably transfected with an empty vector and stimulated for 10 minutes with 25 ng/mL of the indicated cytokines. STAT3 phosphorylation reflects mOSMR and/or mLIFR activation, with total STAT3 and pan-Actin serving as loading controls. **(B)** Western blot of NIH3T3 cell samples stably transfected with shRNA against mLIFR, harvested after a 10-minute stimulation with 25 ng/mL of the indicated cytokines. In this case STAT3 phosphorylation mainly reflects mOSMR activation, with total STAT3 and pan-Actin serving as loading controls. **(C)** Quantitative analysis of STAT3 phosphorylation levels for the mutants tested, relative to WT mOSM. Values were normalized against

total STAT3 levels and presented as mean ± s.e.m. (n=5). Statistical significance was determined by Welch's T-test, with (**) indicating p-values < 0.01.

This observation was complemented by employing the two specific readout systems for mOSMR and mLIFR, which confirmed the existence of receptor-mediated signaling in these variants (Fig. 39A-C).

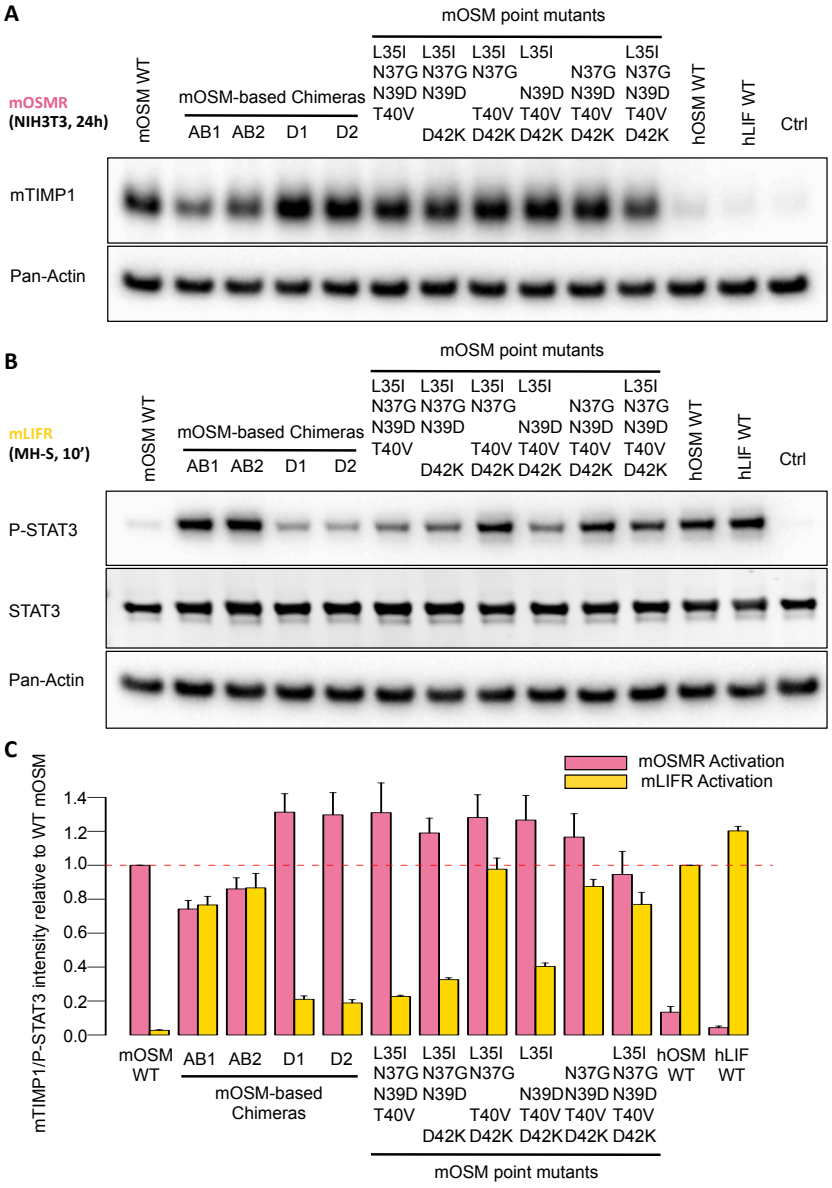

Figure 39: Specific readout system confirms different mOSM chimeras are able to activate the mLIFR. (A) Western blot of NIH3T3 cell samples stimulated for 24 hours with 25 ng/mL of the indicated cytokines. mTIMP1 expression reflects mOSMR activation, with pan-Actin being used as a loading control. **(B)** Western blot of MH-S cell samples harvested after a 10-minute stimulation with 25 ng/mL of the indicated cytokines. In this case STAT3 phosphorylation reflects mLIFR activation, with total

STAT3 and pan-Actin serving as loading controls. **(C)** Quantitative analysis of mOSMR and mLIFR activation levels for the mutants tested, relative to WT mOSM. Values were normalized against pan-Actin levels (for mTIMP1) or total STAT3 levels (for P-STAT3) and presented as mean ± s.e.m. (n=5).

As could be expected this finding was extensible to the single, double and triple mOSM mutants: their signaling remained unaffected after knockdown of the mLIFR (Fig. 40A-C).

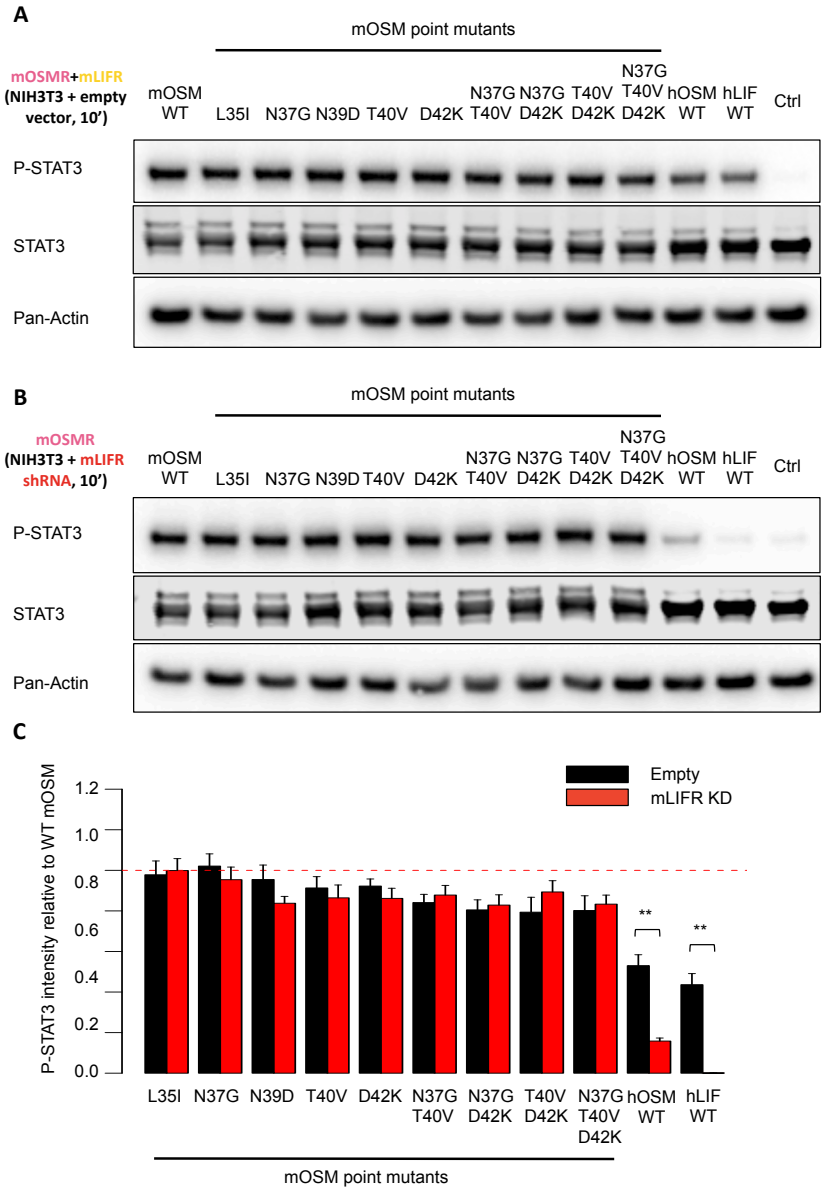

Figure 40: Short-term stimulations with mOSM point mutants hint at conserved mOSMR activation abilities. (A) Western blot of NIH3T3 cell samples stably transfected with an empty vector and stimulated for 10 minutes with 25 ng/mL of the indicated cytokines. STAT3 phosphorylation reflects mOSMR and/or mLIFR

activation, with total STAT3 and pan-Actin serving as loading controls. **(B)** Western blot of NIH3T3 cell samples stably transfected with shRNA against mLIFR, harvested after a 10-minute stimulation with 25 ng/mL of the detailed cytokines. In this case STAT3 phosphorylation reflects mainly mOSMR activation, with total STAT3 and pan-Actin serving as loading controls. **(C)** Quantitative analysis of STAT3 phosphorylation levels for the mutants tested, relative to WT mOSM. Values were normalized against total STAT3 levels and presented as mean ± s.e.m. (n=5). Statistical significance was determined by Welch's T-test, with (**) indicating p-values < 0.01.

Specific readouts confirmed that these variants show uneven mLIFR activation ability, closely reflecting their human receptor activation abilities, but all of them without exception were still capable of signaling through the mOSMR to drive TIMP1 production in NIH3T3 cells (Fig. 41A-C). Taken together, these experiments demonstrate that mutations in the AB loop of mOSM confer the ability to signal through the mLIFR and both human receptor complexes without impacting mOSMR interaction.

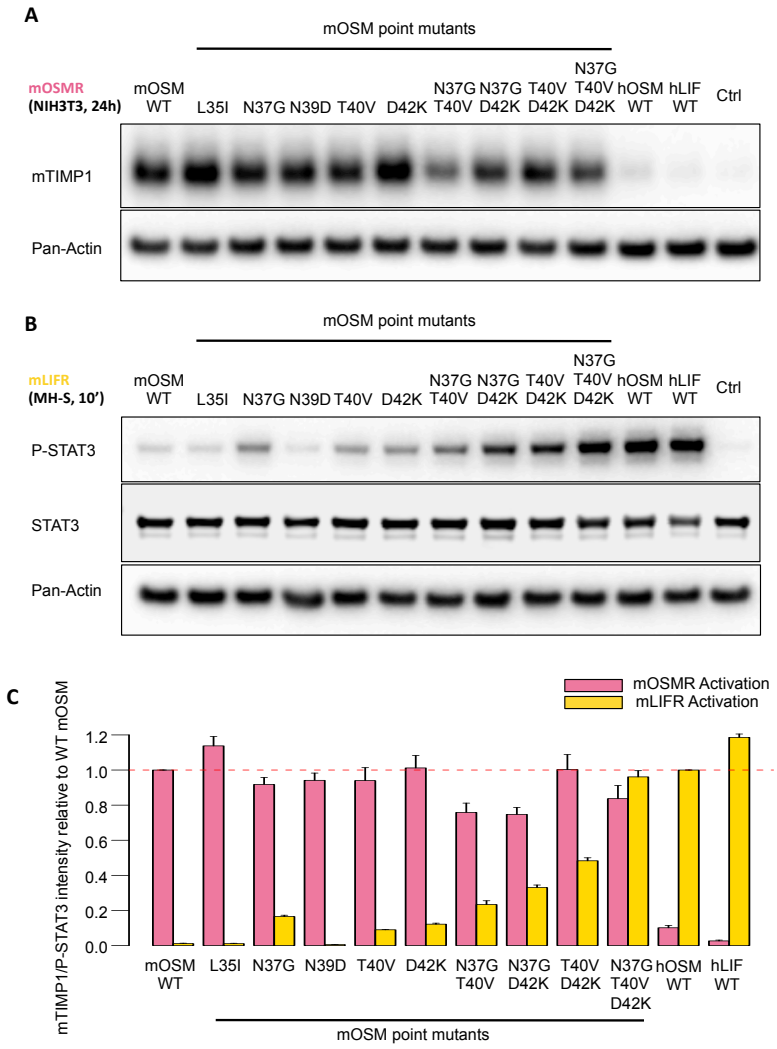

Figure 41: Specific readout system confirms murine receptor promiscuity of various mOSM point mutants. (A) Western blot of NIH3T3 cell samples stimulated for 24 hours with 25 ng/mL of the indicated cytokines. mTIMP1 expression reflects mOSMR activation, with pan-Actin being used as a loading control. **(B)** Western blot of MH-S cell samples harvested after a 10-minute stimulation with 25 ng/mL of the indicated cytokines. In this case STAT3 phosphorylation reflects mLIFR activation, with total STAT3 and pan-Actin serving as loading controls. **(C)** Quantitative analysis of mOSMR and mLIFR activation levels for the mutants tested, relative to WT mOSM. Values were normalized against pan-Actin levels (for mTIMP1) or total STAT3 levels (for P-STAT3) and presented as mean ± s.e.m. (n=5).

4.2.5. Substitutions in the residues involved in species specificity in human Oncostatin M enable murine OSMR activation

The lack of effect of any AB loop substitution in the activation of the mOSMR by mOSM greatly contrasts with the prior observations in the human system, and might reflect the existence of a different binding interface not involving the AB loop in the mouse complex. To investigate this point in more detail, hOSM point mutants carrying the mouse residues in the pivotal positions identified for mOSM (G39N, V42T and K44D), as well as a chimera with the full N-terminal AB loop replaced by its murine equivalent, were created by overlapping PCR, expressed and purified following the previously established protocols.

As could be expected, given that the glycine in position 39 of hOSM had previously proved critical for hOSMR activation in the alanine scanning experiment, every cytokine variant incorporating the mutation G39N was no longer able to signal through the hOSMR (Fig. 42A-C).

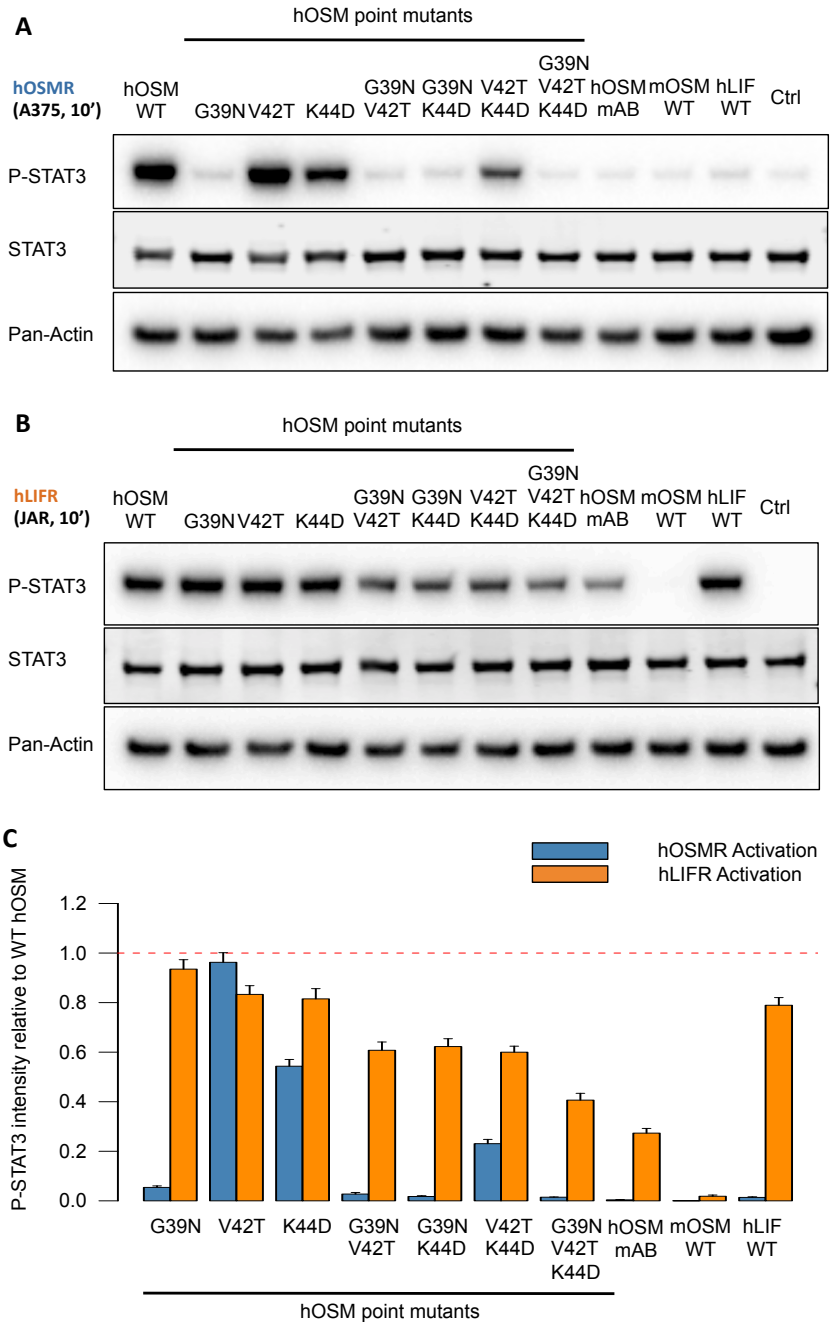

Figure 42: Short-term receptor activation ability of hOSM point mutants reinforces the importance of G39 for hOSMR signaling. (A) Western blot of A375 cell samples after a 10-minute stimulation with 25 ng/mL of WT mOSM, WT hOSM, WT hLIF and the point mutants detailed. STAT3 phosphorylation reflects hOSMR activation, while total STAT3 and pan-Actin serve as loading controls. **(B)** Western blot of JAR cell samples after a 10-minute stimulation with 25 ng/mL of the indicated cytokines. In this case STAT3 phosphorylation reflects hLIFR activation, while total STAT3 and pan-Actin serve as loading controls. **(C)** Quantitative analysis of hOSMR and hLIFR activation levels after the 10-minute stimulation experiments, relative to the observed activation for WT hOSM. Values were normalized against total STAT3 levels and presented as mean ± s.e.m. (n=5).

This observation could be confirmed through the longer-term readout systems: while hLIFR signaling is still preserved to some extent for all the mutants assayed, hOSMR signaling is abrogated in the absence of G39 (Fig. 43A-D).

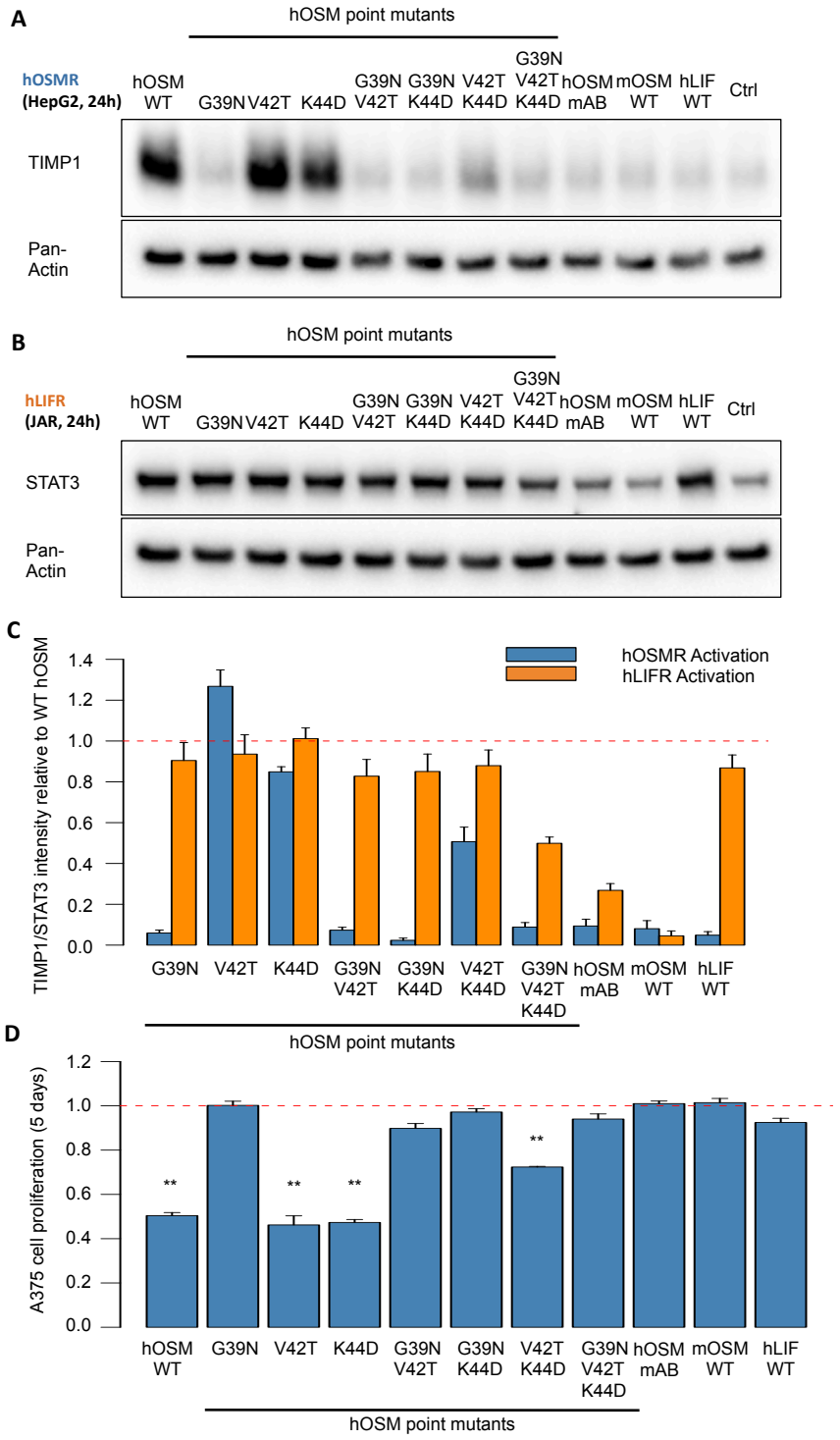

Figure 43: Long-term receptor activation ability of hOSM point mutants confirms G39 as critical to initiate hOSMR signaling. (A) Western blot of HepG2 cell samples

after a 24-hour stimulation with 25 ng/mL of WT mOSM, WT hOSM, WT hLIF and the point mutants indicated. TIMP1 levels reflect hOSMR activation, while total pan-Actin levels serve as loading control. **(B)** Western blot of JAR cell samples after a 24-hour stimulation with the detailed cytokines. In this case STAT3 levels reflect hLIFR activation, while pan-Actin level is used as a loading control. **(C)** Quantitative analysis of hOSMR and hLIFR activation levels after the 24-hour stimulation experiments, relative to the observed activation for WT hOSM. Values were normalized against pan-Actin levels and presented as mean ± s.e.m. (n=5). **(D)** A375 proliferation levels 5 days after stimulation with 10 ng/mL of the indicated cytokines, relative to the proliferation of the control group. Values are given as mean ± s.e.m. (n=3). Statistical significance was determined by Welch's T-test, with (**) indicating p-values < 0.01.

Surprisingly, when the cell stimulation experiments in murine cells were carried out, replacing the lysine in position 44 by aspartic acid appeared sufficient to confer the mutants with mOSMR signaling ability (Fig. 44A-C).

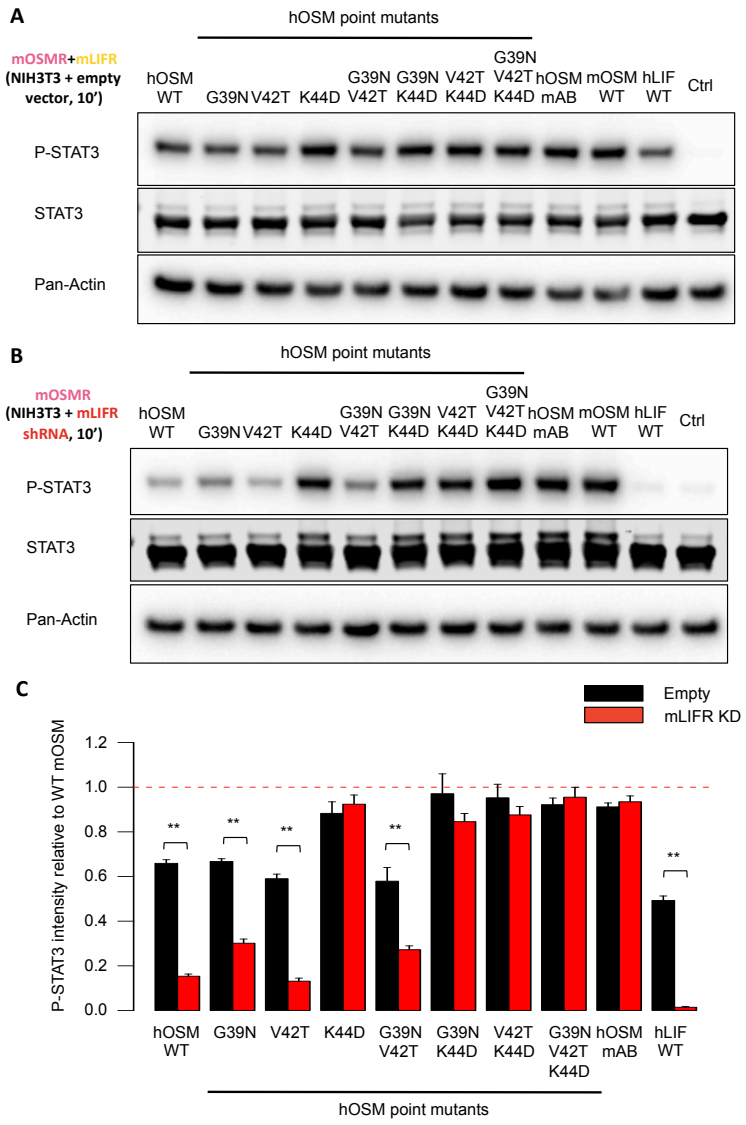

Figure 44: Short-term stimulations with hOSM-based mutants indicate apparent mOSMR activation abilities. (A) Western blot of NIH3T3 cell samples stably transfected with an empty vector and stimulated for 10 minutes with 25 ng/mL of the indicated cytokines. STAT3 phosphorylation reflects mOSMR and/or mLIFR activation, with total STAT3 and pan-Actin serving as loading controls. **(B)** Western blot of NIH3T3 cell samples stably transfected with shRNA against mLIFR, harvested after a 10-minute stimulation with 25 ng/mL of the indicated cytokines. In this case STAT3 phosphorylation reflects mainly mOSMR activation, with total STAT3 and pan-Actin serving as loading controls. **(C)** Quantitative analysis of STAT3 phosphorylation levels for the mutants tested, relative to WT mOSM. Values were normalized against total STAT3 levels and presented as mean ± s.e.m. (n=5). Statistical significance was determined by Welch's T-test, with (**) indicating p-values < 0.01.

Confirmatory experiments employing specific readouts left no doubt that K44 is responsible for the lack of cross-species reactivity of hOSM with the mOSMR, and that its substitution by aspartic acid is sufficient for the mutant cytokine to display a signaling ability in murine cells that mirrors the human situation (Fig. 45A-C). Furthermore, these mutants indicate that the AB loop of the cytokine does play an important role in mOSMR activation, as was the case for the N-terminal D-helix region in the human receptor, despite the fact that the native murine cytokine can withstand modifications in this region without affecting OSMR signaling.

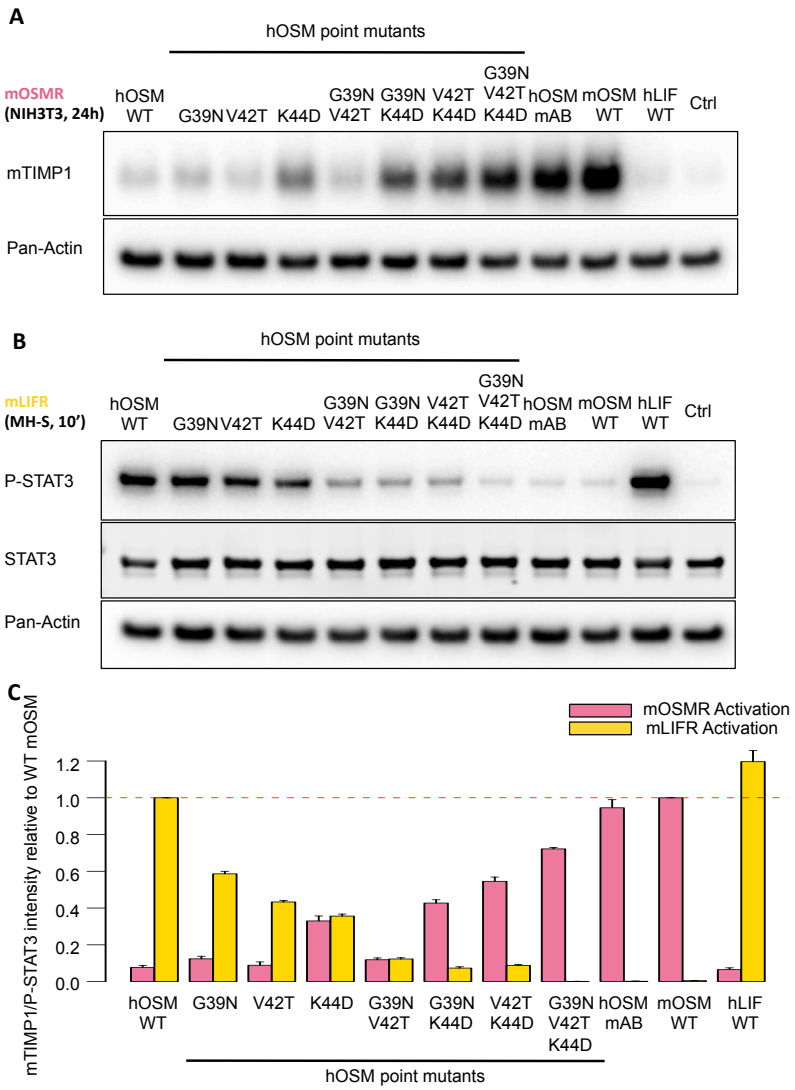

Figure 45: Specific readout system confirms acquisition of mOSMR activation by hOSM variants. (A) Western blot of NIH3T3 cell samples stimulated for 24 hours with 25 ng/mL of the indicated cytokines. mTIMP1 expression reflects mOSMR activation, with pan-Actin being used as a loading control. **(B)** Western blot of MH-S cell samples harvested after a 10-minute stimulation with 25 ng/mL of the indicated cytokines. In this case STAT3 phosphorylation reflects mLIFR activation, with total STAT3 and pan-Actin serving as loading controls. **(C)** Quantitative analysis of mOSMR and mLIFR activation levels for the mutants tested, relative to WT mOSM. Values were normalized against pan-Actin levels (for mTIMP1) or total STAT3 levels (for P-STAT3) and presented as mean ± s.e.m. (n=5).

As a summary of the results comprising this thesis, the signaling properties of the main mutant variants used in this work have been collected in figure 46.

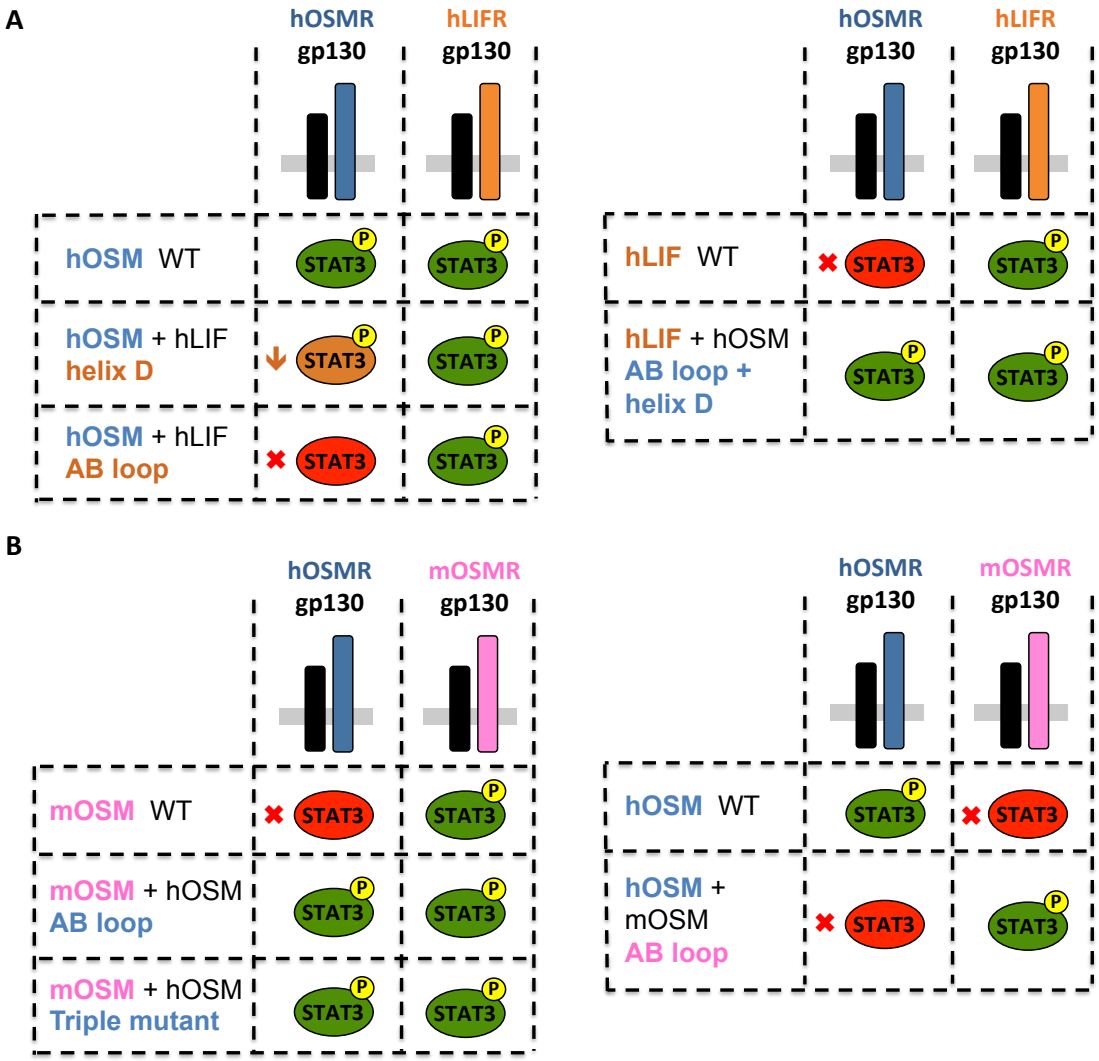

Figure 46: Signaling properties of the main mutant variants created. (A) The substitution of the AB loop region of hOSM by its equivalent hLIF sequence disrupted STAT3 phosphorylation through the hOSMR, while a replacement of the N-terminal helix D region only had a small impact. Conversely, substitutions of both AB loop and N-terminal helix D sequences in hLIF by their corresponding hOSM sequence was required for the chimeric cytokine to signal through the hOSMR complex. **(B)** Replacement of the AB loop of mOSM by the human loop enabled the cytokine to signal through the hOSMR while maintaining affinity for the murine receptor. This change in affinity is determined by just three amino acid substitutions, as evidenced by the mOSM triple mutant. In contrast, exchanging the AB loop of hOSM by the one in mOSM leads to a switch in receptor signaling.

5. Discussion

The availability of detailed data on cytokine-receptor interactions for potential immunotherapeutic cytokines is critical, as it has led to the development of a whole new approach to protein engineering: by employing this information as a basis to manipulate signaling, striking improvements can be achieved in terms of potency, affinity and specificity. (Spangler et al. 2015)

In this regard, the interaction of IL-6 with its receptors has been well characterized: the crystal structure of the complex between IL-6, the IL6R and the extracellular region of gp130 provided detailed information on the interacting residues between these molecules. (Boulanger, Chow, et al. 2003) The same holds true for many of the other IL-6 family members: crystallization experiments have provided valuable insight into the binding between LIF and gp130, LIF and LIFR, and CNTF and the LIFR/CNTFR/gp130 complex. (Boulanger, Bankovich, et al. 2003) (Huyton et al. 2007) (Skiniotis et al. 2008)

In contrast, despite the fact that OSM possesses the broadest signaling abilities within the IL-6 class and thus the widest range of possible applications, little evidence regarding the interaction between OSM and its receptor complexes is available to date. (Hermanns 2015) In order to address this lack of information the present work employs molecular biology tools such as the creation of chimeric proteins, successfully used in the past to examine differences in binding and downstream signaling in a variety of receptor systems including OSMR, LIFR and gp130. (Kallen et al. 1999) (Hermanns et al. 1999)

By these means the particular features of hOSM that enable it to activate multiple receptors could be identified, and variants with a modified receptor activation profile in respect to the native human cytokine could be obtained. In addition, the same techniques were applied to locate the molecular determinants causing the well-described difference in receptor specificity between hOSM and mOSM, which hinders the translation of results obtained in murine models to the human situation. (Ichihara et al. 1997) This research is expected to have immediate practical applications, as some of the OSM variants created show the potential to improve the translatability of future OSM studies in mouse models.

Finally, the data collected in this work supports the possibility that OSM may have adopted an evolutionary path so far unreported for other cytokines, attaining a new function through the evolution of a promiscuous intermediate which would finally derive into a new specific molecule. This process, widely accepted in enzymology, will be discussed in depth in section 5.5. (Khersonsky & Tawfik 2010)

5.1. Novel recombinant OSM production and receptor activation readout systems

The experiments comprising this work relied on the ability to express and purify several wild-type cytokines (hOSM, hLIF and mOSM), as well as different point mutants and chimeric proteins. This is generally a laborious and time-consuming process: these particular proteins tend to aggregate and form insoluble inclusion bodies when overexpressed in a prokaryotic system, requiring additional steps in order to be refolded into their native secondary structure. (Sporeno et al. 1994) An alternative approach consists of the fusion of the cytokine to a solubility tag such as GST, which avoids the aggregation of the protein into inclusion bodies but implies an additional step to remove the tag after expression. (Deller et al. 2000)

To improve on the reported methods, two different solutions were developed: at first, soluble prokaryotic expression was achieved by employing a modified *E. coli* strain expressing a chaperone/disulfide bond isomerase. This method led to the production and direct recovery of wild type and point mutant cytokines without additional steps, confirming that the observed recombinant cytokine aggregation in the common bacterial strains is consequence of a lack of disulfide bond formation in the prokaryotic cytoplasm. (Baneyx & Mujacic 2004)

However, expression of soluble chimeric proteins could not be achieved in bacteria, perhaps due to the substantial modifications in their native amino acid sequence. This led to a mammalian expression system being established: human FreeStyle™ 293-F cells proved able to produce recombinant proteins, including the chimeric variants, in sufficient amounts for later use in stimulation experiments. The fact that these cells are adapted to serum-free medium facilitated downstream recovery and purification of the recombinant proteins. In both prokaryotic and mammalian expression systems the presence of a C-terminal His-tag enabled the recombinant proteins to be purified using Ni-NTA affinity resins. (Schmitt et al. 1993)

In respect to monitoring receptor activation in response to the array of cytokines created, the short-term indicator selected was downstream phosphorylation of STAT3. As discussed in section 1.3, this signaling component is shared by all the IL-6 family receptors and plays a crucial role after their activation: OSM is no exception, as STAT3 mediates most of its biological effects including hematopoiesis, cardioprotection and liver regeneration. (Takizawa et al. 2003) (Hilfiker-Kleiner et al. 2004) (Lörchner et al. 2015) (Li et al. 2002) (Nakamura et al. 2004) By taking advantage of well-characterized cell lines exclusively expressing hOSMR or hLIFR, as well as novel mOSMR or mLIFR-specific cell types in the murine situation, STAT3

phosphorylation became the main readout for receptor activity in most of the experiments contained in this work. (Auguste et al. 1997)

Additional readout systems at later time points were employed in order to confirm the initial observations derived from the measurement of STAT3 phosphorylation levels after a 10-minute stimulation. In the case of OSMR activation, TIMP1 was selected as a known specific target of this receptor in contrast to the LIFR: 24 hours of stimulation are sufficient for TIMP1 expression levels to increase dramatically in both human and murine systems. (Richards et al. 1993) (Bugno et al. 1995) In addition, given that hOSM was first identified as a proliferation inhibitor in a melanoma cell line, its ability to perform this activity was also leveraged as a measure of hOSMR activation. (Zarling et al. 1986)

Finding specific LIFR targets that were not shared with the OSMR proved to be more of a challenge, so in the end the decision was made to employ an hLIFR-specific cell line and monitor total STAT3 levels after 24 hours as a reflection of hLIFR activity. (Bugno et al. 1995) In all these cases, longer-term stimulation results agreed with those obtained in the initial STAT3 phosphorylation readouts.

5.2. The AB loop of Oncostatin M influences activation of the human OSMR

The key role of the N terminus of helix D is well documented: it has been described in the past that the hOSM residues F160 and K163 are critical for hOSMR binding. (Deller et al. 2000) As a consequence, when the phenylalanine and/or lysine were replaced by alanine, the mutant cytokines became unable to elicit any biological activity or initiate hOSMR/hLIFR signaling. (Deller et al. 2000)

The FXXK motif formed by these two amino acids is a conserved feature in all LIFR-binding cytokines, such as LIF, CNTF and CT-1. (Di Marco et al. 1996) (Plun-Favreau et al. 2003) The positive region constituted by this motif appears to interact with a negative core formed by an aspartic acid residue in the immunoglobin-like domain of the LIFR, as site-directed mutagenesis of this domain resulted in a mutant receptor with impaired cytokine binding ability. (Plun-Favreau et al. 2003)

However, since hOSM is the only one of these cytokines able to activate the hOSMR in addition to the hLIFR, it stands to reason that this conserved FXXK motif cannot be the only structural feature involved in hOSMR recognition. Structural comparisons between the IL-6 class members suggested the lengthened BC loop in hOSM might act as a possible hOSMR-specific recognition site, since it forms part of the general binding region for both receptors. (Chollangi et al. 2012) However, the importance of this loop for hOSMR specificity was disproved by the production of hOSM mutants

with a shortened BC loop region, which were still able to activate the hOSMR and displayed higher affinity for both receptor types. (Chollangi et al. 2012)

The work presented here took advantage of the similarities between hOSM and hLIF to create a series of chimeric cytokines based on hOSM, in which different regions of binding site III were exchanged by their hLIF equivalents. By these means it could be proved that the main region of hOSM enabling specific human hOSMR activation is neither the longer BC loop nor the N-terminal helix D region containing the FXXK motif, since replacing them barely had any impact on cytokine signaling.

It was instead the AB loop of hOSM that proved to be crucial for hOSMR activation: replacements of as little as 10 amino acids by their corresponding hLIF residues resulted in chimeric cytokines that were unable to initiate hOSMR signaling, while still displaying normal function through the hLIFR. After this initial finding, alanine mutants of all individual positions within the AB loop of human OSM led to a more detailed assessment of the relative importance of each amino acid in receptor binding.

Interestingly, a mutation in L40 resulted in complete abrogation of signaling through hOSMR and hLIFR, which could reflect either a crucial role in the activation of both receptors or an improper structural organization of the L40A mutant. This second supposition appears more likely, since amino acids with aliphatic side chains such as leucine are very non-reactive: they tend to be buried in the protein interior, particularly in alpha helices, seldom being directly involved in protein function. (Betts & Russell 2003) Disruption of the secondary structure of hOSM also explains the lack of signaling by the C49 mutant, as this residue is part of an essential disulfide bond between C49 and C167. (Kallestad et al. 1991) The presence of the disulfide bond likely ensures that all regions of binding site III are in the correct orientation and distance to interact with the receptor.

Additionally, the alanine scanning analysis performed uncovered four different residues in the AB loop that seem to be exclusively required for hOSMR activation. Stimulation with Q38, G39 and L45 mutants led to normal hLIFR activation but complete absence of hOSMR-dependent signaling, while Y34 resulted in partial impairment of hOSMR activation.

As stated above, the leucine in position 45 is probably not directly interacting with the hOSMR due to its hydrophobicity, but could instead be required to maintain the α-helical structure in this region of the cytokine. The glutamine at position 38, on the other hand, is a polar residue frequently found in the protein surface: glutamines are often involved in protein binding sites, interacting with other amino acids with polar

side chains or charged atoms. (Betts & Russell 2003) An example of one such interaction is the bovine papillomavirus type 1 E5 oncoprotein, in which a single glutamine residue is responsible for its association with a transmembrane component in the vacuole. (Goldstein et al. 1992) Therefore, it seems reasonable to assume that in the case of hOSM the direct binding of Q38 to a polar residue in the hOSMR is necessary for receptor recognition.

The glycine in position 39 is perhaps the most intriguing of the four identified residues, given the influence it also has in species-specific OSMR activation. Glycine is the amino acid with the smallest side chain, containing only a hydrogen atom without any carbons: this leads to a much higher conformational flexibility, so that glycine can be found in structures, such as tight turns, in which no other amino acid can reside. (Betts & Russell 2003) This particularity also allows glycine to perform unique functional roles, such as binding phosphates through its backbone without employing a side chain, which makes them particularly important for kinase proteins. (Schulze-Gahmen et al. 1996) (Betts & Russell 2003)

In the case of hOSM, however, G39 is located exactly in the turn between the end of helix A and the AB loop, which suggests that its importance is more likely structural. In this way, the presence of a glycine in that position would enable the AB loop and D-helix regions of the molecule to be placed at the exact distance and orientation required to enable hOSMR recognition and activation.

The last relevant residue for hOSMR binding, albeit to a lesser degree than Q38, G39 or L45, is the tyrosine in position 34. This partially hydrophobic amino acid is regularly found buried in protein cores, but unlike leucine the side chain of tyrosine contains an aromatic ring with a reactive hydroxyl group, which makes it more likely to interact with atoms other than carbon. (Betts & Russell 2003) In particular, aromatic amino acids have been proposed to be able to stack on top of each other, with their aligned aromatic rings creating an electrostatic interaction between proteins. (Hunter et al. 1991)

If this were the case, Y34 of hOSM would be interacting with a phenylalanine, tryptophan, histidine or another tyrosine in the binding interface of the hOSMR. However, this possible interaction would not be essential for hOSMR binding and/or activation, since alanine replacement of Y34 only causes a partial impairment of signaling.

While the importance of the AB loop in terms of hOSMR activation appears clear based on the data presented, the exact mechanism behind the observed loss of signaling has yet to be determined. Taking into account the nature of the common

activation mechanism for type I cytokine receptor complexes, which undergo conformational changes that lead to transphosphorylation in their cytoplasmatic regions, there seem to be two main possibilities to explain this lack of activation.

Perhaps the most intuitive hypothesis is that the mutant cytokine completely loses its ability to bind the hOSMR due to changes in its AB loop. However, it cannot be ruled out that this AB loop modification would result in a molecule that still maintains affinity for the hOSMR, but is no longer able to induce the required conformational changes to initiate intracellular signaling after ligand binding.

To conclusively answer this question, direct measurements of the binding affinity between the different cytokine variants and the OSMR would have to be performed. Assays such as isothermal titration calorimetry (ITC) and surface plasmon resonance (SPR) are nowadays widely used to this end, due to the small amount of unlabeled sample required and the speed and reliability of its results. (Besenicar et al. 2006) (Pierce et al. 1999) However, applying these techniques to study the binding of hOSM to the hOSMR/gp130 complex has proved challenging: both ITC and SPR rely on reconstituting the ligand-receptor system outside the cellular environment, in solution for ITC and in a sensor chip for SPR. Unfortunately, the lack of direct OSM - OSMR interaction has so far prevented SPR measurements for hOSMR to be performed successfully, (Chollangi et al. 2012) while the binding affinity of cytokine-receptor interactions might be below the lower limit of 1 nM in ITC. (Rajarathnam & Rösgen 2014)

For these reasons, the method of choice to analyze the interaction of hOSM-derived variants to the hOSMR would appear to be radioligand binding. By radiolabeling the cytokines with iodine 125 and measuring binding of increasing amounts of the cytokine to a monolayer of A375 cells, a Scatchard analysis could be performed to determine its affinity constants. (Linsley et al. 1989) In this manner, WT hOSM could be compared to the mutants of interest to determine whether replacement of the AB loop has a direct effect on receptor binding ability, or only affects the conformational changes required for signaling initiation after binding.

5.3. Differences between human Oncostatin M and human Leukemia Inhibitory Factor influencing receptor complex activation

Intuitively, the central role that the hOSM AB loop region plays in hOSMR activation would suggest the existence of major differences in this region between hLIF and hOSM. However, a close examination of the aligned loop regions reveals this not to be the case: in fact, the four key hOSM amino acids (Y34, Q38, G39 and L45) specifically influencing hOSMR activation are also present in hLIF (Fig. 15A). This

indicates a high degree of conservation in the region, which is perhaps unexpected in the case of hLIF since a detailed site-directed mutagenesis study did not identify any of the individual residues in its AB loop region to play a major role in receptor binding. (Hudson et al. 1996)

One relevant difference between these cytokines seems to be the residue right after the conserved QG sequence, with leucine 40 of hOSM being replaced by glutamate in hLIF. Unlike leucine, glutamate is a negatively charged polar amino acid that tends to be exposed in the protein surface, and can form salt bridges with positively charged residues to contribute to protein stability or protein-protein interactions. (Betts & Russell 2003) But while mutations in L40 of hOSM result in an inactive cytokine, hLIF is still able to bind to the hLIFR despite this replacement: this may be a reflection of the slightly different interaction mechanism for both cytokines in terms of hLIFR activation, for which experimental evidence had already been provided in the past. (Plun-Favreau et al. 2003)

However, the main differential feature between the AB loops of hOSM and hLIF seems to be the presence of an additional amino acid in the hLIF sequence (Fig. 15A). Taking into account that the nearby cysteine has a fixed spatial position due to the disulfide bond it forms with helix D in both cytokines, the presence of an extra residue in the hLIF AB loop results in the spatial rearrangement of most of the residues forming this region. In this way, even if nearly all the amino acids necessary for hOSMR activation in hOSM are conserved in hLIF, their orientation relative to helix D would make hOSMR recognition and/or binding impossible (Fig. 47).

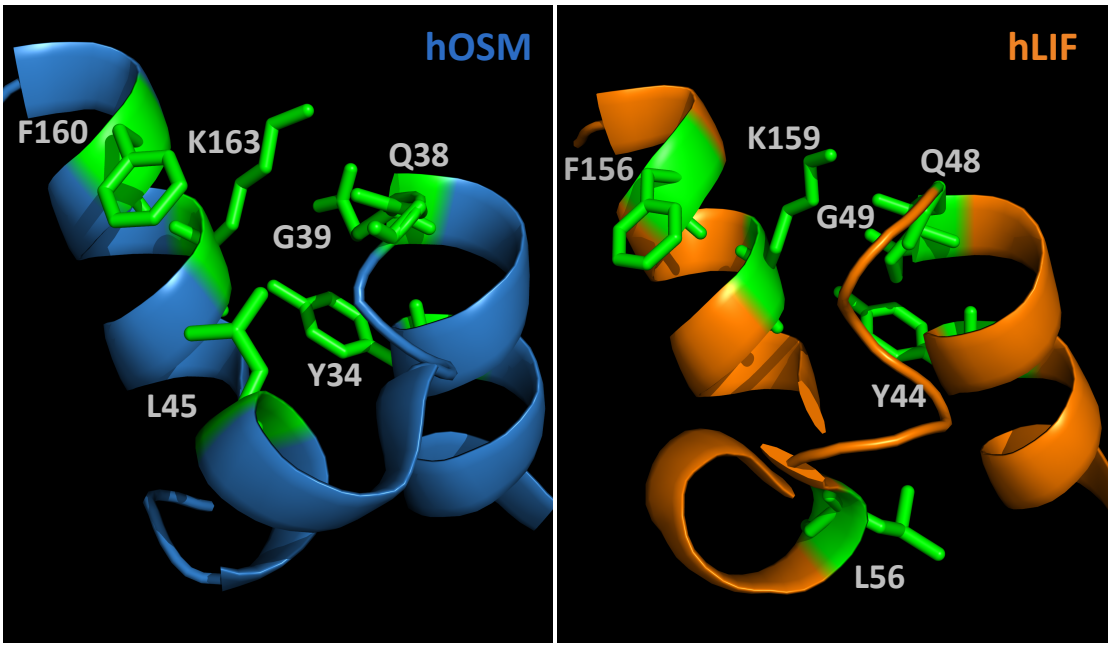

Figure 47: Spatial organization of binding site III in human OSM and human LIF. The residues in the N-terminal AB loop and N-terminal helix D regions of hOSM (left) and hLIF (right) are depicted, with the critical residues for hOSMR activation in hOSM and its equivalents in hLIF highlighted. Note the difference between the spatial location of L45 in hOSM and its corresponding L56 in hLIF, due to the presence of one additional amino acid in this region in the hLIF sequence.

Many more differences between these two proteins can be found in other regions outside the AB loop, but previous reports indicated that in the case of hLIFR interaction the regions outside binding site III (N-terminal AB loop, BC loop and N-terminal helix D) do not appear to play a major role. (Kallen et al. 1999) Thus when the binding site III regions of CNTF were transferred to another IL-6 family member, such as IL-6, the chimeric protein acquired the ability to initiate hLIFR signaling without additional modifications. (Kallen et al. 1999)

To determine whether this was also the case for the hOSMR, hLIF-based chimeras incorporating hOSM site III regions were employed. These experiments evidenced that a combined replacement of the N-terminal AB loop and N-terminal D helix is sufficient to enable hOSMR signaling by hLIF, confirming binding site III as the key region modulating recognition of the different gp130 co-receptors within the IL-6 family. It should be stressed, however, that other regions in hOSM outside binding site III also impact hOSMR interaction, as the AB loop and D-helix regions only confer limited hOSMR activation abilities when placed into hLIF. This would also explain why the N-terminal D-helix regions of hOSM and hLIF appear to be exchangeable for the hOSM-based chimeras, but in contrast only transferring the AB loop into hLIF is insufficient to initiate hOSMR signaling.

5.4. Molecular determinants of Oncostatin M species specificity

The existence of species-specific differences in receptor activation abilities between the human and murine OSM orthologs was originally described 20 years ago. (Ichihara et al. 1997) (Lindberg et al. 1998) While some recent evidence suggests that mOSM may act through the mLIFR complex in particular situations, (Walker et al. 2016) classical mOSM signaling via phosphorylation of mediator proteins such as STATs is generally only apparent upon mOSMR activation and does not take place if only the mLIFR is present. (Ichihara et al. 1997)

Despite this being a well-known phenomenon, the underlying mechanisms behind these species-dependent modes of action had never been addressed until now. Through the generation of human/mouse OSM chimeric cytokines, this work proves that differences in the AB loop of the orthologs can explain the lack of cross-

reactivity of the human and mouse ligands: exchanging even a small 12 amino acid region of mOSM by its human equivalent was sufficient to enable human receptor activation, initiating both hOSMR and hLIFR signaling.

Following up on this initial result, the creation of different combinations of mOSM point mutants within the identified region resulted in a more accurate identification of the structural features involved in determining species specificity of mOSM. Surprisingly, only two/three modifications in the murine cytokine were sufficient to ensure signaling through the human receptors (Fig. 48).

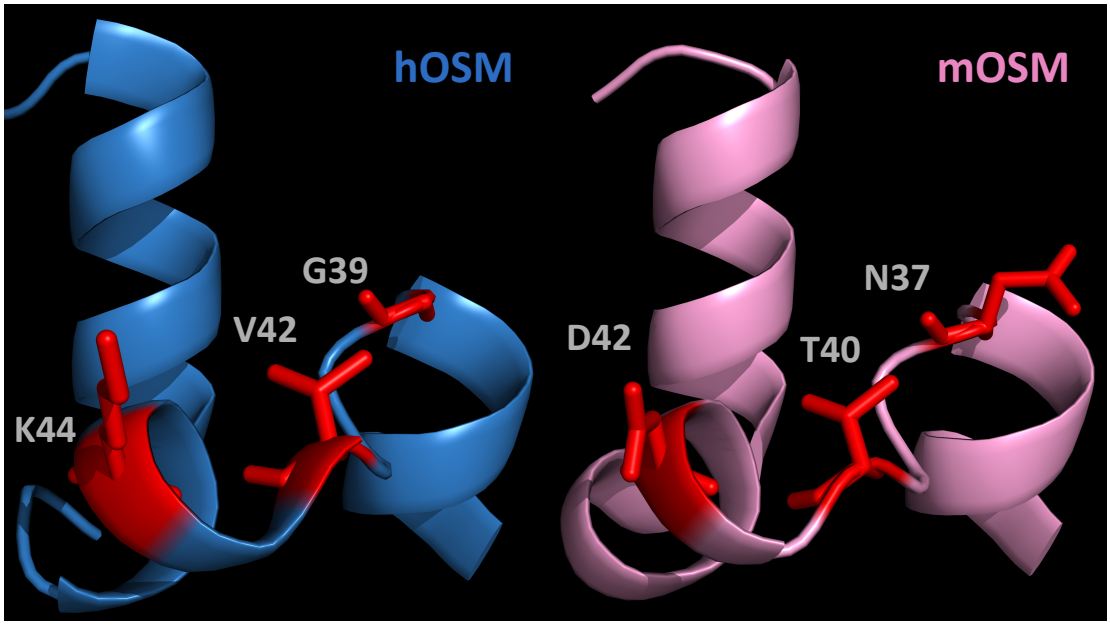

Figure 48: Mutations in the N-terminal AB loop of mouse OSM influencing species-specific receptor activation. The residues in the N-terminal AB loop and N-terminal helix D regions of hOSM (left) and mOSM (middle) are depicted, with the critical residues differentiating both cytokines highlighted in red. A mOSM variant with the substitutions N37G, T40V and D42K acquires the ability to activate the mLIFR, in addition to the mOSMR.

The most critical alteration appears to be the replacement of a glycine residue at the start of the mOSM AB loop by asparagine. As discussed in section 5.1, this glycine at position 39 in the human cytokine is required for hOSMR activation. Thus it should come as no surprise that only mOSM mutant proteins incorporating the N37G replacement became capable of activating the hOSMR. However, while the presence of this modification was clearly necessary, the single N37G point mutant only evidenced residual human receptor activation abilities, indicating that other residues in the AB loop must also be contributing towards the lack of affinity between mOSM and hOSMR.

The main additional difference between the human and mouse orthologs proved to be the presence of an aspartate instead of a lysine in position 42 of mOSM. Unlike the glycine involved in the first substitution, this lysine (K44 in hOSM) had not been identified as critical in the prior alanine scanning experiments. This fact suggests that the relevance of this amino acid replacement is most likely related to the nature of the substituting residue, and not of the lysine itself: while both are polar amino acids, lysine is positively charged and aspartate is negatively charged. (Betts & Russell 2003)

In this way, while the presence of a positively charged residue in that position of the AB loop may not be a strict requirement for hOSMR binding, it appears that a negatively charged amino acid in the same position can hinder human receptor activation. The opposite applies for the mouse receptor, since the presence of K44 appears to be the main factor impeding mOSMR activation by the human cytokine: the hOSM point mutants carrying a K44D substitution became able to initiate mOSMR signaling, although always at the expense of lower hOSMR signaling ability when compared to WT hOSM.

In addition to N37G and D42K, the replacement of threonine 40 by the corresponding valine in hOSM resulted in further enhancement of human receptor signaling. In this case there is no drastic difference in side chain properties between these residues, both being C-beta branched and hydrophobic, so the preference for valine over threonine is likely based on slight differences in the spatial conformation of the binding interface of mOSM. (Betts & Russell 2003)

However, none of these modifications in the AB loop of mOSM affected its ability to activate the mOSMR: this could be explained by the influence of other regions outside binding site III in OSMR interaction, as first discussed in section 5.1. Although the AB loop clearly plays an important role in mOSMR activation, mOSM has likely incorporated additional modifications in other regions of the protein favoring receptor interaction, which would allow for a certain degree of flexibility in the residue composition of the loop. In contrast hOSM, lacking these extra modifications, is forced to meet more stringent requirements in terms of its AB loop sequence to initiate mOSMR signaling.

5.5. Evolutionary implications

It has been reported in the past that genes of the immune system are subjected to directional selection, defined as a selection process favoring change: as a result these genes evolve rapidly, most likely in order to enhance the ability of the

organism to respond against new pathogens. (Hurst & Smith 1999) In light of this fact, it should come as no surprise that cytokines are among the most rapidly evolving genes in vertebrates. (Scapigliati et al. 2006)

Additionally, it is clear that gene duplication processes have played a major role in the diversification of both cytokines and its receptors: only two type I cytokine receptors, one of which is homologous to gp130, were identified in an urochordate (sea squid, *Ciona intestinalis*), which diverged from vertebrates approximately 794 million years ago. (Liongue & Ward 2007) In contrast 27 core receptors, including members of all 5 structural groups present in mammals, could be traced to the last common ancestor between teleosts and mammals, which separated around 476 million years ago. (Liongue & Ward 2007)

IL-6 family cytokines and its receptors are no exception, showing clear signs of a common origin through gene duplication: this is most evident for LIF and OSM, which are linked in tandem in human chromosome 22q12. (Rose et al. 1993) (Jeffery et al. 1993) (Giovannini et al. 1993) LIFR and OSMR are also thought to have originated after duplication of a common ancestral receptor, as they are found within a cluster of cytokine receptor loci in the chromosome 5p12-p13 in humans. (Gearing et al. 1993) (Arita et al. 2008) Moreover, there is by now ample evidence that ligands and receptors co-evolve to attain specific interaction, but little is known about how specificity evolves in natural proteins. (Moyle et al. 1994) (Richter et al. 1995) (Eick et al. 2012)

This work offers detailed molecular insight on a possible mechanism for the evolution of new cytokines. Human and murine LIF sport around 80% amino acid identity, compared to the approximately 50% observed for OSM, implying that LIF has a slower rate of evolution and should thus be closer to the common ancestral cytokine. (Layton et al. 1994) The experiments performed illustrate how a reduced number of modifications in the AB loop and N-terminal D-helix regions are sufficient to confer a new function to LIF, offering a clear molecular path to explain how the ancestral cytokine may have developed the additional ability to activate the OSMR (and thus become promiscuous) after the initial gene duplication event took place.

Protein promiscuity has gradually come to the forefront as a relevant mechanism in molecular evolution since it was first proposed as a driving force for the acquisition of new enzymatic functions. (Jensen 1976) (Khersonsky & Tawfik 2010) According to this theory, the most evolutionarily favorable path for the evolution of a new function is the appearance of a promiscuous variant of the original protein, which would still preserve its original function while simultaneously displaying a new one. (Aharoni et al. 2005)

In this way protein evolution would take place gradually, with very unspecific primitive enzymes steadily giving way to more specialized ones by means of gene duplication and divergence processes, resulting in increased metabolic efficiency. (Khersonsky et al. 2006) It has also been shown that a small number of modifications in the amino acid sequence of an enzyme can lead to drastic changes in their substrate affinity: as an example, the replacement of a single residue in a bacterial endopeptidase was sufficient for it to specifically cleave alanine-arginine bonds instead of the arginine-arginine sequences preferred by the WT enzyme. (Varadarajan et al. 2005)

Originally described in enzymes, the evolutionary role of promiscuity has been since extended to protein-protein interactions, with the first such report studying bacterial toxin-antitoxin systems: many bacteria express both toxins capable of inhibiting growth and specific antitoxins capable of sequestering it, similar to apoptotic genes in higher organisms. (Yamaguchi et al. 2011) Site-directed mutagenesis experiments showed that the apparition of a promiscuous toxin led first to the mutations in the antitoxin to specifically recognize it, followed by the toxin finally shedding its original affinity to become specific for the new antitoxin. (Aakre et al. 2015)

The acquisition of specificity can be attributed to the well-described evolutionary pressures favoring specificity in complex biological interaction networks in order to minimize crosstalk. (Capra et al. 2012) Thus, proteins participating in signaling pathways that are derived from a common origin have often incorporated mutations conferring specificity: such proved to be the case for SH3, a protein-interaction domain with multiple variants in the yeast genome. (Zarrinpar et al. 2003)

Taken together, this final stage in the evolution of a new protein is consistent with the situation observed for OSM in the murine system, in which it has lost the original function of its ancestral protein and can no longer interact with the LIFR. The present work indicates that this step would have involved the development of additional interactions between mOSM and the mOSMR, enabling the cytokine to modify its N-terminal AB loop in such a way as to inhibit mLIFR activation while maintaining mOSMR activity. Phylogenetic analyses for OSM and the OSMR are consistent with this hypothesis, identifying the murine orthologs (*Mus musculus*) as the most evolutionarily distant to the common ancestor in both cases (Fig. 26).

Additional evidence supporting the evolutionary divergence of the murine receptor along with its ligand can be found in the fact that IL-31, which is the only other known cytokine signaling through a complex including the OSMR, displays the same species specificity as OSM: human IL-31 is only able to activate the hOSMR/IL31RA

complex, while mouse IL-31 can only act through mOSMR/IL31RA. (Broxmeyer et al. 2007)

Despite the amount of circumstantial evidence available, conclusive proof of this hypothesis would most likely require the identification of the ligand-receptor binding interfaces in both human and mouse systems, which remain unknown so far. This could be achieved by cross-linking techniques coupled with mass spectrometry, (Rappsilber et al. 2000) which would allow the identification and comparison of particular regions of the different human and murine receptors in direct contact with OSM.

5.6. Consequences for future studies on Oncostatin M

Protein-based therapies constitute a particularly promising approach in the search for new medical treatments, since they are generally more specific and better tolerated by the body than small-molecule drugs. (Leader et al. 2008) These compounds achieve their therapeutic goals by activating specific molecular pathways in a wide array of ailments, including cardiovascular diseases. (Ichiki & Burnett 2012)

Within this frame, interest in the therapeutic applications of external OSM administration has steadily increased since the initial description of its beneficial effects in a murine model of myocardial infarction (MI). (Kubin et al. 2011) OSM cardioprotection is mediated by different mechanisms: the first of these is a direct effect on cardiomyocytes, promoting their dedifferentiation and enabling them to better survive the hypoxic conditions characteristic of a MI injury. (Pöling et al. 2012) Additionally, OSM is able to modulate the response of the immune system after MI, regulating macrophage accumulation in the heart through the induction of Reg protein production to drive cardiac healing. (Lörchner et al. 2015)

Other studies have since confirmed the protective effects of OSM in the heart after infarction in otherwise healthy animals, linking it to an increase in angiogenesis and autophagy in order to limit cardiac remodeling after infarction. (Zhang et al. 2015) (Hu et al. 2017) OSM also proved able to alleviate cardiac injury in diabetic mice through the inhibition of apoptotic processes. (Sun et al. 2015) In addition to acute heart disease, potential therapeutic usage of OSM has also been extended to cerebral ischemic stroke and spinal cord injury in other works. (Guo et al. 2015) (Slaets et al. 2014)

However, since all these studies were carried out in murine models, their translatability to the human situation is jeopardized by the receptor promiscuity of human OSM. It is possible that additional activation of the LIFR would enhance the

protective effects observed in mice after infarction, since LIF has been described to promote cardiomyocyte survival and stimulate regeneration after MI. (Zou et al. 2003) (Kanda et al. 2016) In addition, LIF administration outside the context of MI seemed to have modest positive effects on cardiac function without evidence of harmful effects on cardiomyocytes. (Zgheib et al. 2012)

Nevertheless, LIFR activation has also been linked to potentially harmful side effects such as hematologic alterations or cachexia, which could compromise its usefulness in a clinical setting. (Wallace et al. 1995) (Juan et al. 2009) Particularly worrying is the reported increase in platelet numbers, which was significantly higher for LIFR-activating cytokines in a comparative study. (Juan et al. 2009) This is due to the link between a higher platelet count and higher blood/plasma viscosity, as this last parameter has been positively associated with increased mortality rates in different patient cohorts in a variety of studies. (Ho 2004) (Keatinge et al. 1986) (Patterson et al. 2015) (Peters et al. 2017)

The human-like murine cytokines created in this work are expected to constitute a very useful tool in order to address this issue. Showing the ability to simultaneously activate mOSMR and mLIFR, these OSM variants can improve the human relevance of preclinical studies carried out in mice by mimicking the receptor activation profile that would take place in humans.

Along this line, future research plans are focused on assessing the impact of this human-like mouse OSM *in vivo* in terms of survival and functional recovery of the heart after MI, and comparing its beneficial effects to those evidenced by the unmodified mouse LIF and mouse OSM. Additionally, these cytokines will be administered to mice with no cardiac injury, monitoring their changes in weight and comparing their blood profiles to examine the existence of possible side effects.

In case the harmful side effects of LIFR activation were to outweigh its beneficial effects in these experiments, some of the mutant cytokines generated evidenced a certain preference towards hOSMR activation when compared to WT hOSM. These variants could thus become therapeutically relevant in the human situation, leading to a decrease in concomitant hLIFR activity due to hOSM treatment.

Finally, the generation of a transgenic mouse strain incorporating the described promiscuity-inducing substitutions into the endogenous mOSM sequence would result in a humanized mouse model of OSM action. Humanized models have been extensively used in the field of human hematopoiesis and immune function to minimize the significant differences developed between the murine and human immune systems after 65-75 million years of evolution, ranging from a different

lymphocyte/neutrophil balance to variations in cytokines/chemokines and its corresponding receptors. (Mestas & Hughes 2004)

Thus, in order to minimize the discrepancy between murine and human immune system biology, increasingly sophisticated humanized mouse models have been developed since the human growth hormone gene was first introduced into mice more than 30 years ago. (Brinster & Palmiter 1984) Nowadays such models employ genetically modified mice strains carrying mutations leading to immunodeficiency, such as the severe combined immunodeficiency (Scid) mutation: these animals are then subjected to sublethal irradiation or chemotherapy followed by transplants of human hematopoietic stem/progenitor cells, which are then able to engraft and give rise to the different human immune cell lineages. (Rongvaux et al. 2013)

Complemented with the substitution of several murine immunomodulatory cytokines by their human orthologs, the degree of complexity achieved by such a humanized mouse immune system can approach that of the native human system in terms of subset diversity and numbers. (Rongvaux et al. 2014) The use of these humanized murine models has been instrumental in the study of processes such as early human hematopoietic development, the initiation of acute myeloid leukemia, infectious diseases that exclusively target human cells such as the human immunodeficiency virus (HIV) or autoimmune diseases, among many others. (Doulatov et al. 2010) (Lapidot et al. 1994) (Rämer et al. 2011) (Namikawa et al. 1988) (Brehm et al. 2010)

In case of OSM, the generation of a humanized animal model would facilitate the study of its physiological actions *in vivo* in a manner more easily translatable to the human situation, while at the same time avoiding the difficulties presented by other animal models closer to humans such as primates, in which research activities are restricted due to both ethical considerations and economic reasons. (Rongvaux et al. 2013)

In conclusion, the work presented offers substantial insight into the structural features determining OSM interaction with its receptors in both the human and murine systems. This knowledge has important evolutionary implications for OSM and cytokines as a whole, suggesting a likely evolutionary path after duplication of the ancestral protein through promiscuous intermediates. In addition, some of the OSM variants created are expected to have promising applications in the field, improving the translatability of preclinical research studying the potential therapeutic application of OSM in murine models

6. Summary

Oncostatin M (OSM) is a prominent member of the IL-6 cytokine family. It signals through a heterodimeric OSM receptor/gp130 (OSMR) complex, specific for this cytokine and driving its many biological effects. Especially interesting are its potential therapeutic applications, as OSM has been beneficial in several murine cardiovascular disease models. Unfortunately, the translatability of these results to the human situation is not assured due to the different receptor activation abilities of human and mouse OSM (hOSM/mOSM). While mOSM is specific for the OSMR, hOSM signals through the leukemia inhibitory factor receptor/gp130 (LIFR) in addition to the OSMR, which could result in additional effects besides those reflected in preclinical mouse models. Taken together, there is a clear need for more information on these ligand-receptor interactions, the exclusive features of OSM governing OSMR activation and the divergence between hOSM and mOSM.

This thesis contributes new insights into these topics by means of molecular biology tools: in the first place, a mammalian expression system was established to obtain recombinant hOSM, mOSM and human leukemia inhibitory factor (hLIF) as well as an array of mutant variants of these cytokines. Cytokine stimulation experiments were then carried out in cell lines with specific readouts for each receptor complex, such as A375 cells for hOSMR, JAR cells for hLIFR, NIH3T3 cells for mOSMR or MH-S cells for mLIFR. Both shorter- and longer-term readouts were used, monitoring the phosphorylation of a key downstream signaling component (STAT3) 10 minutes after stimulation and measuring expression levels of well-known target genes (e.g. TIMP1) after 24 hours.

In a first approach, different binding site regions in hOSM or hLIF were exchanged to create hOSM/hLIF chimeras. Cell-stimulation experiments using these chimeric variants pointed to the N-terminal AB loop and N-terminal helix D regions of hOSM as responsible for hOSMR signaling, enabling hOSMR activation by a hLIF-based chimera with these two hOSM regions. Subsequently, site-directed mutagenesis studies individually targeting all the residues within these regions identified the amino acids Y34, Q38, G39, L45 and P153 as critical for hOSMR activation.

Similar methods were applied to study the receptor specificity of mOSM, which was mapped to its N-terminal AB loop by means of chimeric mouse/human OSM cytokines. In this case, point mutagenesis experiments revealed residues N37, T40 and D42 of the murine cytokine to be responsible for mOSMR specificity. This specificity was lost upon replacing these amino acids by their hOSM counterparts, resulting in a mOSM variant able to activate mLIFR as well as mOSMR. Finally, phylogenetic analyses indicated that the acquisition of specificity likely constitutes

the final stage in OSM evolution, as it is associated with a larger evolutionary distance from the ancestral form of the protein.

In sum, new key features of OSM enabling human and murine OSMR signaling have been identified and characterized in detail by using a variety of recombinant mutant cytokines. These results illustrate a novel path for cytokine evolution within the IL-6 family, in which an initial gene duplication event in the LIF/OSM ancestral gene was followed first by the acquisition of a new function (OSMR activation) and finally by the loss of the ancestral function (LIFR activation) to attain specificity. In addition, some of the mOSM mutants generated are expected to improve the translatability of future research on the therapeutic applications of OSM. Given that these mutant variants possess a human-like receptor signaling profile, their use in murine preclinical disease models will more closely reflect the potential effect of hOSM in the human situation, with LIFR being activated along with the OSMR.

7. Zusammenfassung

Oncostatin M (OSM) ist ein Zytokin der Interleukin-6 Familie. Die vielfältigen biologischen Funktionen von OSM werden auf molekularer Ebene durch die Aktivierung eines spezifischen heterodimeren Rezeptorkomplexes, bestehend aus OSM Rezeptor (OSMR) und gp130, vermittelt. Dabei implizieren insbesondere die aus murinen Tiermodellen gewonnenen Erkenntnisse eine protektive Wirkung von OSM in der Progression diverser kardiovaskulärer Erkrankungen. Eine direkte Ableitung für den Mensch und Fortführung translationaler Studien wird allerdings durch speziesspezifische Unterschiede in der Aktivierung unterschiedlicher Rezeptordimere erschwert. So vermittelt murines OSM (mOSM) seine Effekte exklusiv durch den OSMR/gp130 Komplex, wohingegen humanes OSM (hOSM) zusätzlich den leukemia inhibitory factor receptor (LIFR)/gp130 Komplex aktivieren kann. Insbesondere vor dem Hintergrund einer potentiell therapeutischen Bedeutung bedarf es weiterführende Untersuchungen, die jene Ligand-Rezeptor-Interkationen, sowie die Divergenz von mOSM und hOSM analysieren.

Die hier vorgelegte Studie adressiert jene Fragestellungen mittels folgender molekularbiologischer Methoden: Etablierung eines Säugertier-Expressionssystems zur Generierung von rekombinanten, unmodifizierten als auch mutierten Varianten von hOSM, mOSM und hLIF; gefolgt von Zytokinstimulationsstudien in Zelllinien, die exklusiv den hOSMR (A375), hLIFR (JAR), mOSMR (NIH3T3) und mLIFR (MH-S) exprimieren. Ferner wurden Kurzzeit- sowie Langzeitstimulationen durchgeführt, in der die Phosphorylierung des Signalmoleküls STAT3 nach 10 Minuten, als auch die vermehrte Expression von bekannten Zielgenen (u.a. TIMP-1) nach 24 Stunden bestimmt und so als distinkte Parameter zur Aktivierung des OSMR genutzt wurden.

Zur Identifikation zytokinspezifischer Bindungsstellen von OSM und LIF wurden anfänglich chimäre hOSM/hLIF Varianten generiert, in dem unterschiedliche Bindungsstellen von hOSM und hLIF wechselseitig ausgetauscht wurden. Nachfolgende Stimulationsstudien mit chimären hOSM und hLIF charakterisierten dabei die N-terminale AB-Schleife, sowie die N-terminale helikale D-Region als hauptverantwortliche Regionen für die Aktivierung des OSMR, indem die Aktivierung des hOSMR durch eine chimäre hLIF Variante mit beiden Regionen reproduziert werden konnte. Durch die systematische Generierung von Punktmutationen in beiden Regionen konnten ferner die Aminosäurenreste Y34, Q38, G39, L45 and P153 als kritische Komponenten für die spezifische Aktivierung des OSMR durch OSM identifiziert werden.

Vergleichbare Methoden und Analysen wurden zur Charakterisierung der Bindungsspezifizität von mOSM an den mOSMR genutzt. Hier konnte die N-terminale

AB-Schleife und die darin befindlichen Aminosäurenreste N37, T40 und D42 durch die Generierung von chimären mOSM und hOSM Proteinen und nachfolgender Punktmutationen als entscheidende Größen für die Spezifität von mOSM identifiziert werden. Zusätzlich konnte durch die simultane Substitution dieser drei Aminosäuren eine murine OSM Variante generiert werden, die den mLIFR als auch den mOSMR aktiviert. Mit Hilfe von phylogenetischen Modellen konnte gezeigt werden, dass die hier identifizierten unterschiedlichen Bindungsspezifitäten von humanen und murinen OSM einen evolutionären Prozess reflektiert, deren Ursprung auf einem gemeinsamen Vorläufer-Gen begründet ist.

Insgesamt charakterisiert und identifiziert die vorgelegte Studie molekulare Unterschiede, die zur speziesspezifischen Aktivierung des OSMR durch humanes und murines OSM führen. Die durchgeführten Analysen liefern somit einen molekularen Erklärungsansatz für den Entwicklungsprozess und die dadurch erworbene Spezifität der IL-6 Zytokinfamilie, d.h. dass die Duplikation des Vorläufergens zunächst zur Akquisition neuer (Aktivierung des OSMR) und anschließend zum Verlust ursprünglicher Funktionen (Inaktivierung des LIFR) führte. Schließlich ergeben sich durch die Generierung von murinen OSM Varianten, die sich in der Aktivierung der Rezeptorensysteme äquivalent zu hOSM verhalten, neue Anwendungsmöglichkeiten in präklinischen, murinen Tiermodellen, um die Aktivität von humanem OSM unter (patho-)physiologischen Bedingungen zu studieren.

8. List of Abbreviations

BSA	Bovine serum albumin
cDNA	Complementary DNA
CLC	Cardiotrophin-like cytokine
CNTF	Ciliary neurotrophic factor
CNTFR	Ciliary neurotrophic factor receptor
CT-1	Cardiotrophin-1
DMEM	Dulbecco's modified Eagle medium
DMSO	Dimethyl sulfoxide
EBI-3	Epstein-Barr virus induced 3
EDTA	Ethylenediaminetetraacetic acid
FBS	Fetal bovine serum
gp130	Glycoprotein 130
h (prefix)	Human
His-tag	Hexahistidine tag
HIV	Human immunodeficiency virus
IL-6	Interleukin-6
IL-6R	Interleukin-6 receptor
IL-11	Interleukin-11
IL-11RA	Interleukin-11 receptor alpha
IL-27	Interleukin-27
IL-27RA	Interleukin-27 receptor subunit alpha
IL-31	Interleukin-31
IL-31RA	Interleukin-31 receptor alpha
IPTG	Isopropyl β-D-1-thiogalactopyranoside
ITC	Isothermal titration calorimetry
JAK	Janus kinase family
JNK	c-Jun N-terminal kinase
KD	Knockdown
LB	Lysogeny broth
LDL	Low-density lipoprotein
LIF	Leukemia inhibitory factor
LIFR	Leukemia inhibitory factor receptor
m (prefix)	Mouse
MAPK	Mitogen-activated protein kinases
metaGA	Metapopulation genetic algorithm
MI	Myocardial infarction
MS	Mass spectrometry
Ni-NTA	Nickel-nitrilotriacetic acid
NMR	Nuclear magnetic resonance

NP	Neuropoietin
OSM	Oncostatin M
OSMR	Oncostatin M receptor
PCR	Polymerase chain reaction
PEG-6000	Polyethylene Glycol 6000
PI3K/Akt	Phosphoinositide 3-kinase/protein kinase B
PMSF	Phenylmethylsulfonylfluorid
RefSeq	Reference Sequence database
RPMI	Roswell Park Memorial Institute
RT	Room temperature
Scid	Severe combined immunodeficiency
SDS	Sodium dodecyl sulfate
SDS-PAGE	SDS-polyacrylamide gel electrophoresis
SO	Sequence-optimized
SPR	Surface plasmon resonance
STAT	Signal transducer and activator of transcription
TAE	Tris-acetate-EDTA
TBS-T	Tris-buffered saline + Tween 20
TE	Tris-EDTA
TEMED	Tetramethylethylenediamine
TIMP1	Tissue inhibitor of metalloproteinase 1
WT	Wild-type

9. List of Figures

10. References

Aakre, C.D. et al., 2015. Evolving new protein-protein interaction specificity through promiscuous intermediates. *Cell*, 163(3), pp.594–606.

Aharoni, A. et al., 2005. The "evolvability" of promiscuous protein functions. *Nature genetics*, 37(1), pp.73–6.

Akira, S. et al., 1994. Molecular cloning of APRF, a novel IFN-stimulated gene factor 3 p91-related transcription factor involved in the gp130-mediated signaling pathway. *Cell*, 77(1), pp.63–71.

Albasanz-Puig, A. et al., 2011. Oncostatin M is expressed in atherosclerotic lesions: a role for Oncostatin M in the pathogenesis of atherosclerosis. *Atherosclerosis*, 216(2), pp.292–8.

Arita, K. et al., 2008. Oncostatin M receptor-beta mutations underlie familial primary localized cutaneous amyloidosis. *American journal of human genetics*, 82(1), pp.73–80.

Auguste, P. et al., 1997. Signaling of type II oncostatin M receptor. *The Journal of biological chemistry*, 272(25), pp.15760–4.

Baneyx, F. & Mujacic, M., 2004. Recombinant protein folding and misfolding in Escherichia coli. *Nature biotechnology*, 22(11), pp.1399–408.

Baumann, H. et al., 1996. Complex of the soluble IL-11 receptor and IL-11 acts as IL-6-type cytokine in hepatic and nonhepatic cells. *Journal of immunology (Baltimore, Md. : 1950)*, 157(1), pp.284–90.

Bazan, J.F., 1990. Haemopoietic receptors and helical cytokines. *Immunology today*, 11(10), pp.350–4.

Besenicar, M. et al., 2006. Surface plasmon resonance in protein-membrane interactions. *Chemistry and physics of lipids*, 141(1–2), pp.169–78.

Betts, M.J. & Russell, R.B., 2003. Amino Acid Properties and Consequences of Substitutions. In *Bioinformatics for Geneticists*. Chichester, UK: John Wiley & Sons, Ltd, pp. 289–316.

Biasini, M. et al., 2014. SWISS-MODEL: modelling protein tertiary and quaternary structure using evolutionary information. *Nucleic acids research*, 42(Web Server issue), pp.W252-8.

Boniface, K. et al., 2007. Oncostatin M secreted by skin infiltrating T lymphocytes is a potent keratinocyte activator involved in skin inflammation. *Journal of immunology (Baltimore, Md. : 1950)*, 178(7), pp.4615–22.

Boulanger, M.J., Bankovich, A.J., et al., 2003. Convergent mechanisms for recognition of divergent cytokines by the shared signaling receptor gp130. *Molecular cell*, 12(3), pp.577–89.

Boulanger, M.J., Chow, D., et al., 2003. Hexameric structure and assembly of the interleukin-6/IL-6 alpha-receptor/gp130 complex. *Science (New York, N.Y.)*, 300(5628), pp.2101–4.

Brehm, M.A. et al., 2010. Human immune system development and rejection of human islet allografts in spontaneously diabetic NOD-Rag1null IL2rgammanull Ins2Akita mice. *Diabetes*, 59(9), pp.2265–70.

Brinster, R.L. & Palmiter, R.D., 1984. Transgenic mice containing growth hormone fusion genes. *Philosophical transactions of the Royal Society of London. Series B, Biological sciences*, 307(1132), pp.309–12.

Broxmeyer, H.E. et al., 2007. Regulation of myeloid progenitor cell proliferation/survival by IL-31 receptor and IL-31. *Experimental hematology*, 35(4 Suppl 1), pp.78–86.

Bugno, M. et al., 1995. Identification of the interleukin-6/oncostatin M response element in the rat tissue inhibitor of metalloproteinases-1 (TIMP-1) promoter. *Nucleic acids research*, 23(24), pp.5041–7.

Cannon, J.G., 2000. Inflammatory Cytokines in Nonpathological States. *News in physiological sciences*, 15, pp.298–303.

Capra, E.J. et al., 2012. Adaptive mutations that prevent crosstalk enable the expansion of paralogous signaling protein families. *Cell*, 150(1), pp.222–32.

Chalmers, M.J. et al., 2006. Probing protein ligand interactions by automated hydrogen/deuterium exchange mass spectrometry. *Analytical chemistry*, 78(4), pp.1005–14.

Chattopadhyay, S. et al., 2007. Interleukin-31 and oncostatin-M mediate distinct signaling reactions and response patterns in lung epithelial cells. *The Journal of biological chemistry*, 282(5), pp.3014–26.

Chollangi, S. et al., 2012. A unique loop structure in oncostatin M determines binding affinity toward oncostatin M receptor and leukemia inhibitory factor receptor. *The Journal of biological chemistry*, 287(39), pp.32848–59.

Cunningham, B.C. & Wells, J.A., 1989. High-resolution epitope mapping of hGH-receptor interactions by alanine-scanning mutagenesis. *Science (New York, N.Y.)*, 244(4908), pp.1081–5.

Davis, S., Aldrich, T.H., Stahl, N., et al., 1993. LIFR beta and gp130 as heterodimerizing signal transducers of the tripartite CNTF receptor. *Science (New York, N.Y.)*, 260(5115), pp.1805–8.

Davis, S., Aldrich, T.H., Ip, N.Y., et al., 1993. Released form of CNTF receptor alpha component as a soluble mediator of CNTF responses. *Science (New York, N.Y.)*, 259(5102), pp.1736–9.

Deller, M.C. et al., 2000. Crystal structure and functional dissection of the cytostatic cytokine oncostatin M. *Structure*, 8, pp.863–74.

Derouet, D. et al., 2004. Neuropoietin, a new IL-6-related cytokine signaling through the ciliary neurotrophic factor receptor. *Proceedings of the National Academy of Sciences of the United States of America*, 101(14), pp.4827–32.

Devergne, O., Birkenbach, M. & Kieff, E., 1997. Epstein-Barr virus-induced gene 3 and the p35 subunit of interleukin 12 form a novel heterodimeric hematopoietin.

Proceedings of the National Academy of Sciences of the United States of America, 94(22), pp.12041–6.

Dillon, S.R. et al., 2004. Interleukin 31, a cytokine produced by activated T cells, induces dermatitis in mice. *Nature immunology*, 5(7), pp.752–60.

Diveu, C. et al., 2003. GPL, a novel cytokine receptor related to GP130 and leukemia inhibitory factor receptor. *The Journal of biological chemistry*, 278(50), pp.49850–9.

Doulatov, S. et al., 2010. Revised map of the human progenitor hierarchy shows the origin of macrophages and dendritic cells in early lymphoid development. *Nature immunology*, 11(7), pp.585–93.

Drechsler, J., Grötzinger, J. & Hermanns, H.M., 2012. Characterization of the rat oncostatin M receptor complex which resembles the human, but differs from the murine cytokine receptor. *PloS one*, 7(8), p.e43155.

Dreuw, A. et al., 2004. Characterization of the signaling capacities of the novel gp130-like cytokine receptor. *The Journal of biological chemistry*, 279(34), pp.36112–20.

Eick, G.N. et al., 2012. Evolution of minimal specificity and promiscuity in steroid hormone receptors. *PLoS genetics*, 8(11), p.e1003072.

Elson, G.C. et al., 2000. CLF associates with CLC to form a functional heteromeric ligand for the CNTF receptor complex. *Nature neuroscience*, 3(9), pp.867–72.

Fritz, D.K. et al., 2006. Oncostatin-M up-regulates VCAM-1 and synergizes with IL-4 in eotaxin expression: involvement of STAT6. *Journal of immunology (Baltimore, Md. : 1950)*, 176(7), pp.4352–60.

Gearing, D.P. et al., 1991. Leukemia inhibitory factor receptor is structurally related to the IL-6 signal transducer, gp130. *The EMBO journal*, 10(10), pp.2839–48.

Gearing, D.P. et al., 1992. The IL-6 signal transducer, gp130: an oncostatin M receptor and affinity converter for the LIF receptor. *Science (New York, N.Y.)*, 255(5050), pp.1434–7.

Gearing, D.P. et al., 1993. The leukemia inhibitory factor receptor (LIFR) gene is located within a cluster of cytokine receptor loci on mouse chromosome 15 and human chromosome 5p12-p13. *Genomics*, 18(1), pp.148–50.

Giovannini, M. et al., 1993. Tandem linkage of genes coding for leukemia inhibitory factor (LIF) and oncostatin M (OSM) on human chromosome 22. *Cytogenetics and cell genetics*, 64(3–4), pp.240–4.

Goldie, K.N. et al., 2014. Cryo-electron microscopy of membrane proteins. *Methods in molecular biology (Clifton, N.J.)*, 1117, pp.325–41.

Goldstein, D.J. et al., 1992. A glutamine residue in the membrane-associating domain of the bovine papillomavirus type 1 E5 oncoprotein mediates its binding to a transmembrane component of the vacuolar H(+)-ATPase. *Journal of virology*, 66(1), pp.405–13.

Grenier, A. et al., 1999. Oncostatin M production and regulation by human

polymorphonuclear neutrophils. *Blood*, 93(4), pp.1413–21.
Grove, R.I. et al., 1991. Oncostatin M up-regulates low density lipoprotein receptors in HepG2 cells by a novel mechanism. *The Journal of biological chemistry*, 266(27), pp.18194–9.
Guihard, P. et al., 2012. Induction of osteogenesis in mesenchymal stem cells by activated monocytes/macrophages depends on oncostatin M signaling. *Stem cells (Dayton, Ohio)*, 30(4), pp.762–72.
Guilloteau, K. et al., 2010. Skin Inflammation Induced by the Synergistic Action of IL-17A, IL-22, Oncostatin M, IL-1{alpha}, and TNF-{alpha} Recapitulates Some Features of Psoriasis. *Journal of immunology (Baltimore, Md. : 1950)*.
Guo, S. et al., 2015. Oncostatin M Confers Neuroprotection against Ischemic Stroke. *The Journal of neuroscience : the official journal of the Society for Neuroscience*, 35(34), pp.12047–62.
Gyotoku, E. et al., 2001. The IL-6 family cytokines, interleukin-6, interleukin-11, oncostatin M, and leukemia inhibitory factor, enhance mast cell growth through fibroblast-dependent pathway in mice. *Archives of dermatological research*, 293(10), pp.508–14.
Hegyi, H. & Gerstein, M., 1999. The relationship between protein structure and function: a comprehensive survey with application to the yeast genome. *Journal of molecular biology*, 288(1), pp.147–64.
Heinrich, P.C. et al., 1998. Interleukin-6-type cytokine signalling through the gp130/Jak/STAT pathway. *The Biochemical journal*, 334 (Pt 2, pp.297–314.
Heinrich, P.C. et al., 2003. Principles of interleukin (IL)-6-type cytokine signalling and its regulation. *The Biochemical journal*, 374(Pt 1), pp.1–20.
Helaers, R. & Milinkovitch, M.C., 2010. MetaPIGA v2.0: maximum likelihood large phylogeny estimation using the metapopulation genetic algorithm and other stochastic heuristics. *BMC bioinformatics*, 11, p.379.
Hermanns, H.M. et al., 1999. Contributions of leukemia inhibitory factor receptor and oncostatin M receptor to signal transduction in heterodimeric complexes with glycoprotein 130. *Journal of immunology (Baltimore, Md. : 1950)*, 163(12), pp.6651–8.
Hermanns, H.M. et al., 2000. Non-redundant signal transduction of interleukin-6-type cytokines. The adapter protein Shc is specifically recruited to rhe oncostatin M receptor. *The Journal of biological chemistry*, 275(52), pp.40742–8.
Hermanns, H.M., 2015. Oncostatin M and interleukin-31: Cytokines, receptors, signal transduction and physiology. *Cytokine & growth factor reviews*, 26(5), pp.545–58.
Hibi, M. et al., 1990. Molecular cloning and expression of an IL-6 signal transducer, gp130. *Cell*, 63(6), pp.1149–57.
Hilfiker-Kleiner, D. et al., 2004. Signal transducer and activator of transcription 3 is

required for myocardial capillary growth, control of interstitial matrix deposition, and heart protection from ischemic injury. *Circulation research*, 95(2), pp.187–95.

Hirano, T. et al., 1986. Complementary DNA for a novel human interleukin (BSF-2) that induces B lymphocytes to produce immunoglobulin. *Nature*, 324(6092), pp.73–6.

Hirano, T. et al., 1985. Purification to homogeneity and characterization of human B-cell differentiation factor (BCDF or BSFp-2). *Proceedings of the National Academy of Sciences of the United States of America*, 82(16), pp.5490–4.

Ho, C.-H., 2004. Relationship between blood cells and blood viscosity. *American journal of hematology*, 75(4), p.264.

de Hooge, A.S.K. et al., 2003. Growth plate damage, a feature of juvenile idiopathic arthritis, can be induced by adenoviral gene transfer of oncostatin M: a comparative study in gene-deficient mice. *Arthritis and rheumatism*, 48(6), pp.1750–61.

Hoover, D.M. & Lubkowski, J., 2002. DNAWorks: an automated method for designing oligonucleotides for PCR-based gene synthesis. *Nucleic acids research*, 30(10), p.e43.

Horn, D. et al., 1990. Regulation of cell growth by recombinant oncostatin M. *Growth factors (Chur, Switzerland)*, 2(2–3), pp.157–65.

Hu, J. et al., 2017. OSM mitigates post-infarction cardiac remodeling and dysfunction by up-regulating autophagy through Mst1 suppression. *Biochimica et biophysica acta*, 1863(8), pp.1951–1961.

Hudson, K.R., Vernallis, A.B. & Heath, J.K., 1996. Characterization of the receptor binding sites of human leukemia inhibitory factor and creation of antagonists. *The Journal of biological chemistry*, 271(20), pp.11971–8.

Hui, W. et al., 2005. A model of inflammatory arthritis highlights a role for oncostatin M in pro-inflammatory cytokine-induced bone destruction via RANK/RANKL. *Arthritis research & therapy*, 7(1), pp.R57-64.

Hunter, C.A., Singh, J. & Thornton, J.M., 1991. Pi-pi interactions: the geometry and energetics of phenylalanine-phenylalanine interactions in proteins. *Journal of molecular biology*, 218(4), pp.837–46.

Hurst, L.D. & Smith, N.G., 1999. Do essential genes evolve slowly? *Current biology : CB*, 9(14), pp.747–50.

Huyton, T. et al., 2007. An unusual cytokine:Ig-domain interaction revealed in the crystal structure of leukemia inhibitory factor (LIF) in complex with the LIF receptor. *Proceedings of the National Academy of Sciences of the United States of America*, 104(31), pp.12737–42.

Ichihara, M. et al., 1997. Oncostatin M and leukemia inhibitory factor do not use the same functional receptor in mice. *Blood*, 90(1), pp.165–73.

Ichiki, T. & Burnett, J.C., 2012. Protein therapeutics for cardiovascular disease: it is all

about delivery. *Journal of the American College of Cardiology*, 60(24), pp.2558–60.

Ip, N.Y. et al., 1992. CNTF and LIF act on neuronal cells via shared signaling pathways that involve the IL-6 signal transducing receptor component gp130. *Cell*, 69(7), pp.1121–32.

Jahani-Asl, A. et al., 2016. Control of glioblastoma tumorigenesis by feed-forward cytokine signaling. *Nature neuroscience*, 19(6), pp.798–806.

Jeffery, E., Price, V. & Gearing, D.P., 1993. Close proximity of the genes for leukemia inhibitory factor and oncostatin M. *Cytokine*, 5(2), pp.107–11.

Jensen, R.A., 1976. Enzyme recruitment in evolution of new function. *Annual review of microbiology*, 30, pp.409–25.

Juan, T.S.-C. et al., 2009. Mice overexpressing murine oncostatin M (OSM) exhibit changes in hematopoietic and other organs that are distinct from those of mice overexpressing human OSM or bovine OSM. *Veterinary pathology*, 46(1), pp.124–37.

Kallen, K.J. et al., 1999. Receptor recognition sites of cytokines are organized as exchangeable modules. Transfer of the leukemia inhibitory factor receptor-binding site from ciliary neurotrophic factor to interleukin-6. *The Journal of biological chemistry*, 274(17), pp.11859–67.

Kallestad, J.C., Shoyab, M. & Linsley, P.S., 1991. Disulfide bond assignment and identification of regions required for functional activity of oncostatin M. *The Journal of biological chemistry*, 266(14), pp.8940–5.

Kanda, M. et al., 2016. Leukemia Inhibitory Factor Enhances Endogenous Cardiomyocyte Regeneration after Myocardial Infarction. *PloS one*, 11(5), p.e0156562.

Keatinge, W.R. et al., 1986. Increased platelet and red cell counts, blood viscosity, and plasma cholesterol levels during heat stress, and mortality from coronary and cerebral thrombosis. *The American journal of medicine*, 81(5), pp.795–800.

Khersonsky, O., Roodveldt, C. & Tawfik, D.S., 2006. Enzyme promiscuity: evolutionary and mechanistic aspects. *Current opinion in chemical biology*, 10(5), pp.498–508.

Khersonsky, O. & Tawfik, D.S., 2010. Enzyme promiscuity: a mechanistic and evolutionary perspective. *Annual review of biochemistry*, 79, pp.471–505.

Kishimoto, T., Taga, T. & Akira, S., 1994. Cytokine signal transduction. *Cell*, 76(2), pp.253–62.

Kong, N. et al., 2009. Pilot-scale fermentation, purification, and characterization of recombinant human Oncostatin M in Pichia pastoris. *Protein expression and purification*, 63(2), pp.134–9.

Kubin, T. et al., 2011. Oncostatin M is a major mediator of cardiomyocyte dedifferentiation and remodeling. *Cell stem cell*, 9(5), pp.420–32.

Lafuse, W.P., 1991. Molecular biology of murine MHC class II genes. *Critical reviews*

in immunology, 11(3–4), pp.167–94.
Lapidot, T. et al., 1994. A cell initiating human acute myeloid leukaemia after transplantation into SCID mice. *Nature*, 367(6464), pp.645–8.
Layton, M.J. et al., 1994. Conversion of the biological specificity of murine to human leukemia inhibitory factor by replacing 6 amino acid residues. *The Journal of biological chemistry*, 269(47), pp.29891–6.
Leader, B., Baca, Q.J. & Golan, D.E., 2008. Protein therapeutics: a summary and pharmacological classification. *Nature reviews. Drug discovery*, 7(1), pp.21–39.
Lemmon, A.R. & Milinkovitch, M.C., 2002. The metapopulation genetic algorithm: An efficient solution for the problem of large phylogeny estimation. *Proceedings of the National Academy of Sciences of the United States of America*, 99(16), pp.10516–21.
Leurs, U., Mistarz, U.H. & Rand, K.D., 2015. Getting to the core of protein pharmaceuticals--Comprehensive structure analysis by mass spectrometry. *European journal of pharmaceutics and biopharmaceutics : official journal of Arbeitsgemeinschaft fur Pharmazeutische Verfahrenstechnik e.V*, 93, pp.95–109.
Levy, G. et al., 2015. Long-term culture and expansion of primary human hepatocytes. *Nature biotechnology*, 33(12), pp.1264–1271.
Li, W. et al., 2002. STAT3 contributes to the mitogenic response of hepatocytes during liver regeneration. *The Journal of biological chemistry*, 277(32), pp.28411–7.
Lieberman, R.L., Peek, M.E. & Watkins, J.D., 2013. Determination of soluble and membrane protein structures by X-ray crystallography. *Methods in molecular biology (Clifton, N.J.)*, 955, pp.475–93.
Lindberg, R.A. et al., 1998. Cloning and characterization of a specific receptor for mouse oncostatin M. *Molecular and cellular biology*, 18(6), pp.3357–67.
Linsley, P.S. et al., 1989. Identification and characterization of cellular receptors for the growth regulator, oncostatin M. *The Journal of biological chemistry*, 264(8), pp.4282–9.
Liongue, C. & Ward, A.C., 2007. Evolution of Class I cytokine receptors. *BMC evolutionary biology*, 7, p.120.
Liu, Z. et al., 2016. Transient protein-protein interactions visualized by solution NMR. *Biochimica et biophysica acta*, 1864(1), pp.115–22.
Lörchner, H. et al., 2015. Myocardial healing requires Reg3β-dependent accumulation of macrophages in the ischemic heart. *Nature medicine*, 21(4), pp.353–62.
Luo, P. et al., 2016. Hepatic Oncostatin M Receptor β Regulates Obesity-Induced Steatosis and Insulin Resistance. *The American journal of pathology*, 186(5), pp.1278–92.
Lütticken, C. et al., 1994. Association of transcription factor APRF and protein kinase

Jak1 with the interleukin-6 signal transducer gp130. *Science (New York, N.Y.)*, 263(5143), pp.89–92.

Maglott, D.R. et al., 2000. NCBI's LocusLink and RefSeq. *Nucleic acids research*, 28(1), pp.126–8.

Malik, N. et al., 1989. Molecular cloning, sequence analysis, and functional expression of a novel growth regulator, oncostatin M. *Molecular and cellular biology*, 9(7), pp.2847–53.

de Marco, A., 2009. Strategies for successful recombinant expression of disulfide bond-dependent proteins in Escherichia coli. *Microbial cell factories*, 8, p.26.

Di Marco, A. et al., 1996. Identification of ciliary neurotrophic factor (CNTF) residues essential for leukemia inhibitory factor receptor binding and generation of CNTF receptor antagonists. *Proceedings of the National Academy of Sciences of the United States of America*, 93(17), pp.9247–52.

Marion, D., 2013. An introduction to biological NMR spectroscopy. *Molecular & cellular proteomics : MCP*, 12(11), pp.3006–25.

McDonald, J.H., 2014. Handbook of Biological Statistics (3rd ed.). Sparky House Publishing, Baltimore, Maryland.

McDonald, N.Q., Panayotatos, N. & Hendrickson, W.A., 1995. Crystal structure of dimeric human ciliary neurotrophic factor determined by MAD phasing. *The EMBO journal*, 14(12), pp.2689–99.

Mestas, J. & Hughes, C.C.W., 2004. Of mice and not men: differences between mouse and human immunology. *Journal of immunology (Baltimore, Md. : 1950)*, 172(5), pp.2731–8.

Miyaoka, Y. et al., 2006. Oncostatin M inhibits adipogenesis through the RAS/ERK and STAT5 signaling pathways. *The Journal of biological chemistry*, 281(49), pp.37913–20.

Morikawa, Y. et al., 2004. Essential function of oncostatin m in nociceptive neurons of dorsal root ganglia. *The Journal of neuroscience : the official journal of the Society for Neuroscience*, 24(8), pp.1941–7.

Morrison, K.L. & Weiss, G.A., 2001. Combinatorial alanine-scanning. *Current opinion in chemical biology*, 5(3), pp.302–7.

Mosley, B. et al., 1996. Dual oncostatin M (OSM) receptors. Cloning and characterization of an alternative signaling subunit conferring OSM-specific receptor activation. *The Journal of biological chemistry*, 271(51), pp.32635–43.

Mosmann, T., 1983. Rapid colorimetric assay for cellular growth and survival: application to proliferation and cytotoxicity assays. *Journal of immunological methods*, 65(1–2), pp.55–63.

Moyle, W.R. et al., 1994. Co-evolution of ligand-receptor pairs. *Nature*, 368(6468), pp.251–5.

Murakami, M. et al., 1993. IL-6-induced homodimerization of gp130 and associated activation of a tyrosine kinase. *Science (New York, N.Y.)*, 260(5115), pp.1808–10.

Nakamura, K. et al., 2004. Hepatocyte proliferation and tissue remodeling is impaired after liver injury in oncostatin M receptor knockout mice. *Hepatology (Baltimore, Md.)*, 39(3), pp.635–44.

Namikawa, R. et al., 1988. Infection of the SCID-hu mouse by HIV-1. *Science (New York, N.Y.)*, 242(4886), pp.1684–6.

Nandurkar, H.H. et al., 1996. The human IL-11 receptor requires gp130 for signalling: demonstration by molecular cloning of the receptor. *Oncogene*, 12(3), pp.585–93.

Negoro, S. et al., 2001. Glycoprotein 130 regulates cardiac myocyte survival in doxorubicin-induced apoptosis through phosphatidylinositol 3-kinase/Akt phosphorylation and Bcl-xL/caspase-3 interaction. *Circulation*, 103(4), pp.555–61.

Newell, J.G., Davies, M. & Bateson, A.N., 2000. The use of site-directed mutagenesis, transient transfection, and radioligand binding. A method for the characterization of receptor-ligand interactions. *Molecular biotechnology*, 14(1), pp.25–45.

O'Hara, K.A. et al., 2003. Oncostatin M: an interleukin-6-like cytokine relevant to airway remodelling and the pathogenesis of asthma. *Clinical and experimental allergy : journal of the British Society for Allergy and Clinical Immunology*, 33(8), pp.1026–32.

Patterson, C.C. et al., 2015. Which biomarkers are predictive specifically for cardiovascular or for non-cardiovascular mortality in men? Evidence from the Caerphilly Prospective Study (CaPS). *International journal of cardiology*, 201, pp.113–8.

Pellecchia, M. et al., 2008. Perspectives on NMR in drug discovery: a technique comes of age. *Nature reviews. Drug discovery*, 7(9), pp.738–45.

Pennica, D. et al., 1995. Cardiotrophin-1. Biological activities and binding to the leukemia inhibitory factor receptor/gp130 signaling complex. *The Journal of biological chemistry*, 270(18), pp.10915–22.

Peters, S.A. et al., 2017. Plasma and blood viscosity in the prediction of cardiovascular disease and mortality in the Scottish Heart Health Extended Cohort Study. *European journal of preventive cardiology*, 24(2), pp.161–167.

Pflanz, S. et al., 2002. IL-27, a heterodimeric cytokine composed of EBI3 and p28 protein, induces proliferation of naive CD4+ T cells. *Immunity*, 16(6), pp.779–90.

Pflanz, S. et al., 2004. WSX-1 and glycoprotein 130 constitute a signal-transducing receptor for IL-27. *Journal of immunology (Baltimore, Md. : 1950)*, 172(4), pp.2225–31.

Pierce, M.M., Raman, C.S. & Nall, B.T., 1999. Isothermal titration calorimetry of protein-protein interactions. *Methods (San Diego, Calif.)*, 19(2), pp.213–21.

Plun-Favreau, H. et al., 2003. Leukemia inhibitory factor (LIF), cardiotrophin-1, and oncostatin M share structural binding determinants in the immunoglobulin-like

domain of LIF receptor. *The Journal of biological chemistry*, 278(29), pp.27169–79.

Pöling, J. et al., 2012. The Janus face of OSM-mediated cardiomyocyte dedifferentiation during cardiac repair and disease. *Cell cycle (Georgetown, Tex.)*, 11(3), pp.439–45.

Pöling, J. et al., 2014. Therapeutic targeting of the oncostatin M receptor-β prevents inflammatory heart failure. *Basic research in cardiology*, 109(1), p.396.

Radtke, S. et al., 2002. Novel role of Janus kinase 1 in the regulation of oncostatin M receptor surface expression. *The Journal of biological chemistry*, 277(13), pp.11297–305.

Rajarathnam, K. & Rösgen, J., 2014. Isothermal titration calorimetry of membrane proteins - progress and challenges. *Biochimica et biophysica acta*, 1838(1 Pt A), pp.69–77.

Rämer, P.C. et al., 2011. Mice with human immune system components as in vivo models for infections with human pathogens. *Immunology and cell biology*, 89(3), pp.408–16.

Rappsilber, J. et al., 2000. A generic strategy to analyze the spatial organization of multi-protein complexes by cross-linking and mass spectrometry. *Analytical chemistry*, 72(2), pp.267–75.

Richards, C.D. et al., 1992. Recombinant oncostatin M stimulates the production of acute phase proteins in HepG2 cells and rat primary hepatocytes in vitro. *Journal of immunology (Baltimore, Md. : 1950)*, 148(6), pp.1731–6.

Richards, C.D. et al., 1993. Selective regulation of metalloproteinase inhibitor (TIMP-1) by oncostatin M in fibroblasts in culture. *Journal of immunology (Baltimore, Md. : 1950)*, 150(12), pp.5596–603.

Richards, C.D., 2013. The enigmatic cytokine oncostatin m and roles in disease. *ISRN inflammation*, 2013, p.512103.

Richter, G. et al., 1995. The rat interleukin 4 receptor: coevolution of ligand and receptor. *Cytokine*, 7(3), pp.237–41.

Robinson, R.C. et al., 1994. The crystal structure and biological function of leukemia inhibitory factor: implications for receptor binding. *Cell*, 77(7), pp.1101–16.

Rongvaux, A. et al., 2014. Development and function of human innate immune cells in a humanized mouse model. *Nature biotechnology*, 32(4), pp.364–72.

Rongvaux, A. et al., 2013. Human hemato-lymphoid system mice: current use and future potential for medicine. *Annual review of immunology*, 31, pp.635–74.

Rose, T.M. et al., 1993. The genes for oncostatin M (OSM) and leukemia inhibitory factor (LIF) are tightly linked on human chromosome 22. *Genomics*, 17(1), pp.136–40.

Rose, T.M. & Bruce, A.G., 1991. Oncostatin M is a member of a cytokine family that includes leukemia-inhibitory factor, granulocyte colony-stimulating factor, and interleukin 6. *Proceedings of the National Academy of Sciences of the United*

States of America, 88(19), pp.8641–5.
Sadowski, H.B. et al., 1993. A common nuclear signal transduction pathway activated by growth factor and cytokine receptors. *Science (New York, N.Y.)*, 261(5129), pp.1739–44.
Scapigliati, G., Buonocore, F. & Mazzini, M., 2006. Biological activity of cytokines: an evolutionary perspective. *Current pharmaceutical design*, 12(24), pp.3071–81.
Schiemann, W.P., Bartoe, J.L. & Nathanson, N.M., 1997. Box 3-independent signaling mechanisms are involved in leukemia inhibitory factor receptor alpha- and gp130-mediated stimulation of mitogen-activated protein kinase. Evidence for participation of multiple signaling pathways which converge at Ras. *The Journal of biological chemistry*, 272(26), pp.16631–6.
Schmidt, T., Bergner, A. & Schwede, T., 2014. Modelling three-dimensional protein structures for applications in drug design. *Drug discovery today*, 19(7), pp.890–7.
Schmitt, J., Hess, H. & Stunnenberg, H.G., 1993. Affinity purification of histidine-tagged proteins. *Molecular biology reports*, 18(3), pp.223–30.
Schroeder, T., 2010. Hematopoietic stem cell heterogeneity: subtypes, not unpredictable behavior. *Cell stem cell*, 6(3), pp.203–7.
Schulze-Gahmen, U., De Bondt, H.L. & Kim, S.H., 1996. High-resolution crystal structures of human cyclin-dependent kinase 2 with and without ATP: bound waters and natural ligand as guides for inhibitor design. *Journal of medicinal chemistry*, 39(23), pp.4540–6.
Schwartz, D.M. et al., 2016. Type I/II cytokines, JAKs, and new strategies for treating autoimmune diseases. *Nature reviews. Rheumatology*, 12(1), pp.25–36.
Shuai, K. et al., 1994. Interferon activation of the transcription factor Stat91 involves dimerization through SH2-phosphotyrosyl peptide interactions. *Cell*, 76(5), pp.821–8.
Shuai, K. et al., 1993. Polypeptide signalling to the nucleus through tyrosine phosphorylation of Jak and Stat proteins. *Nature*, 366(6455), pp.580–3.
Sievers, F. et al., 2011. Fast, scalable generation of high-quality protein multiple sequence alignments using Clustal Omega. *Molecular systems biology*, 7, p.539.
Skiniotis, G. et al., 2008. Structural organization of a full-length gp130/LIF-R cytokine receptor transmembrane complex. *Molecular cell*, 31(5), pp.737–48.
Slaets, H. et al., 2014. Oncostatin M reduces lesion size and promotes functional recovery and neurite outgrowth after spinal cord injury. *Molecular neurobiology*, 50(3), pp.1142–51.
Smyth, D.C., Kerr, C. & Richards, C.D., 2006. Oncostatin M-induced IL-6 expression in murine fibroblasts requires the activation of protein kinase Cdelta. *Journal of immunology (Baltimore, Md. : 1950)*, 177(12), pp.8740–7.
Somers, W., Stahl, M. & Seehra, J.S., 1997. 1.9 A crystal structure of interleukin 6: implications for a novel mode of receptor dimerization and signaling. *The EMBO*

journal, 16(5), pp.989–97.

Spangler, J.B. et al., 2015. Insights into cytokine-receptor interactions from cytokine engineering. *Annual review of immunology*, 33, pp.139–67.

Sporeno, E. et al., 1994. Production and structural characterization of amino terminally histidine tagged human oncostatin M in E. coli. *Cytokine*, 6(3), pp.255–64.

Stahl, N. et al., 1994. Association and activation of Jak-Tyk kinases by CNTF-LIF-OSM-IL-6 beta receptor components. *Science (New York, N.Y.)*, 263(5143), pp.92–5.

Stahl, N. et al., 1993. Cross-linking identifies leukemia inhibitory factor-binding protein as a ciliary neurotrophic factor receptor component. *The Journal of biological chemistry*, 268(11), pp.7628–31.

Suda, T. et al., 2002. Oncostatin M production by human dendritic cells in response to bacterial products. *Cytokine*, 17(6), pp.335–40.

Sun, D. et al., 2015. Oncostatin M (OSM) protects against cardiac ischaemia/reperfusion injury in diabetic mice by regulating apoptosis, mitochondrial biogenesis and insulin sensitivity. *Journal of cellular and molecular medicine*, 19(6), pp.1296–307.

Taga, T. et al., 1989. Interleukin-6 triggers the association of its receptor with a possible signal transducer, gp130. *Cell*, 58(3), pp.573–81.

Takizawa, M. et al., 2003. Requirement of gp130 signaling for the AGM hematopoiesis. *Experimental hematology*, 31(4), pp.283–9.

Tanaka, M. et al., 2003. Targeted disruption of oncostatin M receptor results in altered hematopoiesis. *Blood*, 102(9), pp.3154–62.

Thoma, B. et al., 1994. Oncostatin M and leukemia inhibitory factor trigger overlapping and different signals through partially shared receptor complexes. *The Journal of biological chemistry*, 269(8), pp.6215–22.

Underhill-Day, N. & Heath, J.K., 2006. Oncostatin M (OSM) cytostasis of breast tumor cells: characterization of an OSM receptor beta-specific kernel. *Cancer research*, 66(22), pp.10891–901.

Varadarajan, N. et al., 2009. Construction and flow cytometric screening of targeted enzyme libraries. *Nature protocols*, 4(6), pp.893–901.

Varadarajan, N. et al., 2005. Engineering of protease variants exhibiting high catalytic activity and exquisite substrate selectivity. *Proceedings of the National Academy of Sciences of the United States of America*, 102(19), pp.6855–60.

de Vos, A.M., Ultsch, M. & Kossiakoff, A.A., 1992. Human growth hormone and extracellular domain of its receptor: crystal structure of the complex. *Science (New York, N.Y.)*, 255(5042), pp.306–12.

Walker, E.C. et al., 2016. Murine Oncostatin M Acts via Leukemia Inhibitory Factor Receptor to Phosphorylate Signal Transducer and Activator of Transcription 3 (STAT3) but Not STAT1, an Effect That Protects Bone Mass. *The Journal of biological chemistry*, 291(41), pp.21703–21716.

Wallace, P.M. et al., 1995. In vivo properties of oncostatin M. *Annals of the New York Academy of Sciences*, 762, pp.42–54.

Wang, Y. et al., 2000. Receptor subunit-specific action of oncostatin M in hepatic cells and its modulation by leukemia inhibitory factor. *The Journal of biological chemistry*, 275(33), pp.25273–85.

West, N.R. et al., 2017. Oncostatin M drives intestinal inflammation and predicts response to tumor necrosis factor-neutralizing therapy in patients with inflammatory bowel disease. *Nature medicine*, 23(5), pp.579–589.

Wiesmann, C. et al., 1999. Crystal structure of nerve growth factor in complex with the ligand-binding domain of the TrkA receptor. *Nature*, 401(6749), pp.184–8.

Wildhagen, K.C.A.A. et al., 2011. The structure-function relationship of activated protein C. Lessons from natural and engineered mutations. *Thrombosis and haemostasis*, 106(6), pp.1034–45.

Yamaguchi, Y., Park, J.-H. & Inouye, M., 2011. Toxin-antitoxin systems in bacteria and archaea. *Annual review of genetics*, 45, pp.61–79.

Yin, T. et al., 1993. Involvement of IL-6 signal transducer gp130 in IL-11-mediated signal transduction. *Journal of immunology (Baltimore, Md. : 1950)*, 151(5), pp.2555–61.

Yonath, A., 2011. X-ray crystallography at the heart of life science. *Current opinion in structural biology*, 21(5), pp.622–6.

Zarling, J.M. et al., 1986. Oncostatin M: a growth regulator produced by differentiated histiocytic lymphoma cells. *Proceedings of the National Academy of Sciences of the United States of America*, 83(24), pp.9739–43.

Zarrinpar, A., Park, S.-H. & Lim, W.A., 2003. Optimization of specificity in a cellular protein interaction network by negative selection. *Nature*, 426(6967), pp.676–80.

Zauberman, A. et al., 1999. Stress activated protein kinase p38 is involved in IL-6 induced transcriptional activation of STAT3. *Oncogene*, 18(26), pp.3886–93.

Zgheib, C. et al., 2012. Chronic treatment of mice with leukemia inhibitory factor does not cause adverse cardiac remodeling but improves heart function. *European cytokine network*, 23(4), pp.191–7.

Zhang, X. et al., 2017. Oncostatin M receptor β deficiency attenuates atherogenesis by inhibiting JAK2/STAT3 signaling in macrophages. *Journal of lipid research*, 58(5), pp.895–906.

Zhang, X. et al., 2015. OSM Enhances Angiogenesis and Improves Cardiac Function after Myocardial Infarction. *BioMed research international*, 2015, p.317905.

Zou, Y. et al., 2003. Leukemia inhibitory factor enhances survival of cardiomyocytes and induces regeneration of myocardium after myocardial infarction. *Circulation*, 108(6), pp.748–53.

11. Erklärung zur Dissertation

I declare that I have completed this dissertation single-handedly without the unauthorized help of a second party and only with the assistance acknowledged therein. I have appropriately acknowledged and cited all text passages that are derived verbatim from or are based on the content of published work of others, and all information relating to verbal communications. I consent to the use of an anti-plagiarism software to check my thesis. I have abided by the principles of good scientific conduct laid down in the charter of the Justus Liebig University Giessen "Satzung der Justus-Liebig-Universität Gießen zur Sicherung guter wissenschaftlicher Praxis" in carrying out the investigations described in the dissertation.

Bad Nauheim, .2017 _____

(Juan Manuel Adrián Segarra)

12. Publications and scientific presentations

12.1. Peer-reviewed publications

Lörchner, H., Pöling, J., Gajawada, P., Hou, Y., Polyakova, V., Kostin, S., **Adrian-Segarra, J.M.**, Boettger, T., Wietelmann, A., Warnecke, H., Richter, M., Kubin, T. & Braun, T., 2015. Myocardial healing requires Reg3β-dependent accumulation of macrophages in the ischemic heart. *Nature medicine*, 21(4), pp.353–62.

Hou, Y., **Adrian-Segarra, J.M.,** Richter, M., Kubin, N., Shin, J., Werner, I., Walther, T., Schönburg, M., Pöling, J., Warnecke, H., Braun, T., Kostin, S. & Kubin, T., 2015. Animal Models and "Omics" Technologies for Identification of Novel Biomarkers and Drug Targets to Prevent Heart Failure. *BioMed research international*, 2015, 2015:212910.

12.2. Scientific presentations

Adrian-Segarra, J.M., Al-Furoukh, N., Lörchner, H., Gajawada, P., Kubin, T., Pöling, J. & Braun, T., 2016. Structural features of Oncostatin M enabling specific ligand-receptor interactions. **Poster & Flash Talk** presentations at **EMBO Chemical Biology 2016**.

13. Acknowledgements

"Caminante, no hay camino; se hace camino al andar"
"Walker, there is no path; the path is made by walking"
- Antonio Machado, Proverbios y Cantares XXIX

Scientific work at times involves walking uncertain and unexplored paths, and this PhD project was no exception. Despite being an individual work, I would never have reached this point without the help and support of many people along the way, for which I am deeply grateful.

In first place I would like to thank my supervisor, Prof. Dr. Dr. Thomas Braun, for his trust and unwavering support; none of this would have been possible without his faith in an unproved PhD candidate nearly five years ago. I am also indebted to my direct supervisor, Dr. Jochen Pöling, whose encouragement and guidance proved instrumental in crafting a project above and beyond my initial expectations.

Several people made key contributions without which the present work could not have been undertaken: foremost were Dr. Natalie Al-Furoukh, who introduced me to molecular cloning, and Dr. Krishnamoorthy Sreenivasan, who created lentiviral-transfected NIH3T3 cell lines to use as murine receptor activation readouts. I am also thankful to Dr. Holger Lörchner, Dr. Praveen Gajawada, Dr. André Schneider, Dr. Heike Hermanns and Dr. Sarah Tonack for donating cell lines and plasmid constructs used in this study, to Jutta Wetzel and Kerstin Richter for their invaluable technical assistance and to Dr. Thomas Kubin for his role in recruiting me for this project.

I have been fortunate to come across some very special people during my stay in Germany: life would not be the same without my group members (Holger, Jochen, Praveen, Jutta, Jenny, Julia, Kerstin and Yunlong) and many other colleagues from the Institute (in particular Krishna, Daniela and Yu Ting). The same is true for my friends back in Spain (especially Ernesto, Marta, Sylvia, Tania, Helena, Mari Carmen, Àngel and Arnau), who have not let distance be an obstacle.

Finally, I have no words to describe how much my family has helped throughout this time: my mother María José, my uncle Silvestre, my siblings Verónica and Silvestre and my cousin Francisco have provided an incredible amount of love, support and encouragement since the first day. This work is dedicated to my father Manuel: despite passing away twenty years ago, his loving memory continues to be a driving force to this day.